INFORMATION TO USERS

This manuscript has been reproduced from the microfilm master. UMI films the text directly from the original or copy submitted. Thus, some thesis and dissertation copies are in typewriter face, while others may be from any type of computer printer.

The quality of this reproduction is dependent upon the quality of the copy submitted. Broken or indistinct print, colored or poor quality illustrations and photographs, print bleedthrough, substandard margins, and improper alignment can adversely affect reproduction.

In the unlikely event that the author did not send UMI a complete manuscript and there are missing pages, these will be noted. Also, if unauthorized copyright material had to be removed, a note will indicate the deletion.

Oversize materials (e.g., maps, drawings, charts) are reproduced by sectioning the original, beginning at the upper left-hand corner and continuing from left to right in equal sections with small overlaps. Each original is also photographed in one exposure and is included in reduced form at the back of the book.

Photographs included in the original manuscript have been reproduced xerographically in this copy. Higher quality 6" x 9" black and white photographic prints are available for any photographs or illustrations appearing in this copy for an additional charge. Contact UMI directly to order.

UMI®

Bell & Howell Information and Learning
300 North Zeeb Road, Ann Arbor, MI 48106-1346 USA
800-521-0600

Numerical Analysis of Elastic Membrane Structures Subjected to Hydrostatic Pressure Loading

Ying Liu

A Thesis

in

The Department

of

Mechanical Engineering

Presented in Partial Fulfillment of the Requirements
for the Degree of Master of Applied Science at
Concordia University
Montreal, Quebec, Canada

August 1997

Abstract

Membrane structures play an important role in a wide variety of applications, ranging from solar sails, satellites and aircraft, to pneumatic structures, lightweight temporary constructions and biological tissues.

In this research project a numerical model has been developed for stress analysis in isotropic elastic membranes undergoing finite deformations, while partly or totally subjected to pressure loading of the hydrostatic type. The possibility of wrinkling is accounted for by employing a ***Relaxed Strain Energy Density***. The numerical procedure is based on the ***Dynamic Relaxation Method***. This is an explicit, iterative technique in which the static solution is obtained as the steady state part of the damped dynamic response of the structure. The numerical scheme is constructed by applying Green's theorem differencing method for the spatial discretization of the partial differential equations describing the damped motion of the membrane. The resulting system of ordinary differential equations is further integrated in time by a central difference time integrator. Solutions of typical boundary value problems are obtained and analyzed. The effects of various loading and boundary conditions on the response of the membrane are examined. The predictions of the numerical method are in good agreement with the results obtained with experimental models.

Acknowledgments

I would like to express my sincere gratitude to my thesis supervisor, Dr. Eliza M. Haseganu, for her constant guidance and help throughout my graduate studies.

I would like to thank Mr. Danius Juras and Mr. Dale Rathwell for their help during my experimental investigation. I would also like to thank the other professors at CONCAVE Research Center for their help in the realization of this work.

Appreciation is extended to Concordia University and the Department of Mechanical Engineering. The financial support provided by the Natural Sciences and Engineering Research Council of Canada and by Concordia University, through the Faculty Research and Development Program are gratefully acknowledged.

Finally, I sincerely thank my husband Binlai and my parents for their patience, understanding, encouragement and support.

Table of Contents

List of Figures

List of Symbols

$A^{k,l}$	—	nodal area
$A^{k+1/2,l+1/2}$	—	zonal area
c	—	damping matrix coefficient
C	—	Cauchy-Green strain tensor
e	—	error vector
$\{e_\alpha\}$	—	fixed orthonormal basis ($\alpha = 1,2$)
$\{e_i\}$	—	fixed orthonormal basis ($i = 1,2,3$)
$e_{\alpha\beta}$	—	2D alternator symbol
e_{ijk}	—	3D alternator symbol
E	—	Young's modulus
F	—	deformation gradient
$\tilde{F}$	—	external force
G	—	shear modulus
g	—	gravitational acceleration
h	—	time step
h_{ll}	—	height of liquid measured along e_3 direction

$\boldsymbol{J}$	—	Jacobian
$\boldsymbol{K}$	—	stiffness matrix
${}^{l}\boldsymbol{K}$	—	local diagonal stiffness matrix
${}^{t}\boldsymbol{K}$	—	tangential stiffness matrix
$\boldsymbol{L}, \boldsymbol{M}$	—	principal vectors of strain in reference configuration
$\boldsymbol{l}, \boldsymbol{m}$	—	principal vectors of strain in deformed configuration
m_{ii}	—	element of diagonal mass matrix
$\boldsymbol{M}$	—	mass matrix
$\boldsymbol{n}$	—	unit vector normal to deformed surface at $\boldsymbol{r}$
O	—	truncation error
$\boldsymbol{p}$	—	pressure loading
$\boldsymbol{P}$	—	internal force
$\tilde{P}$	—	load potential
$\boldsymbol{r}$	—	position vector of material particle in deformed configuration
r_1, r_2, r_3	—	components of $\boldsymbol{r}$ with respect to $\{e_i\}$
$\boldsymbol{R}$	—	residual vector
$\boldsymbol{t}$	—	traction vector
$\boldsymbol{T}$	—	Piola stress tensor
$\boldsymbol{u}$	—	displacement vector
$\boldsymbol{U}$	—	strain energy per unit intial volume
ν	—	natrual width in simple tension

W	—	strain energy per unit area of reference configuration
w_λ, w_μ	—	principal Piola stresses
x	—	position vector of material particle in reference configuration
x_1, x_2	—	components of x with respect to $\{e_\alpha\}$

Greek Symbols

Δ	—	2D unit tensor
δ	—	kronecker delta symbol
ε	—	typical zone width
λ, μ	—	principal stretches
ν	—	unit vector normal to undeformed surface at x
ω_0, ω_{max}	—	fundamental and maximum natural frequencies of structure
Ω	—	bounded region of (x_1, x_2)-plane
$\partial\Omega$	—	boundary of region Ω
ϱ	—	spectral radius
ϱ_0, ϱ_l	—	mass densities of membrane and liquid
σ	—	Cauchy stress tensor

Superscripts

(k, l)	—	label of node
$(k+1/2, l+1/2)$	—	label of zone and zone center

n	—	label of time step
0	—	label of time step at $t = 0$
-1	—	inverse of matrix, tensor
T	—	transpose of tensor

Subscripts

i	—	component with respect to $\boldsymbol{e}_i$ $(i = 1, 2, 3)$
j	—	component with respect to $\boldsymbol{e}_j$ $(j = 1, 2, 3)$
α	—	component with respect to $\boldsymbol{e}_\alpha$ $(\alpha = 1, 2)$
β	—	component with respect to $\boldsymbol{e}_\beta$ $(\beta = 1, 2)$
$,\alpha$	—	partial derivative with respect to x_α $(\alpha = 1, 2)$
λ, μ	—	partial derivatives with respect to principal stretches

Abbreviations

DOF	—	degree of freedom
ODE	—	ordinary differential equation
PDE	—	partial differential equation
2D	—	two dimensions
3D	—	three dimensions

Chapter 1

Introduction

Membrane structures play an important role in a wide variety of applications, ranging from solar sails, satellites and aircraft, to pneumatic structures, lightweight temporary constructions and biological tissues. The deformations occurring in such structures are generally of the large rotation or large strain type, and are therefore inherently nonlinear. Partial or total wrinkling of the membrane may be observed in many equilibrium configurations. The problems of static analysis associated with membrane structures are of two types: (i) form (shape) finding, (ii) response (deformation and/or stress) analysis. In this work, the second type of problems is considered.

A numerical model has been developed for the static analysis of isotropic elastic membranes subjected to pressure loading of hydrostatic type and different displacement boundary conditions. The membranes may have arbitrary planar stress-free reference configurations and may undergo finite deformations. The possibility of wrinkling is taken into account.

This numerical model is based on the ***Dynamic Relaxation*** (DR) method (Frankel, 1950, Otter, 1965, Day, 1965, Underwood, 1983). DR is an explicit iterative method developed to solve static problems in structural mechanics. The static problem is

transformed into an equivalent dynamic problem by adding inertia and damping terms. The static solution is then obtained as the steady state part of the transient response of the structure.

The numerical model is obtained from the spatial and temporal discretization of the partial differential equations (PDEs) describing the damped motion of the structure. The spatial discretization technique used here is a finite difference technique derived from Green's theorem (Wilkins, 1964, Silling, 1985). In addition to its simplicity, this method is suitable to any shape of the boundary. Uniform or irregular meshes may be used. The resulting system of ordinary differential equations (ODEs) is then integrated in time by employing a central difference time integrator.

The DR method has been introduced and applied to engineering problems since the 1960's. It has been successfully used for plates and shell problems, especially the large deflection cases, for form-finding as well as nonlinear static analysis of lightweight tensile structures, such as networks and membranes. Many researchers contributed to improve this method. Welsh (1967) introduced fictitious mass densities. The convergence of the damped solution towards the static solution may be accelerated by using a fictitious mass. Underwood (1983) presented an adaptive DR method. In the adaptive method, the damping coefficient and the fictitious mass densities are computed in every iteration to obtain the least time step. Tangential and local stiffness matrices have to be computed in the adaptive DR method in order to calculate the damping coefficient and the mass matrices. Zhang and Yu (1989) introduced a modified adaptive DR method. They used a different approach to calculate the damping coefficient, and avoided the computation of the local stiffness matrix. Zhang, Kadkhodayan and Mai (1994) improved the modified

adaptive DR method. They showed a way to choose the initial displacement in order to save computation time. The DR method is of interest to many researchers due to its explicit formulation. DR is appropriate to the type of problems considered in this work since it does not involve the computation and inversion of the stiffness matrix, which is ill-conditioned when wrinkling is present. Ordinary stiffness based iterative methods such as Newton-Raphson cannot be used in the presence of wrinkling, since such methods lead to ill-conditioned systems of equations. The solutions obtained with DR are asymptotically dynamically stable, which is another advantage of the method.

Some equilibrium configurations may exhibit partial or total wrinkling. Analysis of wrinkling is important for prediction of structural response. Wrinkling occurs due to the loss of prestress and appearance of compressive stresses, under the action of certain loads and/or certain boundary conditions. The small bending stiffness of the material determines the configuration of the wrinkled region. When wrinkling occurs, membrane theory can not be applied, since the bending stiffness is neglected in this theory, and compressive stresses are obtained. Solutions with compressive stresses are unstable (Steigmann, 1986) and therefore not observable as equilibrium states. Shell theory may be used in the wrinkled regions to get solutions, but it is more complicated in comparison to membrane theory. Wagner (1929) introduced tension field theory to analyze wrinkled membranes. This theory is much simpler from the point of view of analysis. Pipkin (1986) showed that tension field theory can be incorporated into ordinary membrane theory by replacing the strain energy function by a ***Relaxed Strain Energy Density.*** The stress-strain relations derived from the relaxed strain energy deliver stresses that are never compressive. In the wrinkled region, a state of uniaxial stress is obtained, one principal

stress being zero. However only the average deformation in a wrinkled region results from this theory. A relaxed strain energy density is used in this work.

A brief description of the following chapters of the thesis is given in the next paragraphs.

In chapter 2, membrane theory and the relaxed strain energy density are introduced. The global and the local equilibrium equations are presented. The way of incorporating the relaxed strain energy within the membrane theory is shown. The stress-strain relation is derived from the relaxed strain energy density. The stresses and the strains considered here are given by the Piola stress tensor and the Cauchy-Green strain tensor respectively.

In chapter 3, the DR method is presented. The origination of the DR method, the theory of DR, the algorithm and different approaches to choose the iteration parameters in order to obtain a fast stable solution, can be found in this chapter. A finite difference technique derived from Green's theorem for the spatial discretization of the PDEs governing the damped motion of the membrane is also presented. The method to approximate the internal forces which are needed in the DR formulation is shown.

In chapter 4, the algorithm developed to analyze the response of the membrane partially or totally subjected to pressure loading of the hydrostatic type is presented.

In chapter 5, applications of this numerical method are discussed. The reference configuration of the membrane is plane, but the deformed configurations may be three dimensional. A variety of equilibrium problems involving membranes subjected to different displacement boundary conditions and pressure loading of the hydrostatic type are considered. Solutions for the shapes of the deformed configurations, the distribution

of the principal stresses, as well as the principal stretches are obtained, and graphs of these solutions indicating the presence of wrinkling are presented.

In chapter 6, an experimental investigation of the problem involving a square membrane subjected to shear and stretch is described. The experimental results are shown to validate the solution obtained with the numerical model.

Chapter 7 presents a summary, conclusions and future work directions.

Chapter 2

Membrane Theory

2.1 Introduction

The direct theory of elastic membranes is considered (Naghdi, 1972; Steigmann, 1990). In this theory, a membrane is regarded as a two dimensional elastic continuum, endowed with a strain energy $W(\boldsymbol{F})$ measured per unit area of a reference surface, where $\boldsymbol{F}$ is the deformation gradient. The membrane is assumed to be perfectly flexible, thus its bending stiffness is considered to be negligible. Assumptions are also made that the membrane material is isotropic, homogeneous and incompressible. The case of finite deformations is treated.

Under the action of specific loads or certain boundary conditions, wrinkling of the membrane may occur. This represents a localized buckling phenomenon. The configuration of the wrinkled region depends on the small bending stiffness of the material. Membrane theory in its usual form neglects the bending stiffness and cannot give details of the deformation in the wrinkled region. Moreover, it delivers compressive stresses in the wrinkled region, making the solution unstable (Steigmann, 1986) and

therefore physically meaningless. To obtain a solution, shell theory may be used in the wrinkled regions, or tension field theory, which is much simpler from the point of view of analysis. Pipkin (1986) introduced the concept of a relaxed strain energy density. By employing this strain energy, tension field theory is automatically incorporated into ordinary membrane theory, leading to stresses that are never compressive and therefore to deformations that satisfy this necessary condition of stability.

2.2 Kinematics of Deformation

Suppose an elastic membrane has a plane stress-free reference configuration and occupies a bounded region Ω with boundary $\partial\Omega$. Let $\{e_\alpha\}$ be the basis in the reference configuration, where a Greek letter indicates 1 to 2. A material particle of the membrane may be identified by x in the reference configuration, where the position vector x is represented by: $x = x_\alpha e_\alpha$. Here the repetition of a Greek letter indicates a summation over the index from 1 to 2 ($x = x_1 e_1 + x_2 e_2$). A deformation carries the membrane to a three dimensional surface. Let $\{e_i\}$ be the basis in the deformed configuration, where a Latin letter indicates 1 to 3, and $e_3 = e_1 \times e_2$. The material particle of the membrane identified by x in the reference configuration is carried to a new position $r(x)$, which is in three-dimensional space. In the deformed configuration, the position vector $r(x)$ may be represented by $r(x) = r_i(x) e_i$, where the repetition of a Latin letter indicates a summation over the index from 1 to 3. In the direct theory the basic kinematical variable is the deformation gradient F. F maps the material line element dx at x in the reference configuration onto the material line element dr at r in the deformed configuration,

tangential to the deformed surface. Taking the differential of $\boldsymbol{r}(\boldsymbol{x}) = r_i(\boldsymbol{x})e_i$, one obtains $\mathrm{d}r_i = \partial r_i / \partial x_\alpha \, \mathrm{d}x_\alpha$, or in the invariant form $\mathrm{d}\boldsymbol{r}(\boldsymbol{x}) = \boldsymbol{F}\,\mathrm{d}\boldsymbol{x}$. Thus the deformation gradient $\boldsymbol{F}$ is defined by

$$\boldsymbol{F} = F_{i\alpha}(\boldsymbol{x}) e_i \otimes e_\alpha , \tag{2.1a}$$

where $F_{i\alpha}$ is represented by:

$$F_{i\alpha} = \partial r_i \Big/ \partial x_\alpha \; ; \text{ or } F_{i\alpha} = r_{i,\alpha} . \tag{2.1b}$$

If $\boldsymbol{F}\,\mathrm{d}\boldsymbol{x} = \boldsymbol{0}$ for $\mathrm{d}\boldsymbol{x} \neq \boldsymbol{0}$, it implies that at least one line element of material in the reference configuration has its length reduced to zero by the deformation, which is impossible. Thus $\boldsymbol{F}\,\mathrm{d}\boldsymbol{x} \neq \boldsymbol{0}$ for all $\mathrm{d}\boldsymbol{x} \neq \boldsymbol{0}$, $\boldsymbol{F}$ is a non-singular tensor.

The Cauchy-Green strain tensor is defined by

$$\boldsymbol{C} = \boldsymbol{F}^T\boldsymbol{F} = C_{\alpha\beta} e_\alpha \otimes e_\beta . \tag{2.2a}$$

The components of the Cauchy-Green strain tensor may be obtained by substituting (2.1a) into (2.2a), which gives

$$\begin{aligned} \boldsymbol{C} = \boldsymbol{F}^T\boldsymbol{F} &= (F_{i\alpha} e_i \otimes e_\alpha)^T (F_{j\beta} e_j \otimes e_\beta) \\ &= (F_{i\alpha} e_\alpha \otimes e_i)(F_{j\beta} e_j \otimes e_\beta) \\ &= F_{i\alpha} F_{j\beta} \delta_{ij} e_\alpha \otimes e_\beta \\ &= F_{i\alpha} F_{i\beta} e_\alpha \otimes e_\beta , \end{aligned}$$

where δ_{ij} is the Kronecker delta symbol defined by

$$\delta_{ij} = \begin{cases} 1 & i = j \\ 0 & i \neq j \end{cases}$$

So the components of the Cauchy-Green strain tensor are given by:

$$C_{\alpha\beta} = F_{i\alpha} F_{i\beta} . \tag{2.2b}$$

For $(\boldsymbol{F}^T\boldsymbol{F})^T = \boldsymbol{F}^T(\boldsymbol{F}^T)^T = \boldsymbol{F}^T\boldsymbol{F}$, the Cauchy-Green strain tensor $\boldsymbol{C}$ is a symmetric second order tensor. By using the definition of the transpose tensor: $\boldsymbol{v}\cdot(\boldsymbol{T}^T\boldsymbol{u}) = \boldsymbol{u}\cdot(\boldsymbol{T}\boldsymbol{v})$, where $\boldsymbol{T}$ is a tensor and $\boldsymbol{v}$ and $\boldsymbol{u}$ are any vectors, the transpose Cauchy-Green strain tensor $\boldsymbol{C}^T$ may be written as: $\boldsymbol{v}\cdot(\boldsymbol{C}^T\boldsymbol{v}) = \boldsymbol{v}\cdot(\boldsymbol{C}\boldsymbol{v})$. Substituting (2.2a) into the above equation, leads to $\boldsymbol{v}\cdot(\boldsymbol{F}^T\boldsymbol{F}\boldsymbol{v}) = \boldsymbol{v}\cdot(\boldsymbol{F}^T(\boldsymbol{F}\boldsymbol{v})) = (\boldsymbol{F}\boldsymbol{v})\cdot(\boldsymbol{F}\boldsymbol{v}) = |\boldsymbol{F}\boldsymbol{v}|^2 > 0$ for all $\boldsymbol{v} \neq \boldsymbol{0}$. Thus $\boldsymbol{C}$ is a positive definite second order tensor according to the definition.

For a symmetric second-order tensor, the eigenvectors of this tensor are mutually orthogonal and the eigenvalues are real. Let $\{\boldsymbol{L}(x), \boldsymbol{M}(x)\}$ be the orthonormal pair of eigenvectors of the Cauchy-Green tensor $\boldsymbol{C}$, with representations $\boldsymbol{L} = L_\alpha(x)e_\alpha$ and $\boldsymbol{M} = M_\alpha(x)e_\alpha$. $\boldsymbol{L}(x)$ and $\boldsymbol{M}(x)$ are the two principal vectors of strain at x in the reference configuration. Let $\{\boldsymbol{l}(x), \boldsymbol{m}(x)\}$ be an orthonormal pair of eigenvectors of $\boldsymbol{C}$ with respect to the deformed configuration, then $\boldsymbol{l}(x)$ and $\boldsymbol{m}(x)$ are the two principal vectors of strain at r which are tangential to the deformed surface at the material point x with respect to deformed configuration. Let $\mathrm{d}x$ and $\mathrm{d}r$ be along the principal directions $\boldsymbol{L}$ and $\boldsymbol{l}$ respectively, then from $\mathrm{d}\boldsymbol{r}(x) = \boldsymbol{F}\,\mathrm{d}x$, one obtains:

$$\boldsymbol{l}|\mathrm{d}\boldsymbol{r}(x)| = \boldsymbol{F}\boldsymbol{L}|\mathrm{d}x|. \tag{2.3}$$

The vector products of the both hand sides of (2.3) give

$$\boldsymbol{l}|\mathrm{d}\boldsymbol{r}(x)|\cdot\boldsymbol{l}|\mathrm{d}\boldsymbol{r}(x)| = \boldsymbol{F}\boldsymbol{L}|\mathrm{d}x|\cdot\boldsymbol{F}\boldsymbol{L}|\mathrm{d}x|. \tag{2.4a}$$

Simplifying (2.4a) gives:

$$|\mathrm{d}\boldsymbol{r}(x)|^2 = |\boldsymbol{F}\boldsymbol{L}|^2|\mathrm{d}x|^2, \tag{2.4b}$$

and (2.4b) may be rewritten as:

$$\frac{|\mathrm{d}\,r(x)|}{|\mathrm{d}\,x|} = |\boldsymbol{FL}| = \lambda(x), \tag{2.4c}$$

where $\lambda(x)$ is one of the principal stretches along the principal direction $\boldsymbol{L}$ at x. By using the definition of the transpose it can be obtained that

$$|\boldsymbol{FL}| = \{\boldsymbol{L}\cdot(\boldsymbol{F}^T\boldsymbol{FL})\}^{1/2} = \{\boldsymbol{L}\cdot\boldsymbol{CL}\}^{1/2}. \tag{2.5}$$

Thus the non-negative scalars $\lambda(x)$ may be defined as

$$\lambda(x) = |\boldsymbol{FL}| = \{\boldsymbol{L}\cdot\boldsymbol{CL}\}^{1/2}. \tag{2.6a}$$

Then equation (2.6a) gives:

$$\boldsymbol{CL} - \lambda^2(x)\boldsymbol{L} = \boldsymbol{0}, \tag{2.6b}$$

where $\lambda^2(x)$ is one of the eigenvalues of the Cauchy-Green strain tensor.

By the same procedure, let $\mu(x)$ be the other principal stretch along the other principal direction $\boldsymbol{M}$ at x, defined as

$$\mu(x) = |\boldsymbol{FM}| = \{\boldsymbol{M}\cdot\boldsymbol{CM}\}^{1/2}. \tag{2.7a}$$

From equation (2.7a) one can get

$$\boldsymbol{CM} - \mu^2(x)\boldsymbol{M} = \boldsymbol{0}, \tag{2.7b}$$

where $\mu^2(x)$ is the other eigenvalue of the Cauchy-Green strain tensor $\boldsymbol{C}$.

The two eigenvalues of $\boldsymbol{C}$ can be obtained by solving the eigenvalue problem. The characteristic equation for $\boldsymbol{C}$ may be written as:

$$\det(C_{\alpha\beta} - \lambda\delta_{\alpha\beta}) = 0; \qquad \det(C_{\alpha\beta} - \mu\delta_{\alpha\beta}) = 0. \tag{2.8}$$

By solving (2.8), λ and μ can be expressed as

$$\lambda = \left\{\frac{1}{2}\left[\mathrm{tr}\boldsymbol{C} + (\mathrm{discr}\boldsymbol{C})^{1/2}\right]\right\}^{1/2},$$

$$\mu = \left\{\frac{1}{2}\left[\mathrm{tr}\boldsymbol{C} - (\mathrm{discr}\boldsymbol{C})^{1/2}\right]\right\}^{1/2}, \tag{2.9}$$

where $\mathrm{tr}\boldsymbol{C} = C_{\alpha\alpha} = C_{11} + C_{22}$ and $\mathrm{discr}\boldsymbol{C} = (\mathrm{tr}\boldsymbol{C})^2 - 4\det\boldsymbol{C}$ are the invariants of $\boldsymbol{C}$. Substituting λ and μ into equation (2.6b) and (2.7b), the components of $\boldsymbol{L}$ and $\boldsymbol{M}$ can be obtained:

$$L_1 = \frac{C_{12}}{\sqrt{(\lambda^2 - C_{11})^2 + C_{12}^2}}, \qquad L_2 = \frac{\lambda^2 - C_{11}}{C_{12}} L_1,$$

$$M_1 = \frac{C_{12}}{\sqrt{(\mu^2 - C_{11})^2 + C_{12}^2}}, \qquad M_2 = \frac{\mu^2 - C_{11}}{C_{12}} M_1. \tag{2.10}$$

In the case of $C_{12} = 0$, according to the definition, C_{11} and C_{22} are the two scalar values of the two principal strains and the two principal directions are along the x_1 and x_2 axes. The components of $\boldsymbol{L}$ and $\boldsymbol{M}$ are:

$$L_1 = 1, \qquad L_2 = 0, \tag{2.11}$$

$$M_1 = 0, \qquad M_2 = 1.$$

The unit vectors $\boldsymbol{l}$ and $\boldsymbol{m}$ can be defined as:

$$\boldsymbol{l}(\boldsymbol{x}) = \lambda^{-1}\boldsymbol{F}\boldsymbol{L}, \qquad \boldsymbol{m}(\boldsymbol{x}) = \mu^{-1}\boldsymbol{F}\boldsymbol{M} \tag{2.12}$$

Substituting (2.1b) into (2.12), one obtains:

$$\boldsymbol{l}(\boldsymbol{x}) = \lambda^{-1} r_{i,\alpha}\boldsymbol{e}_i \otimes \boldsymbol{e}_\alpha \cdot L_\beta \boldsymbol{e}_\beta = \lambda^{-1} r_{i,\alpha} L_\beta \delta_{\alpha\beta}\boldsymbol{e}_i = \lambda^{-1} r_{i,\alpha} L_\alpha \boldsymbol{e}_i, \tag{2.13}$$

$$\boldsymbol{m}(\boldsymbol{x}) = \mu^{-1} r_{i,\alpha}\boldsymbol{e}_i \otimes \boldsymbol{e}_\alpha \cdot M_\beta \boldsymbol{e}_\beta = \mu^{-1} r_{i,\alpha} M_\beta \delta_{\alpha\beta}\boldsymbol{e}_i = \mu^{-1} r_{i,\alpha} M_\alpha \boldsymbol{e}_i.$$

Thus the components of $\boldsymbol{l}$ and $\boldsymbol{m}$ are given by:

$$l_1 = \lambda^{-1}(L_1 r_{1.1} + L_2 r_{1.2}), \qquad m_1 = \mu^{-1}(M_1 r_{1.1} + M_2 r_{1.2}),$$

$$l_2 = \lambda^{-1}(L_1 r_{2.1} + L_2 r_{2.2}), \qquad m_2 = \mu^{-1}(M_1 r_{2.1} + M_2 r_{2.2}), \tag{2.14}$$

$$l_3 = \lambda^{-1}(L_1 r_{3.1} + L_2 r_{3.2}), \qquad m_3 = \mu^{-1}(M_1 r_{3.1} + M_2 r_{3.2}).$$

The unit tensor $\boldsymbol{I}$ may be represented in the form $\boldsymbol{I} = \Delta + \boldsymbol{e}_3 \otimes \boldsymbol{e}_3$, where $\Delta = \boldsymbol{e}_\alpha \otimes \boldsymbol{e}_\alpha$. Considering the orthonomality of $\{\boldsymbol{L}, \boldsymbol{M}\}$, Δ can be expressed as $\Delta = \boldsymbol{L} \otimes \boldsymbol{L} + \boldsymbol{M} \otimes \boldsymbol{M}$ for any $x \in \Omega$.Then $\boldsymbol{F}$ can be written as

$$\boldsymbol{F} = \boldsymbol{F}\Delta = \boldsymbol{F}\boldsymbol{L} \otimes \boldsymbol{L} + \boldsymbol{F}\boldsymbol{M} \otimes \boldsymbol{M}. \tag{2.15}$$

Substituting (2.12) into (2.15), one obtains:

$$\boldsymbol{F} = \lambda \boldsymbol{l} \otimes \boldsymbol{L} + \mu \boldsymbol{m} \otimes \boldsymbol{M}. \tag{2.16}$$

Then the Cauchy-Green strain is

$$\begin{aligned} \boldsymbol{C} &= \boldsymbol{F}^T \boldsymbol{F} \\ &= (\lambda \boldsymbol{l} \otimes \boldsymbol{L} + \mu \boldsymbol{m} \otimes \boldsymbol{M})^T (\lambda \boldsymbol{l} \otimes \boldsymbol{L} + \mu \boldsymbol{m} \otimes \boldsymbol{M}) \\ &= \{\lambda (\boldsymbol{l} \otimes \boldsymbol{L})^T + \mu (\boldsymbol{m} \otimes \boldsymbol{M})^T\} (\lambda \boldsymbol{l} \otimes \boldsymbol{L} + \mu \boldsymbol{m} \otimes \boldsymbol{M}) \\ &= \lambda^2 \boldsymbol{L} \otimes \boldsymbol{L} + \mu^2 \boldsymbol{M} \otimes \boldsymbol{M} + \lambda\mu \boldsymbol{l} \cdot \boldsymbol{m} (\boldsymbol{L} \otimes \boldsymbol{M} + \boldsymbol{M} \otimes \boldsymbol{L}). \end{aligned} \tag{2.17}$$

Since $\boldsymbol{l}$ and $\boldsymbol{m}$ are orthonormal vectors, $\boldsymbol{l} \cdot \boldsymbol{m} = \boldsymbol{0}$. Thus the spectral form of $\boldsymbol{C}$ may be written as:

$$\boldsymbol{C} = \lambda^2 \boldsymbol{L} \otimes \boldsymbol{L} + \mu^2 \boldsymbol{M} \otimes \boldsymbol{M}. \tag{2.18}$$

The Jacobian J which is the ratio of the elemental area of the deformed surface to the elemental area of the reference configuration, $J = \mathrm{d}a / \mathrm{d}A$, is:

$$J = \sqrt{\det \boldsymbol{C}} = \lambda\mu. \tag{2.19}$$

2.3 Stress and Equilibrium

The existence of a strain energy $\boldsymbol{W}(\boldsymbol{F})$ per unit area of reference configuration Ω represents the basic constitutive hypothesise of elastic membrane theory (e.g. Cohen and Wang, 1984).

The total potential energy due to a deformation $x \rightarrow r(x)$ is $E(r) = \iint_{\Omega} W(\boldsymbol{F})\mathrm{d}A - \tilde{P}[r]$, where $\mathrm{d}A = \mathrm{d}x_1\mathrm{d}x_2$ and $\tilde{P}[r]$ is the load potential associated with the particular type of pressure loading. The values of $W(\boldsymbol{F})$ should not be affected by superposed rotations, and therefore $W(\boldsymbol{F}) = \hat{W}(\boldsymbol{C})$. For isotropic elastic membranes the strain energy can be expressed as a symmetric function of the principal stretches λ and μ: $W(\boldsymbol{C}) = w(\lambda,\mu) = w(\mu,\lambda)$.

If only normal forces are applied to a unit square of membrane material, the membrane will be stretched into a rectangle of dimensions λ and μ. Let w_λ and w_μ be the two principal forces, they can be obtained from the strain energy by using variational principle:

$$w_\lambda = \partial w(\lambda,\mu)/\partial\lambda\,, \qquad (2.20)$$

$$w_\mu = \partial w(\lambda,\mu)/\partial\mu\,.$$

The two principal stresses which are the forces per unit length measured in the deformed configuration can be expressed as:

$$\sigma_1 = w_\lambda/\mu, \qquad (2.21)$$

$$\sigma_2 = w_\mu/\lambda.$$

Then the Cauchy stress tensor $\sigma = \sigma_{ij} e_i \otimes e_j$ may be written in the sprectal form:

$$\sigma = (w_\lambda / \mu) l \otimes l + (w_\mu / \lambda) m \otimes m. \tag{2.22}$$

Let T be the nominal stress tensor, also called the Piola or first Piola-Kirchhoff stress tensor. The components of this stress tensor are measured as the force per unit length of the arc in the reference configuration. T may be represented in the form $T = T_{i\alpha} e_i \otimes e_\alpha$. It can be shown that $T_{i\alpha} = \partial W / \partial F_{i\alpha}$ and in spectral form, T can be expressed as

$$T = w_\lambda l \otimes L + w_\mu m \otimes M. \tag{2.23}$$

where w_λ and w_μ are the two principal Piola stresses. The components of the Piola stress can be obtained from

$$T_{i\alpha} = e_i \cdot T e_\alpha. \tag{2.24}$$

Substituting (2.23) into (2.24), gives

$$\begin{aligned} T_{i\alpha} &= e_i \cdot (w_\lambda l_j e_j \otimes L_\beta e_\beta + w_\mu m_k e_k \otimes M_\gamma e_\gamma) e_\alpha \\ &= w_\lambda l_i L_\alpha + w_\mu m_i M_\alpha \end{aligned} \tag{2.25}$$

Therefore the components of the Piola stress are given by:

$$\begin{aligned} T_{11} &= l_1 L_1 w_\lambda + m_1 M_1 w_\mu, & T_{12} &= l_1 L_2 w_\lambda + m_1 M_2 w_\mu, \\ T_{21} &= l_2 L_1 w_\lambda + m_2 M_1 w_\mu, & T_{22} &= l_2 L_2 w_\lambda + m_2 M_2 w_\mu, \\ T_{31} &= l_3 L_1 w_\lambda + m_3 M_1 w_\mu, & T_{32} &= l_3 L_2 w_\lambda + m_3 M_2 w_\mu. \end{aligned} \tag{2.26}$$

The two tensor fields are related by

$$\sigma = J^{-1} T F^T, \tag{2.27}$$

where J and F are given by (2.19) and (2.1a).

Consider a membrane occupying the region Ω in the undeformed state. The membrane is in equilibrium under the pressure pn per unit of deformed area, the body forces are

neglected. The unit vector $\boldsymbol{n}$ which is externally normal to the deformed surface at $\boldsymbol{r}$ can be expressed as

$$\boldsymbol{n} = \boldsymbol{l} \times \boldsymbol{m}, \tag{2.28}$$

since $\boldsymbol{l}$ and $\boldsymbol{m}$ are the two principal vectors which are tangential to the deformed surface. The force transmitted across an element of the arc that has length ds is tds, where $t = \boldsymbol{T}\boldsymbol{v}$ is the traction vector and $\boldsymbol{v}$ is the unit vector normal to the arc in the undeformed state.

For the case of pressure loading, and neglecting the body force (Fig. 2.1), the equilibrium of an arbitrary part $D \subset \Omega$ of the membrane, requires that

$$\oint_{\partial D} \boldsymbol{T}\boldsymbol{v}ds + \iint_{D} p\boldsymbol{J}\boldsymbol{n}dA = \boldsymbol{0}. \tag{2.29}$$

By using the divergence theorem, the contour integral in (2.29) may be transformed to an area integral:

$$\oint_{\partial D} \boldsymbol{T}\boldsymbol{v}ds = \iint_{D} D\mathrm{iv}\boldsymbol{T}dA \tag{2.30}$$

where the Divergence of $\boldsymbol{T}$ is given by $D\mathrm{iv}\boldsymbol{T} = T_{i\alpha,\alpha}\boldsymbol{e}_i$. Substituting (2.30) into (2.29) yields the global form of the equilibrium equation of region D

$$\iint_{D} \mathrm{Div}\boldsymbol{T}\,\mathrm{d}\boldsymbol{A} + \iint_{D} p\boldsymbol{J}\boldsymbol{n}dA = \boldsymbol{0}. \tag{2.31}$$

By using the localization theorem, the local (pointwise) equilibrium equation may be obtained from (2.31):

$$\mathrm{Div}\boldsymbol{T} + p\boldsymbol{J}\boldsymbol{n} = \boldsymbol{0} \tag{2.32}$$

In component form, (2.32) can be rewritten as:

$$T_{i\alpha,\alpha} + pJn_i = 0. \tag{2.33}$$

In case of zero pressure and in the absence of point loads, the local equilibrium equations become

$$Div\boldsymbol{T} = \boldsymbol{0}, \qquad T_{i\alpha,\alpha} = 0. \tag{2.34}$$

In order for the equilibrium equations to deliver stable solutions, there are certain necessary conditions to be satisfied by the strain energy density $W(\boldsymbol{F})$. The energy criterion of elastic stability (Knops, Wilkens, 1973) states that an equilibrium configuration $\boldsymbol{r}(\boldsymbol{x})$ is stable if it minimizes the potential energy of deformation: $E(\boldsymbol{r}) \le E(\boldsymbol{r}+\Delta\boldsymbol{r})$, for all small perturbations $\Delta\boldsymbol{r}(\boldsymbol{x})$. Further, according to Graves theorem (Graves, 1939), a deformation $\boldsymbol{r}(\boldsymbol{x})$ minimizes the energy $E(\boldsymbol{r})$ only if its gradient $\boldsymbol{F}(\boldsymbol{x})$ is a point of rank one convexity of the strain energy $W(\boldsymbol{F})$ at every point $x \in \Omega$. This statement leads to necessary conditions of stability requiring the principal stresses be non-negative (Steigmann, 1991): $w_{\lambda} \ge 0$, $w_{\mu} \ge 0$, $\forall x \in \Omega$.

The global equation of motion of an arbitrary part D of Ω, in the presence of pressure loading may be written as

$$\oint_{\partial D} \boldsymbol{T}\boldsymbol{v}ds + \iint_{D} p\boldsymbol{J}\boldsymbol{n}dA = \iint_{D} \varrho_0 \ddot{\boldsymbol{r}}dA, \tag{2.35}$$

where ϱ_0 is the mass density per unit initial area, and $\ddot{\boldsymbol{r}}$ is the acceleration.

Two types of conservative pressure loading have been considered in this work: uniform pressure (p = constant) and pressure loading of the hydrostatic type, having the magnitude $p = \left|\varrho_l g(h_{ll} - r_3)\right|$, where ϱ_l is the density of liquid, g is the gravitational acceleration and h_{ll} is the height of liquid measured along the $\boldsymbol{e}_3$ direction.

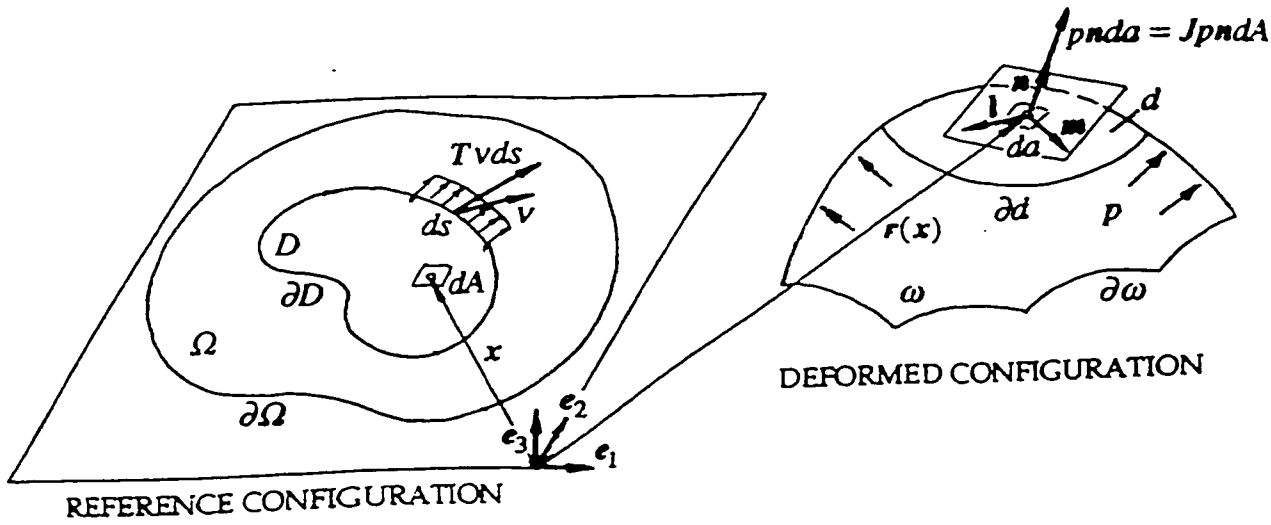

Fig. 2.1 Equilibrium of the region $D \subset \Omega$ of the membrane

2.4 Relaxed Strain Energy Density

In membrane theory, the bending stiffness is neglected, but real membranes often exhibit wrinkled regions, in which the size and configuration of the wrinkles is determined by the bending stiffness. Membrane theory delivers solutions with compressive stresses in the wrinkled regions. This happens because ordinary strain energies do not satisfy the rank one convexity condition. Since states with compressive stresses are unstable, such solutions are not physically meaningful. Instead of using plate theory in the wrinkled regions, tension field theory can be used (Wagner, 1929), which is much simpler from the point of view of analysis. However, when a membrane is partially wrinkled, it is not simple to decide which theory to use in a given part of the membrane. Pipkin (1986) introduced the concept of a relaxed strain energy density. If the relaxed strain energy density is used, tension field theory is automatically incorporated into ordinary membrane theory. The relaxed strain energy satisfies the rank one convexity condition, thus the stress-strain relation obtained from a relaxed strain energy function gives stresses that are never compressive. Such deformations satisfy the necessary conditions for stability. A wrinkled region is simply defined as a region in which the stress is uniaxial at each point in the membrane. In the wrinkled regions, the relaxed strain energy destiny represents the average energy per unit initial area over a region containing numerous wrinkles.

Consider a unit square membrane in simple tension. In the deformed configuration, the sides of the square become λ and μ. Assume λ as the larger ($\lambda > 1$) and μ as the smaller ($\mu < 1$) principal stretches. Since the square is in simple tension the principal

stress w_λ is strictly positive ($w_\lambda > 0$) and w_μ is equal to zero ($w_\mu = 0$). The corresponding smaller principal stretch μ is a function of λ and was named by Pipkin (1986) the natural width in simple tension $\nu(\lambda)$. For isotropic incompressible material in 3D, $\lambda_1\lambda_2\lambda_3 = 1$. For the case of simple tension $\lambda_1 = \lambda$, $\lambda_2 = \lambda_3 = \mu$, leading to $\lambda\mu^2 = 1$. Thus for the unit square membrane in simple tension $\mu = \lambda^{-1/2}$. But μ is the natural width $\nu(\lambda)$, thus $\nu(\lambda) = \lambda^{-1/2}$ for incompressible materials.

Wrinkling occurs if the smaller principal stretch $\mu < \nu(\lambda)$ for $\lambda > 1$. In this instance, ordinary strain energy functions deliver compressive stresses. For the case of the unit square, in order for μ to be smaller than $\nu(\lambda)$, a compressive stress $w_\mu < 0$ would be required, violating the stability conditions.

The relaxed strain energy density is defined to be equal to the value of the original strain energy at the natural width:

$$w_R(\lambda,\mu) = w[\lambda,\nu(\lambda)] = \hat{w}(\lambda). \tag{2.36}$$

The relaxed strain energy can be obtained from the original strain energy by constructing a sequence of finely wrinkled configurations, with closely spaced discontinuities in the deformation gradient. The limit of the sequence is a smooth deformation that is achieved without compressive stress and at no expense in the strain energy (Pipkin, 1986).

Therefore, in the wrinkled region, where $\mu < \nu(\lambda)$, the relaxed strain energy delivers $w_\lambda > 0$ and $w_\mu = 0$, satisfying the requirement that the principal stresses be non-negative, whereas the original strain energy delivers $w_\lambda > 0$ and $w_\mu < 0$, violating the necessary conditions for stability.

Similarly, for $\mu > 1$ and $\lambda < 1$, let $\nu(\mu)$ be the natural width in simple tension, and the relaxed strain energy becomes a function of μ only.

When the membrane is deformed with $\lambda < 1$ and $\mu < 1$, double wrinklings might be achieved such that no stress at all is present, and the relaxed strain energy density is taken to be zero.

$$w_R(\lambda, \mu) = 0. \tag{2.37}$$

So the relaxed strain energy is defined by

$$W_R(\boldsymbol{F}) = w_R(\lambda, \mu) \equiv \begin{cases} w(\lambda, \mu); & \lambda > \nu(\mu), \quad \mu > \nu(\lambda), \\ w(\lambda); & \lambda > 1, \quad \mu \le \nu(\lambda), \\ w(\mu); & \mu > 1, \quad \lambda \le \nu(\mu), \\ 0; & \lambda \le 1, \quad \mu \le 1. \end{cases} \tag{2.38}$$

The principal stresses furnished by the relaxed strain energy automatically satisfy the necessary conditions for all $(\lambda, \mu) \ge 0$. For example for the case of deformation with $\lambda > 1$ and $\mu \le \nu(\lambda)$, the principal stresses are $w_\mu = 0$ and $w_\lambda = \partial \hat{w}(\lambda) / \partial \lambda$, where w_λ is a function of λ alone. The associated state of stress is given by:

$$\boldsymbol{T} = w_\lambda \boldsymbol{l} \otimes \boldsymbol{L}, \tag{2.39}$$

and is called a tension field. The unit vectors $\boldsymbol{L}$ and $\boldsymbol{l}$ are tangential to the tension trajectories (wrinkles) in the reference configuration, respectively in the deformed one.

Thus by using the relaxed strain energy in the equilibrium equations, tension field theory is automatically included into ordinary membrane theory, extending its range of applicability to the case of wrinkled membranes.

A solution within this theory only gives the average deformation in a wrinkled region. To predict the details of the distribution, spacing and amplitude of the wrinkles, a theory

that accounts for the strain energy due to bending must be employed (Hilgers and Pipkin, 1992).

Chapter 3

Numerical Method

3.1 Introduction

The nonlinear static analysis and form-finding of tension structures is usually carried out by employing standard stiffness-based iterative methods, such as Newton-Raphson (Haug and Powell, 1971, and many others). However, in the presence of wrinkling, the element stiffness matrix becomes ill-conditioned and the iterations may not converge. Modifications of these methods to account for the sudden stiffness changes that occur at the transition from tense to wrinkled states have been developed by Miller and Hedgepeth (1982), and other researchers. But these modifications involve complex iterative algorithms.

The numerical model developed in this work is based on the Dynamic Relaxation Method (DR). This is an explicit iterative technique developed to solve structural mechanics problems. This technique does not require the construction and inversion of the stiffness matrix, which in presence of wrinkling is ill-conditioned, and is therefore particularly well suited for the class of problems considered here. Wrinkling is accounted for by employing a relaxed strain energy density. The approximation of the internal

forces is obtained by applying Green's theorem differencing method. Besides its simplicity, this method has the advantage to be applicable to problems involving any shape of the boundary.

The DR method has been already used for form-finding of membrane structures (Barnes, 1974), however without considering the possibility of wrinkling.

3.2 Dynamic Relaxation

3.2.1 Introduction

Dynamic relaxation (DR) is an explicit iterative method used to solve static problems in structural mechanics. The static problem is transformed into an equivalent dynamic problem by adding inertia and damping terms, and by allowing the structure to vibrate under critical damping. The displacements in the static structure may be obtained when the vibration dies out. Thus, this numerical technique is based on the fact that the static solution can be considered as the steady state part of the transient response of the structure.

The DR method originates from the 2^{nd} order Richardson method developed by Frankel (1950). The Richardson Method is an explicit iterative technique, which is using

$$\begin{aligned} \phi^{n+1} &= \phi^n + \alpha L\phi^n, \quad \text{(interior points)} \\ \phi^{n+1} &= \phi^n, \quad \text{(boundary points)} \end{aligned} \tag{3.1}$$

to solve PDEs of the form

$$L\phi = 0, \tag{3.2}$$

where L is a linear difference operator. Frankel (1950) introduces a modified operation method by transforming (3.2) into

$$\frac{\partial^2 \phi}{\partial t^2} + A\frac{\partial \phi}{\partial t} - L\phi = 0. \tag{3.3}$$

He uses an iteration process based on

$$\begin{aligned} \phi^{n+1} &= \phi^n + \alpha L\phi^n + \beta(\phi^n - \phi^{n-1}), \qquad \text{(interior points)} \\ \phi^{n+1} &= \phi^n \qquad\qquad\qquad\quad \text{(boundary points).} \end{aligned} \tag{3.4}$$

Frankel first makes the connection with dynamics, so the second-order Richardson method is also known as Frankel's method.

The DR technique was first applied by Day and Otter (1965) in connection with reactor pressure vessel computations. Day (1965) named the method ***Dynamic Relaxation***. Day and Otter's papers in the mid-60's represent the beginning of the engineer's interest in DR and introduce the idea of obtaining a static solution from a dynamic transient analysis method. After Day and Otter, important improvements of the DR method have been made. Welsh (1967) introduced the fictitious mass densities into the DR method. The use of the fictitious mass densities accelerates the convergence of the DR method, since the oscillations are not of interest in the final solutions to the equilibrium equations. Cundall (1976) suggested an effective damping procedure, termed "kinetic damping", which has been frequently applied in the context of form-finding and static analysis of cable networks and membranes. Underwood (1983) presented an adaptive DR method for nonlinear structural analysis, Zhang and Yu (1989) first introduced a modified adaptive dynamic relaxation (maDR) method, based on the

adaptive DR method of Underwood, and applied the maDR method to the bending and wrinkling of circular plates problems as well. Zhang, Kadkhodayan and Mai (1994) made an improvement of the maDR method. The improved method (DXDR) is developed from the modified adaptive dynamic relaxation, which is more efficient than the maDR method. Other improvements of DR such as the automatic evaluation of the DR iteration parameters were made by Papadrakakis (1981). Zienkiewicz and Löhner (1985), also Tarakanov (1984), accelerated the convergence of DR method. Silling (1985), introduced a versatile spatial discretization method based on Green's theorem in the context of a DR analysis in finite elastostatics. In addition to introducing the adaptive DR method, Underwood did more important work regarding the DR method: in 1983 he published a detailed review of the DR method.

The DR technique was first used to solve linear structural problems, but it is especially attractive for the problems with highly nonlinear geometric and material behavior, which include limit points or regions of very soft stiffness characteristics. This is due to the following features of the DR method: (1) the explicit form of DR makes this method easily to be programmed, (2) since all quantities may be treated as vectors, matrix manipulation is avoided and low computer storage is required. The low storage requirement makes it possible to solve complicated problems using a personal computer.

Rushton made the first application of DR to a nonlinear problem in connection with the large deflection of variable-thickness plates in 1968. Since 1970 researchers have done a large number of studies on nonlinear structural analysis, especially on large deflection of plates and shells (Salehi and Shahidi, 1994, Kommineni and Kant, 1995). This DR technique has also been successfully used to form-finding and nonlinear static

analysis of lightweight tensile structures, such as cable networks and membranes (Haseganu and Seigmann, 1994a,b, Liu and Haseganu, 1997, 1998), tensegrity systems analysis (Motro, 1984, Motro, Najari and Jouanna, 1986), incompressibility in large deformations (Silling, 1987), phase changes and localization in elasticity (Silling, 1988a,b, 1989), elasto-plastic response (Zhang, Yu, Wang, 1989), nonlinear viscoelastic response (French and Jensen, 1991), and materially nonlinear problems in geomechanics (Siddiquee, Tanaka and Tatsuoka, 1995).

The following description of the dynamic relaxation method draws mainly from Underwood's work.

3.2.2 Structural Analysis

The equilibrium equation of a structure may be discretized by using finite difference or finite element discretization techniques. The discretized equilibrium equation of a structure can be written in the general form:

$$\boldsymbol{P}(\boldsymbol{u}) = \tilde{\boldsymbol{F}}, \tag{3.5}$$

where $\boldsymbol{P}$ is the vector of internal forces, $\boldsymbol{u}$ is the solution vector (the displacement vector), $\tilde{\boldsymbol{F}}$ is the vector of the external forces (point loads, body forces, forces due to distributed loads and forces prescribed on the boundaries).

In general $\boldsymbol{P}$ is obtained from variational principles:

$$\boldsymbol{P}(\boldsymbol{u}) = \frac{\partial E(\boldsymbol{u})}{\partial \boldsymbol{u}}, \tag{3.6}$$

where E is the internal energy. Equation (3.6) is suitable for both linear and nonlinear problems to obtain the internal forces. For the linear problem, $\boldsymbol{P}$ may be written in the general form:

$$\boldsymbol{P}(\boldsymbol{u}) = \boldsymbol{K}\boldsymbol{u}, \tag{3.7}$$

where $\boldsymbol{K}$ is the stiffness matrix. For the nonlinear problem, $\boldsymbol{P}$ is commonly in the incremental form:

$$\Delta\boldsymbol{P}(\boldsymbol{u}) = {}^{t}\boldsymbol{K}(\boldsymbol{u})\Delta\boldsymbol{u}, \tag{3.8}$$

where ${}^{t}\boldsymbol{K}(\boldsymbol{u})$ is the tangential stiffness matrix. This may be obtained from:

$${}^{t}\boldsymbol{K}(\boldsymbol{u}) = \frac{\partial \boldsymbol{P}(\boldsymbol{u})}{\partial \boldsymbol{u}}. \tag{3.9}$$

Equation (3.5) may be solved by various methods such as Gauss-elimination, Newton-Raphson, or matrix methods. When the element stiffness obtained from equation (3.9) becomes ill-conditioned, which happens for example when wrinkling is present in the equilibrium configurations of the membranes, the standard stiffness-based iterative methods such as Newton-Raphson may not converge, and solutions can not be obtained by using these methods. Solutions cannot be obtained from matrix methods either, since the element stiffness matrix is singular. This problem can be avoided by using the DR method.

3.2.3 Transient Response

In the DR method, the equilibrium equations are transformed into equivalent equations of motion by adding acceleration and damping terms to the equilibrium equations. The transient response described by the equation of motion is in the from:

$$M\ddot{u}^n + C\dot{u}^n + P(u^n) = \tilde{F}^n, \tag{3.10}$$

where M is the mass matrix, C is the damping matrix, n indicates the n^{th} time increment, and a superimposed dot indicates a temporal derivative ($\ddot{u}$ is the acceleration vector, $\dot{u}$ is the velocity vector).

The DR algorithm (2nd order Richardson) developed by Frankel (1950) is obtained by using the following central difference expression for the temporal derivatives:

$$\dot{u}^{n-1/2} = (u^n - u^{n-1}) / h, \tag{3.11}$$

$$\ddot{u}^n = (\dot{u}^{n+1/2} - \dot{u}^{n-1/2}) / h, \tag{3.12}$$

where h is a fixed time increment. The expression for $\dot{u}^n$ is obtained by the average value:

$$\dot{u}^n = \frac{1}{2}(\dot{u}^{n-1/2} + \dot{u}^{n+1/2}). \tag{3.13}$$

Substituting (3.11)-(3.13) into equation (3.10), the pair of equations used to advance to the next velocity and displacement are given by:

$$\dot{u}^{n+1/2} = \frac{(M/h - \frac{1}{2}C)}{(M/h + \frac{1}{2}C)}\dot{u}^{n-1/2} + \frac{(\tilde{F}^n - P^n)}{(M/h + \frac{1}{2}C)},$$

$$u^{n+1} = u^n + h\dot{u}^{n+1/2}, \tag{3.14}$$

where $P^n = P(u^n)$.

Since the oscillation is not of interest, the mass matrix and the damping matrix need not to represent the physical structure. However P and $\tilde{F}$ must represent the physical problem. A diagonal mass matrix and mass proportional damping is chosen. So

$$\boldsymbol{C} = c\boldsymbol{M}, \tag{3.15}$$

where c is the damping coefficient. Substituting (3.15) into (3.14), equation (3.14) becomes:

$$\dot{\boldsymbol{u}}^{n+1/2} = \frac{(2-ch)}{(2+ch)}\dot{\boldsymbol{u}}^{n-1/2} + \frac{2h}{(2+ch)}\boldsymbol{M}^{-1}(\tilde{\boldsymbol{F}}^{n} - \boldsymbol{P}^{n}),$$

$$\boldsymbol{u}^{n+1} = \boldsymbol{u}^{n} + h\dot{\boldsymbol{u}}^{n+1/2}, \tag{3.16}$$

where $\boldsymbol{M}^{-1}$ indicates the inverse of $\boldsymbol{M}$. Since (3.16) is algebraic, each solution vector component may be computed individually from:

$$\dot{u}_i^{n+1/2} = \frac{(2-ch)}{(2+ch)}\dot{u}_i^{n-1/2} + \frac{2h}{m_{ii}(2+ch)}(\tilde{F}_i^{n} - P_i^{n}),$$

$$u_i^{n+1} = u_i^{n} + h\dot{u}_i^{n+1/2}, \tag{3.17}$$

where the subscript i is the i^{th} vector component and m_{ii} is the i^{th} diagonal element of $\boldsymbol{M}$. Since $\boldsymbol{M}$ is diagonal, equations (3.17) are decoupled. This algorithm doesn't involve matrix manipulation, it is in explicit form, it is easily to program, it requires low storage, and it may be used to solve problems which have ill-conditioned element stiffness matrices.

For starting the DR algorithm, the initial conditions are of the form:

$$\boldsymbol{u}^{0} \neq \boldsymbol{0}; \qquad \dot{\boldsymbol{u}}^{0} = \boldsymbol{0}. \tag{3.18}$$

Equation (3.13) and the second of (3.18), give

$$\dot{\boldsymbol{u}}^{-1/2} = \dot{\boldsymbol{u}}^{1/2}. \tag{3.19}$$

Substituting (3.19) into the first expression of (3.16), considering $n = 0$ as well, the velocity at the time step 1/2 can be obtained:

$$\dot{u}^{1/2} = hM^{-1}(\tilde{F}^0 - P^0)/2. \tag{3.20}$$

It can be noted that the damping coefficient c dose not enter the starting procedure. So the central difference time integrator for diagonal mass and mass proportional damping has the form:

$$\begin{aligned}
&\dot{u}^{1/2} = hM^{-1}(\tilde{F}^0 - P^0)/2 && \text{for } n = 0, \\
&\dot{u}^{n+1/2} = \frac{(2-ch)}{(2+ch)}\dot{u}^{n-1/2} + \frac{2h}{(2+ch)}M^{-1}(\tilde{F}^n - P^n) && \text{for } n \neq 0, \\
&u^{n+1} = u^n + h\dot{u}^{n+1/2} && \text{for all } n.
\end{aligned} \tag{3.21}$$

To obtain a static solution from the transient response equation, the mass matrix M, the damping coefficient c, and the time increment h have to be determined. These parameters are chosen for the purpose of obtaining the fastest convergence.

Once a displacement vector u which is a solution vector of (3.5) is obtained, the oscillations die out and the structure reaches the equilibrium configuration. This displacement vector is the final solution of the equilibrium equation of the static structural problem.

3.2.4 DR Algorithm for Linear Problems and Properties

Formally, the DR algorithm may be written as suggested by Underwood (1983):

(a) choose c, h and M; u^0 is given; $\dot{u}^0 = 0$,

(b) $R^n = \tilde{F}^n - P(u^n)$,

(c) if $R^n \approx 0$ stop, otherwise continue,

(d) for $n=0$, $\dot{u}^{1/2} = hM^{-1}R^0 / 2$,

$$\text{for } n \neq 0, \qquad \dot{u}^{n+1/2} = \frac{(2-ch)}{(2+ch)}\dot{u}^{n-1/2} + \frac{2h}{(2+ch)}M^{-1}R^n, \tag{3.22}$$

(e) $u^{n+1} = u^n + h\dot{u}^{n+1/2}$,

(f) $n = n+1$; return to (b).

It can be observed that step (d) and the step (e) are identical to the central difference time integrator. The only difference is that the parameters M and c in the DR method need not to represent the physical structure, M and c are fictitious values. The mass matrix M and the damping coefficient c are chosen to obtain the static solution $R = 0$ in a minimum number of steps. Also, the choice of h must ensure stability and accuracy of the iterations.

Since the DR algorithm seems quite simple, it has been used for various analyses of structural mechanics problems. The optimum convergence rate of the solution is of interest. For the linear problem, the presentation of Underwood (1983) gives the residual R:

$$R = \tilde{F} - Ku, \tag{3.23}$$

where $P(u) = Ku$. Substituting (3.23) into (3.22d), and using (3.22e) and the expression of (3.11), the equation (3.22d) can be rewritten in the form:

$$u^{n+1} = u^n + \beta(u^n - u^{n-1}) - \alpha Au^n + \alpha b^n,$$
$$\alpha = 2h^2 / (2+ch), \quad \beta = (2-ch) / (2+ch), \tag{3.24}$$

where $\boldsymbol{A} = \boldsymbol{M}^{-1}\boldsymbol{K}$, $\boldsymbol{b} = \boldsymbol{M}^{-1}\tilde{\boldsymbol{F}}$. The general equation for $n \neq 0$ is considered here. In order to obtain the convergence, the error in the iteration at the n^{th} step must be smaller than the error at the last step. The error in the iteration at the n^{th} step is defined as:

$$e^n = u^n - \tilde{u}, \tag{3.25}$$

where $\tilde{u}$ is the solution vector for $\boldsymbol{R} = \boldsymbol{0}$. Substituting (3.25) into (3.24) gives the error equation:

$$e^{n+1} = e^n - \alpha A e^n + \beta(e^n - e^{n-1}). \tag{3.26}$$

Equation (3.26) shows the relationship between successive error vectors. A solution of (3.26) may be obtained by assuming

$$e^{n+1} = ke^n, \tag{3.27}$$

where $|k| = \varrho$ is the spectral radius (Strang, 1976). The fastest convergence is obtained for the smallest possible $|k| < 1$. Substituting (3.27) into (3.26) gives a quadratic equation in k:

$$k^2 - (1 + \beta - \alpha A)k + \beta = 0, \tag{3.28}$$

where A denotes any eigenvalue of $\boldsymbol{A}$. The minimum value of k, which produces uniform convergence over the entire range of eigenvalues $A_0 \leq A \leq A_m$, is desirable for fast convergence. The optimum convergence condition, $\tilde{k}$, is obtained when the roots of (3.28) are real and equal. This condition is achieved by the expression (Paradrakakis, 1981, Underwood, 1983):

$$(1 + \beta - \alpha A) = \pm 2\beta^{1/2}, \tag{3.29}$$

which gives

$$|\tilde{k}| = \tilde{\varrho} = \beta^{1/2}. \tag{3.30}$$

Since (3.29) holds for all possible eigenvalues of $\boldsymbol{A}$, the two equations that satisfy the optimum convergence condition for $\tilde{\varrho}$ are:

$$1+\beta-\alpha A_0 = 2\beta^{1/2}, \tag{3.31}$$

and

$$1+\beta-\alpha A_m = -2\beta^{1/2}. \tag{3.32}$$

Adding (3.31) and (3.32) leads to

$$\alpha(A_0 + A_m) = 2(1+\beta). \tag{3.33}$$

Equation (3.31) can be rewritten as:

$$\alpha A_0 = (\beta^{1/2} - 1)^2. \tag{3.34}$$

Equation (3.33) and (3.34) give

$$\tilde{\varrho} = \beta^{1/2} \approx \left|1 - 2\sqrt{\frac{A_0}{A_m}}\right|, \tag{3.35}$$

where $A_0 << A_m$ has been assumed.

The value of h and c may be chosen to satisfy the condition of optimum convergence (3.29). Equations (3.15) and (3.34), the definitions of α and β and the assumption of $A_0 << A_m$, give

$$h \le 2/\sqrt{A_m} = 2/\omega_{max}, \tag{3.36}$$

and

$$c \approx 2\sqrt{A_0} = 2\omega_0, \tag{3.37}$$

where ω_0 and ω_{max} are the lowest and highest circular frequencies of the undamped equation (3.10). Equation (3.35) can be written in terms of ω_0 and ω_{max} as

$$\tilde{\varrho} = \left| 1 - 2\left(\frac{\omega_0}{\omega_{max}}\right) \right| . \tag{3.38}$$

To produce more rapid convergence, the minimum $\tilde{\varrho}$ is expected. This can be realized by scaling A to maximize the ratio A_0 / A_m or maximizing the ratio ω_0 / ω_m through a judicious choice for M. They are the same.

Equation (3.36) obtained for the optimum convergence condition expresses the stability limit for the central difference time integrator (Leech, 1965). The relationship of the stability limit to the transit time for information between two adjacent nodes in the discrete elements (Courant, Friderichs and Lewy, 1928) has been exploited to develop the idea of a "fictitious mass" (Welsh, 1967), which minimizes $\tilde{\varrho}$ while retaining stability. The expression of critical damping of the lowest natural frequency (3.37) is obtained by considering the optimum convergence condition as well. The critical damping property has been used in the choice of c (Rushton, 1968).

3.2.5 Choice of Iteration Parameters

Choice of M and h

Since the beginning of the application of the DR technique, many methods have been used to determine the iteration parameters. The real mass was used before Welsh (1967) introduced the fictitious mass densities. Day (1965) used the real mass and adjusted the time increment h by trial and error, until a suitable value which satisfies the stability

conditions was found. Otter (1965) also used the real mass, but calculated the time increment h from the Courant-Friedrichs-Lewy condition (1928). Using the real mass is simple and straight forward, but it is not an efficient method, unless the damping coefficient c satisfies the optimum convergence condition.

A general method based on the Courant-Friedrichs-Lewy condition, introduces a fictitious diagonal mass matrix, whose diagonal elements m_{ii} are chosen such that the transit times for information transfer for degree of freedom i to adjacent and like degrees of freedoms is a constant. Welsh (1967) first proposed this approach. This method is suitable for both linear and nonlinear problems, and both finite element or finite difference discretization technique may be used (Silling, 1988a). For convenience this constant is typically chosen, such that $h = 1$. It has been found that evaluating m for $h = 1.1$ and iterating with $h = 1$ provides a sufficient margin to ensure stability (Underwood, 1983).

Another commonly used method is based on Gerschgorin's theorem. This theorem states (Strang, 1976):

Every eigenvalue of A *lies in at least one of the circles* $C_1,\ldots,C_n$ *where* C_i *has its center at the diagonal entry* a_{ii} *and its radius* $r_i = \sum_{j \neq 1} |a_{ij}|$ *equal to the absolute sum along the rest of the row.*

Gerschgorin's theorem shows that all circles will be coincident for equal mesh spacing, and they will be nearly coincident for unequal mesh spacing, if every row is scaled such that the absolute sum along every row is identical (Underwood, 1983). As well it shows that the largest eigenvalue is less than or equal to the sum of the moduli of the elements

along any row. Using (3.36) and Gerschgorin's theorem give the following general expression for m_{ii}:

$$m_{ii} \geq \frac{1}{4} h^2 \sum_j \left| K_{ij} \right|, \tag{3.39}$$

where K_{ij} are the elements of the stiffness matrix $\boldsymbol{K}$, $j = 1,.....,N$, $i = 1,.....,N$. Here N is the total number of DOF of the structure.

Papadrakakis (1981) proposed an approach by assuming $m_{ii} \sim k_{ii}$. An automatic procedure is presented for the evaluation of the iteration parameters, and trial runs or eigenvalue analysis of the modified stiffness matrix are avoided. This method may be applied to geometrically and material nonlinear problems. However, this approach is not suitable for partially wrinkled membrane structures, since the regions of very soft stiffness may lead to a singular stiffness matrix and to a singular mass matrix as well (Hasegnu and Steigmann, 1994).

Choice of c

There are several approaches for determining the damping coefficient c as well. The choice of c should be near the critical value for optimum convergence of the solution.

Day (1965) used a trial and error procedure to find the suitable value of c. Most the researchers (Rushton, 1968, Cassel, 1970) determine c from a numerical experiment when using DR method. This experiment consists of forming the fictitious mass matrix by using one of the previous methods and then computing the response for a number of

iterations with $c = 0$. The number of iterations must be sufficient to observe the lowest frequency ω_0. The damping coefficient c is determined from (3.37), after obtaining the lowest frequency ω_0. Rushton (1968) and other researchers determined a distinct damping coefficient for each intrinsic coordinate. Bunce (1972) introduced an approach based on Rayleigh's quotient, to evaluate the lowest natural frequency. Alwar (1975) proposed an approach in which a small value is chosen for c so that the solution will oscillate about the true solution, but the oscillations will be decaying. The time solution is estimated from the envelope of the decaying oscillations. Papadrakakis (1981) proposed the following approach. He calculated a series of approximations to the dominant eigenvalue from $\lambda_{DR} = \left\| u^{k+1} - u^{k} \right\| / \left\| u^{k} - u^{k-1} \right\|$. When λ_{DR} has converged to almost a constant value, then this gives the minimum eigenvalue. This minimum eigenvalue may be used to evaluate c. Underwood (1983) developed a similar approach based on the Rayleigh's quotient. Details of this approach are presented in the introduction of the adaptive DR method (Underwood, 1983) in the next section. Zhang and Yu (1989) introduced an approach for the choice of c based on of Underwood's method. Details regarding this approach are given in the next section.

3.2.6 DR Algorithms for Nonlinear Problems

An adaptive DR method

An adaptive DR method for the solution of nonlinear problems was proposed by Underwood in 1983. The difference from the linear DR algorithm is that Underwood used

an updated fictitious mass matrix, since the initial fictitious mass matrix may not satisfy the conditions for stability throughout the analysis, due to increases in the stiffness for the nonlinear problem. Underwood evaluated $h \approx 1.1$ and performed the iterations with $h = 1.0$, since this provided a safety margin for stability. Then he used ${}^{t}\boldsymbol{K}_{ij}$ for the nonlinear problem, which represents the tangential stiffness, and obtained the fictitious mass from (3.39). ${}^{t}\boldsymbol{K}_{ij}$ was determined from (3.9).

To determine the damping coefficient c, Underwood developed an approach based on the Rayleigh's quotient. The damping coefficient is computed from (3.37) at each iteration from Rayleigh's quotient as

$$c_n = 2\sqrt{\frac{(\boldsymbol{u}^n)^T\, {}^{t}\boldsymbol{K}^n \boldsymbol{u}^n}{(\boldsymbol{u}^n)^T \boldsymbol{M} \boldsymbol{u}^n}}, \tag{3.40}$$

where the superscript T indicates the transpose, ${}^{t}\mathbf{K}^n$ is a diagonal local stiffness matrix, and it is given by

$${}^{t}K_{ii}^{n} = \left[-P_i(u^{n-1}) + P_i(u^n) \right] / h\dot{u}_i^{n-1/2}. \tag{3.41}$$

Equation (3.40) gives an estimate of the critical damping for the current deformation mode $\boldsymbol{u}^n$, based on an estimate of the local tangent stiffness. This approach gives the critical damping based on the final solution, avoids the overshoot of the solution vector and requires no unproductive iterations (Underwood, 1983). The adaptive DR algorithm may be generally written as (Underwood, 1983):

(a) $\boldsymbol{u}^0$ is given; $\dot{\boldsymbol{u}}^0 = 0$; $n = 0$,

(b) compute $\boldsymbol{M}$ form (3.39) with $h = \tilde{h}$, where $\tilde{h} > h$

and ${}^{t}K_{ij}$ is determined from (3.9),

(c) $R^n = \tilde{F}^n - P(u^n)$,

(d) if $R^n \approx 0$ stop, otherwise continue,

(e) for $n=0$, $\dot{u}^{1/2} = hM^{-1}R^0/2$, (3.42)

for $n \neq 0$, $\dot{u}^{n+1/2} = \frac{(2-ch)}{(2+ch)}\dot{u}^{n-1/2} + \frac{2h}{(2+ch)}M^{-1}R^n$,

(f) $u^{n+1} = u^n + h\dot{u}^{n+1/2}$,

(g) evaluate error and reform M if necessary; repeat (c)-(f),

(h) $n = n+1$; return to (b).

(i) $c_n = 2\sqrt{\frac{(u^n)^T\,{}^{t}K^n u^n}{(u^n)^T M u^n}}$, where ${}^{t}K_{ii}^n = \left[-P_i(u^{n-1}) + P_i(u^n)\right]/h\dot{u}_i^{n-1/2}$,

(j) return to (c).

If in step (i) the value of c_n is not positive, c_n is set to zero. ${}^{t}K^n$ is an estimate and does not always satisfy the physics of the problem. This approach has been successfully used by Zhang and Yu (1989), Haseganu and Steigmann (1994).

A modified adaptive DR algorithm

A modified adaptive DR method is proposed by Zhang and Yu (1989), which is based on the adaptive DR method by Underwood (1983).

This maDR method is similar to the adaptive DR method. The difference is the choice of the damping coefficient of c_n and the initial displacement u^0. The damping

coefficient c_n is calculated by $c_n = 2\left[(\boldsymbol{u}^n)^T \boldsymbol{K}^n \boldsymbol{u}^n / (\boldsymbol{u}^n)^T \boldsymbol{M}^n \boldsymbol{u}^n\right]^{1/2}$, where $\boldsymbol{M}^n$ is calculated from (3.39). It eliminates the need to calculate the local stiffness matrix from (3.41). This approach of choice of c has been used by Haseganu and Steigmann (1994a,b) for the analysis of wrinkled membranes. The initial displacement $\boldsymbol{u}^0$ in the maDR method is determined from $u_i^0 = (u_i^* + u_i^{**})/2$, where u_i^* and u_i^{**} are the values of two neighboring but opposite peaks of the locus u_i detected with $c = 0$.

This method has been applied to the analysis of elastic-plastic bending and wrinkling of circular plates by Zhang and Yu (1989), and Zhang, Yu and Wang (1989) as well. Obviously, the computing time needed to obtain $\boldsymbol{u}^0$ is substantial, compared with the computing time needed to solve the original problem. The algorithm of the maDR method is omitted here.

Zhang, Kadkhodayan and Mai (1994) have improved the maDR method, which is called DXDR. They find that u_i^{**} isn't necessary. The initial displacement $\boldsymbol{u}^0$ is obtained form $\boldsymbol{u}^0 = (\tilde{\boldsymbol{u}}^0 + \boldsymbol{u}^*)/2$, which saves half of the computation time of the method before. The algorithm of this method is omitted here as well.

3.3 Spatial Discretization

3.3.1 Introduction

The spatial discretization needed in the DR method is obtained by using a finite element or finite difference technique.

In the beginning the finite difference method was employed for the spatial discretization needed in the DR method. Otter (1965) and others used central differences with interlacing meshes to approximate partial derivatives. Rushton (1968) used central differences without interlacing meshes to approximate partial derivatives. Interlacing meshes give better approximation for the shear stresses.

The finite element method was first used in DR by Lynch, Kelsey and Saxe (1968). Comparing with the finite difference method, the finite element method has a number of advantages (Otter and Cassell, 1966) such as: (a) each element or subregion could be of an arbitrary shape, it could follow the boundary as closely as possible, (b) an irregular subdivision to economize on the number of unknowns could be used. This technique has been used for solving plates and shells problems (Sauve and Badie, 1993), for form-finding and static analysis of light weight tensile structures (Lewis and Gosling, 1993), and other nonlinear structural analysis (Oakley, David, Knight, and Norman, Warner, 1995a,b,c).

The finite difference method, is still used by many researchers (Turvey and Osman, 1993, Haseganu and Steigmann, 1994, Kodkhodayan and Zhang, 1995), due to its simplicity. A spatial finite difference discretization technique is developed by Wilkins (1969). This technique is called Green's theorem differencing method since it is based on Green's theorem. Silling (1989) describes this theory in detail. This method is suitable for problems involving loss of ellipticity (Silling, 1987) and has also been successfully used for the analysis of wrinkled membranes (Haseganu and Steigmann, 1994a). This discretization technique is of interest in the analysis of wrinkled membranes. Finite difference approximations are applied directly to the field equations of continuum

mechanics in this method. Quadrilateral or non quadrilateral meshes; uniform or irregular meshes may be used. Besides being simple, this method is suitable to any shape of boundary, avoiding the inconvenience of mapping techniques. Silling (1985) describes the theory behind this method in details.

3.3.2 Green's Theorem Differencing Method

This spatial finite difference discretization technique is based on the Green's theorem. The Green's theorem states that

$$\iint_D \partial\phi_\alpha dA = e_{\alpha\beta} \oint_{\partial D} \phi dx_\beta \tag{3.43}$$

where ϕ is any piecewise differentiable field in the plane, $e_{\alpha\beta}$ is the two dimensional alternator symbol ($e_{12} = -e_{21} = 1$, $e_{11} = e_{22} = 0$), and ∂D is the closed piecewise smooth boundary of D.

The reference configuration Ω is assumed to be a plane configuration here, but this spatial finite difference discretization method may be adjusted to curved reference configuration as well. The plane region Ω is discretized into a Q×S meshes of nodes. Each node is labeled by a pairs of integers (k, l). The location of the node (k, l) is indicated by the position vector $x^{k,l}$. In Cartesian coordinates the components of the position vector may be written as $x_\alpha^{k,l}$, where $\alpha = 1,2$. The quadrilateral region between each set of four adjacent nodes is called a zone. Zones are labeled by half-integer indices (k+1/2, l+1/2). The zone (k+1/2, l+1/2) may be identified with the shaded area (Fig. 3.1). After deformation, the plane configuration Ω is changed to a 3 dimensional curved

configuration. The location of the node (k, l) in the deformed configuration at time step n is indicated by the time-dependent position vector $\boldsymbol{r}^{k,l,n}$. The time-dependent position vector $\boldsymbol{r}^{k,l,n}$ may be obtained from $\boldsymbol{r}^{k,l,n} = \boldsymbol{x}^{k,l,n} + \boldsymbol{u}^{k,l,n}$, where $\boldsymbol{u}^{k,l,n}$ is the nodal displacement vector at time step n. In Cartesian coordinates the components of the time-dependent position vector may be written in the form $r_i^{k,l,n} = x_i^{k,l,n} + u_i^{k,l,n}$, where $i = 1, 2, 3$.

The variables identified with nodes are called node-centered variables, others, identified with zones are called zone-centered variables. Node-centered variables include position $\boldsymbol{x}^{k,l}$ and $\boldsymbol{r}^{k,l,n}$, displacement $\boldsymbol{u}^{k,l,n}$, velocity $\dot{\boldsymbol{u}}^{k,l,n}$, acceleration $\ddot{\boldsymbol{u}}^{k,l,n}$, fictitious node mass $m^{k,l}$, internal forces $\boldsymbol{P}^{k,l,n}$ and external forces $\tilde{\boldsymbol{F}}^{k,l}$ which include body forces, points loads, and forces due to pressure acting on a surface. Zone-centered variables include the Piola stress tensor $\boldsymbol{T}^{k+1/2,l+1/2,n}$ and the deformation gradient tensor $\tilde{\boldsymbol{F}}^{k+1/2,l+1/2,n}$.

In the DR method, the solution of a static structural problem is obtained by assuming the structure is undergoing a damped vibration. The spatial discretized version of the damped equation of motion of a structure at the node (k, l) of the mesh may be written in components form as:

$$m_i^{k,l}\ddot{u}_i^{k,l,n} + c\dot{u}_i^{k,l,n} + P_i^{k,l,n} = \tilde{F}_i^{k,l,n}. \tag{3.44}$$

For a membrane (3.44) may be obtained by discretizing the global equilibrium equation (2.31) and then adding the acceleration and the viscous damping terms or by discretizing the global equation of motion (2.35) and then adding the viscous damping term.

For the membrane, the internal force is given by (2.31) as $\boldsymbol{P} = \iint_D T_{i\alpha}\, \mathrm{d}A$.

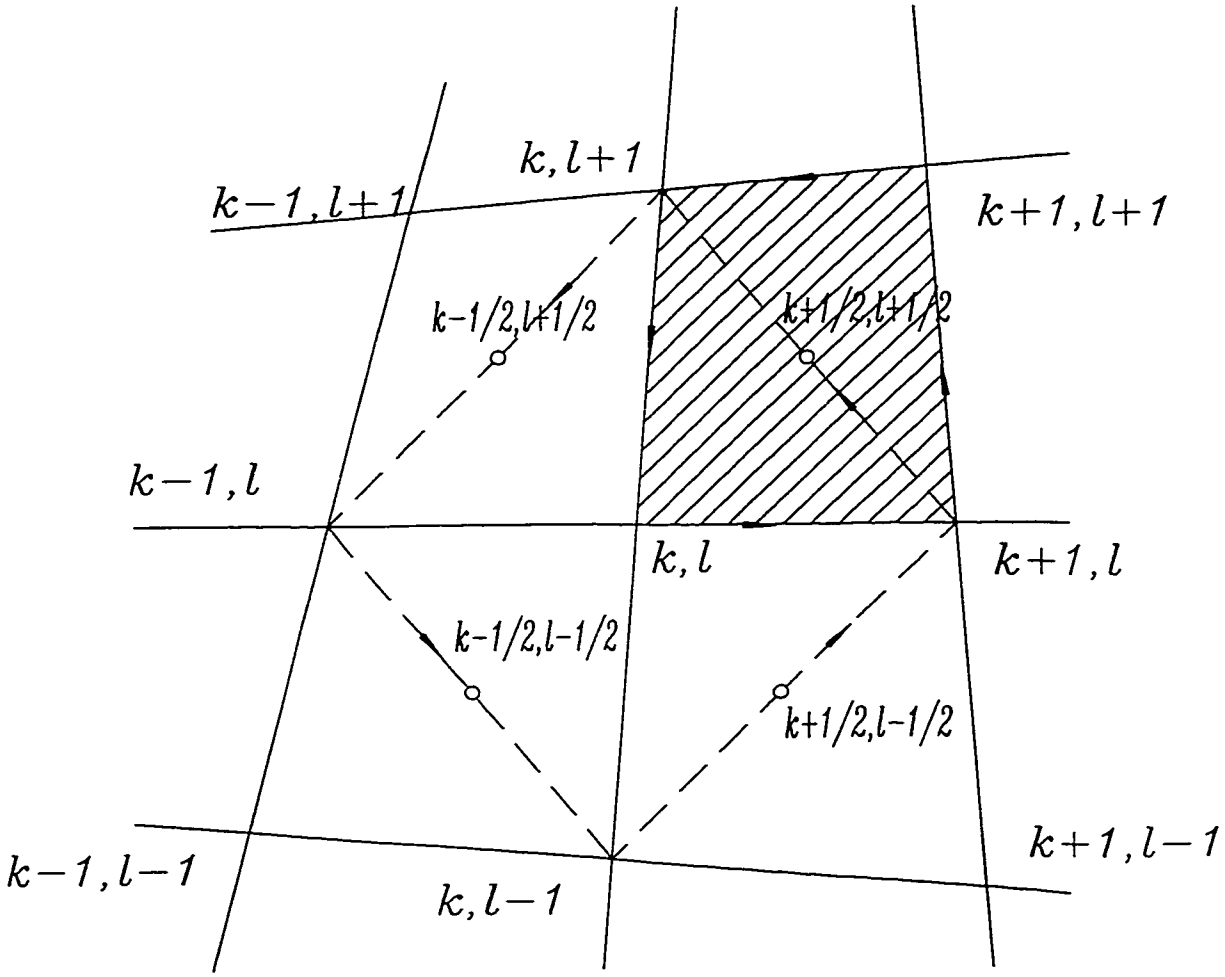

Fig. 3.1 Mesh for spatial discretization, with integration paths used in Green's theorem differencing method

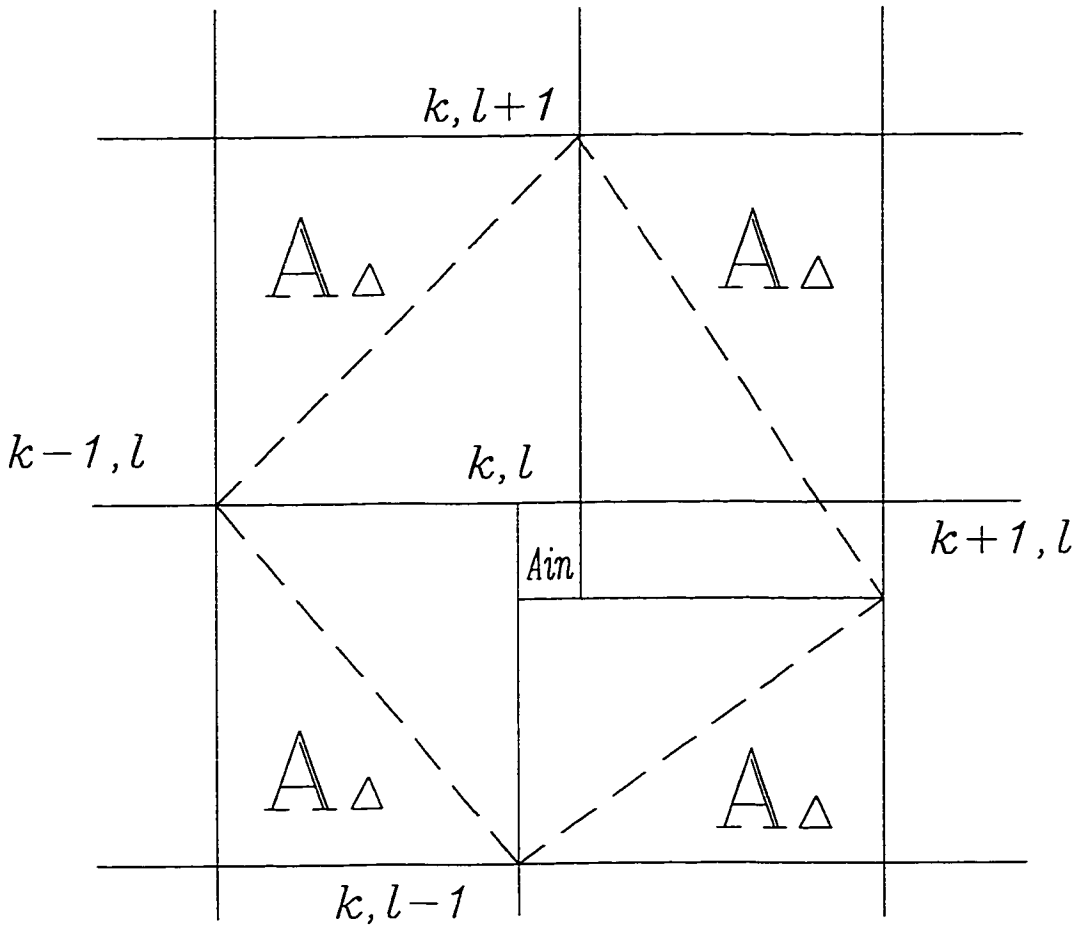

Fig. 3.2 Mesh for the nodal area

The approximation of the internal force $\boldsymbol{P}$ may be obtained by using Green's theorem. For the left hand side of (3.43), let the stress gradient $T_{i\alpha,\alpha}$ be the integrand, let the area $2A^{k,l}$ enclosed by the dashed contour be the integral area D as shown in Fig. 3.1. Then, applying the one point integration rule, $T_{i\alpha,\alpha}$ is set equal to its value at the node (k, l) i.e. $T_{i\alpha,\alpha}^{k,l,n}$. For the right hand side of (3.43), let the stress $T_{i\alpha}$ be the integrand and let the dashed contour be the integral curve as shown in Fig. 3.1. Then, using the one point integration rule, $T_{i\alpha}$ is set equal to the zone-centered stress value $T_{i\alpha}^{k+1/2,l+1/2,n}$, so the components of the stress $T_{i\alpha}$ are zone-centered value. Thus the Green's theorem applied to the internal force $\boldsymbol{P}$ may be written as:

$$\iint_D T_{i\alpha,\alpha} dA = \varepsilon_{\alpha\beta} \oint_{\partial D} T_{i\alpha} dx_\beta \ .$$

Finally, one obtains the following equation:

$$\begin{aligned} 2A^{k,l} T_{i\alpha,\alpha}^{k,l,n} = e_{\alpha\beta} \{ & T_{i\alpha}^{k+1/2,l+1/2,n} (x_\beta^{k,l-1} - x_\beta^{k+1,l}) + T_{i\alpha}^{k-1/2,l+1/2,n} (x_\beta^{k-1,l} - x_\beta^{k,l+1}) \\ & + T_{i\alpha}^{k-1/2,l-1/2,n} (x_\beta^{k,l-1} - x_\beta^{k-1,l}) + T_{i\alpha}^{k+1/2,l-1/2,n} (x_\beta^{k+1,l} - x_\beta^{k,l-1}) \} \ . \end{aligned} \tag{3.45}$$

The area $2A^{k,l}$ enclosed by the dashed quadrilateral in Fig. 3.1 equals the difference between the total area of the node (k, l) $A_{total}^{k,l}$ and the four triangular areas $4A_\Delta^{k,l}$, or the difference between the four triangular areas $4A_\Delta^{k,l}$ and the internal area $A_{in}^{k,l}$, shown in Fig. 3.2. Thus the area $2A^{k,l}$ may be written with respect to the total area $A_{total}^{k,l}$ and the internal area $A_{in}^{k,l}$ as:

$$2A^{k,l} = \frac{1}{2}(A_{total}^{k,l} + A_{in}^{k,l}). \tag{3.46}$$

The total area $A_{total}^{k,l}$ is a rectangle and its area is given by

$$A_{total}^{k,l} = (x_1^{k+1,l} - x_1^{k-1,l})(x_2^{k,l+1} - x_2^{k,l-1}). \tag{3.47}$$

$A_{in}^{k,l}$ is also a rectangle, thus its area is given by

$$A_{in}^{k,l} = (x_1^{k,l+1} - x_1^{k,l-1})(x_2^{k-1,l} - x_2^{k+1,l}). \tag{3.48}$$

Substituting (3.47) and (3.48) into (3.46), gives the area of $2A^{k,l}$ with respect to the two coordinates:

$$2A^{k,l} = \frac{1}{2}\{(x_2^{k-1,l} - x_2^{k+1,l})(x_1^{k,l+1} - x_1^{k,l-1}) - (x_1^{k-1,l} - x_1^{k+1,l})(x_2^{k,l+1} - x_2^{k,l-1})\}. \tag{3.49}$$

Let $A^{k,l}$ be the equivalent nodal area (Herrmann and Bertholf, 1983), so it is equal to one half of the area enclosed by the dashed quadrilateral in Fig. 3.1, thus $A^{k,l}$ is given by

$$A^{k,l} = \frac{1}{4}\{(x_2^{k-1,l} - x_2^{k+1,l})(x_1^{k,l+1} - x_1^{k,l-1}) - (x_1^{k-1,l} - x_1^{k+1,l})(x_2^{k,l+1} - x_2^{k,l-1})\}. \tag{3.50}$$

Since the repetition of a Greek symbol indicates the summation over the index from 1 to 2, the components form of (3.45) may be written as:

$$\begin{aligned}
\text{For } i=1 \quad T_{11,1}^{k,l,n} + T_{12,2}^{k,l,n} &= \{T_{11}^{k+1/2,l+1/2,n}(x_2^{k,l+1} - x_2^{k+1,l}) + T_{11}^{k-1/2,l+1/2,n}(x_2^{k-1,l} - x_2^{k,l+1}) \\
&\quad + T_{11}^{k-1/2,l-1/2,n}(x_2^{k,l-1} - x_2^{k-1,l}) + T_{11}^{k+1/2,l-1/2,n}(x_1^{k+1,l} - x_2^{k,l-1})\} \\
&\quad - \{T_{12}^{k+1/2,l+1/2,n}(x_1^{k,l+1} - x_1^{k+1,l}) + T_{12}^{k-1/2,l+1/2,n}(x_1^{k-1,l} - x_1^{k,l+1}) \\
&\quad + T_{12}^{k-1/2,l-1/2,n}(x_1^{k,l-1} - x_1^{k-1,l}) + T_{12}^{k+1/2,l-1/2,n}(x_1^{k+1,l} - x_1^{k,l-1})\}; \\
\text{For } i=2 \quad T_{21,1}^{k,l,n} + T_{22,2}^{k,l,n} &= \{T_{21}^{k+1/2,l+1/2,n}(x_2^{k,l+1} - x_2^{k+1,l}) + T_{12}^{k-1/2,l+1/2,n}(x_2^{k-1,l} - x_2^{k,l+1}) \\
&\quad + T_{21}^{k-1/2,l-1/2,n}(x_2^{k,l-1} - x_2^{k-1,l}) + T_{21}^{k+1/2,l-1/2,n}(x_1^{k+1,l} - x_2^{k,l-1})\} \\
&\quad - \{T_{22}^{k+1/2,l+1/2,n}(x_1^{k,l+1} - x_1^{k+1,l}) + T_{22}^{k-1/2,l+1/2,n}(x_1^{k-1,l} - x_1^{k,l+1}) \\
&\quad + T_{22}^{k-1/2,l-1/2,n}(x_1^{k,l-1} - x_1^{k-1,l}) + T_{22}^{k+1/2,l-1/2,n}(x_1^{k+1,l} - x_1^{k,l-1})\}; \\
\text{For } i=3 \quad T_{31,1}^{k,l,n} + T_{32,2}^{k,l,n} &= \{T_{31}^{k+1/2,l+1/2,n}(x_2^{k,l+1} - x_2^{k+1,l}) + T_{31}^{k-1/2,l+1/2,n}(x_2^{k-1,l} - x_2^{k,l+1})
\end{aligned} \tag{3.51}$$

$$+T_{31}^{k-1/2,l-1/2,n}(x_2^{k,l-1}-x_2^{k-1,l})+T3_{31}^{k+1/2,l-1/2,n}(x_1^{k+1,i}-x_2^{k,l-1})\}$$
$$-\{T_{32}^{k+1/2,l+1/2,n}(x_1^{k,l-1}-x_1^{k+1,l})+T_{32}^{k-1/2,l+1/2,n}(x_1^{k-1,l}-x_1^{k,l+1})$$
$$+T_{32}^{k-1/2,l-1/2,n}(x_1^{k,l-1}-x_1^{k-1,l})+T_{32}^{k+1/2,l-1/2,n}(x_1^{k+1,l}-x_1^{k,l-1})\}.$$

There is a relation between the Piola stress tensor T and the Cauchy-Green strain tensor C, which may be obtained by using the variational principle. For a membrane, the Cauchy-Green strain tensor C is a function of the deformation gradient. So the stress components $T_{i\alpha}$ depend on the zone-centered components of the deformation gradient $F_{i\alpha}$. The components of the deformation gradient $F_{i\alpha}$ may be approximated by applying Green's formula (3.43). For the left hand side of (3.43), let $F_{i\alpha}$ be the integrand and let the shaded zone in Fig. 3.1 be the integral area. Notice that $F_{i\alpha}=r_{i,\alpha}$, let $r_i(x,t^n)$ be the integrand and let the contour which encloses the shade zone be the integral curve. Then set the integrand equal to the average of its end-point values along the zone edge, and $F_{i,\alpha}^{k+1/2,l+1/2,n}$ may be obtained as

$$A^{k+1/2,l+1/2}F_{i\alpha}^{k+1/2,l+1/2,n}=e_{\alpha\beta}\{\frac{r_i^{k+1,l+1}+r_i^{k+1,l}}{2}(x_\beta^{k+1,l+1}-x_\beta^{k+1,l})$$
$$+\frac{r_i^{k,l+1}+r_i^{k+1,l+1}}{2}(x_\beta^{k,l+1}-x_\beta^{k+1,l+1})$$
$$+\frac{r_i^{k,l}+r_i^{k,l+1}}{2}(x_\beta^{k,l}-x_\beta^{k,l+1})$$
$$+\frac{r_i^{k+1,l}+r_i^{k,l}}{2}(x_\beta^{k+1,l}-x_\beta^{k,l})\}. \qquad (3.52a)$$

After some simplifications from (3.52a), the zone-centered components of the deformation gradient at time step n may be rewritten as:

$$F_{i\alpha}^{k+1/2,l+1/2,n}=\frac{e_{\alpha\beta}}{2A^{k+1/2,l+1/2}}\{(x_\beta^{k,l+1}-x_\beta^{k+1,l})(r_\beta^{k+1,l+1}-r_\beta^{k,l})-(x_\beta^{k+1,l+1}-x_\beta^{k,l})(r_\beta^{k,l+1}-r_\beta^{k+1,l}), \qquad (3.52b)$$

where $A^{k+1/2,l+1/2}$ is the area of the shaded zone. By employing the same procedure used to obtain $2A^{k,l}$, $A^{k+1/2,l+1/2}$ is given by

$$A^{k+1/2,l+1/2} = \frac{1}{2}\{(x_2^{k,l+1} - x_2^{k+1,l})(x_1^{k+1,l+1} - x_1^{k,l}) - (x_1^{k,l+1} - x_1^{k+1,l})(x_2^{k+1,l+1} - x_2^{k,l})\}. \tag{3.53}$$

The component form of (3.52b) may be written as:

For $i = 1$ $$F_{11}^{k+1/2,\,l+1/2,\,n} = \frac{1}{2A^{k+1/2,\,l+1/2}}\{(x_2^{k,l+1} - x_2^{k+1,l})(r_1^{k+1,l+1} - r_1^{k,l}) - (x_2^{k+1,l+1} - x_2^{k,l})(r_1^{k,l+1} - r_1^{k+1,l})\}, \tag{3.54}$$

$$F_{12}^{k+1/2,\,l+1/2,\,n} = \frac{-1}{2A^{k+1/2,\,l+1/2}}\{(x_1^{k,l+1} - x_1^{k+1,l})(r_1^{k+1,l+1} - r_1^{k,l}) - (x_1^{k+1,l+1} - x_1^{k,l})(r_1^{k,l+1} - r_1^{k+1,l})\};$$

For $i = 2$ $$F_{21}^{k+1/2,\,l+1/2,\,n} = \frac{1}{2A^{k+1/2,\,l+1/2}}\{(x_2^{k,l+1} - x_2^{k+1,l})(r_2^{k+1,l+1} - r_2^{k,l}) - (x_2^{k+1,l+1} - x_2^{k,l})(r_2^{k,l+1} - r_2^{k+1,l})\},$$

$$F_{22}^{k+1/2,\,l+1/2,\,n} = \frac{-1}{2A^{k+1/2,\,l+1/2}}\{(x_1^{k,l+1} - x_1^{k+1,l})(r_2^{k+1,l+1} - r_2^{k,l}) - (x_1^{k+1,l+1} - x_1^{k,l})(r_2^{k,l+1} - r_2^{k+1,l})\};$$

For $i = 3$ $$F_{31}^{k+1/2,\,l+1/2,\,n} = \frac{1}{2A^{k+1/2,\,l+1/2}}\{(x_2^{k,l+1} - x_2^{k+1,l})(r_3^{k+1,l+1} - r_3^{k,l}) - (x_2^{k+1,l+1} - x_2^{k,l})(r_3^{k,l+1} - r_3^{k+1,l})\},$$

$$F_{32}^{k+1/2,\,l+1/2,\,n} = \frac{-1}{2A^{k+1/2,\,l+1/2}}\{(x_1^{k,l+1} - x_1^{k+1,l})(r_3^{k+1,l+1} - r_3^{k,l}) - (x_1^{k+1,l+1} - x_1^{k,l})(r_3^{k,l+1} - r_3^{k+1,l})\}.$$

The same approximations (3.45) or (3.52) may be obtained by using Taylor series expansions (Herrmann and Bertholf, 1983). They show that the local truncation error is $O(\varepsilon^3)$ for an uniform mesh and $O(\varepsilon^2)$ for other types of meshes, where ε is a typical

zone width. When calculating the approximation of the stress gradient difference by using the deformation gradient approximation, their truncation errors combine. Therefore the local truncation error for the method is $O(\varepsilon^2)$ for uniform rectangular meshes and $O(\varepsilon)$ for the other types of meshes (Silling, 1985).

3.3.3 Internal and External Forces

The i-th internal force component on the node (k, l) at time step n due to internal stresses is given by:

$$P_i^{k,l,n} = A^{k,l} T_{i\alpha,\alpha}^{k,l,n}. \tag{3.56}$$

Using (3.45) gives

$$\begin{aligned} P_i^{k,l,n} = \frac{e_{\alpha\beta}}{2} \{ & T_{i\alpha}^{k+1/2,l+1/2,n} (x^{k,l+1} - x^{k+1,l}) + T_{i\alpha}^{k-1/2,l+1/2,n} (x_\beta^{k-1,l} - x_\beta^{k,l+1}) \\ & + T_{i\alpha}^{k-1/2,l-1/2,n} (x_\beta^{k,l-1} - x_\beta^{k-1,l}) + T_{i\alpha}^{k+1/2,l-1/2,n} (x_\beta^{k+1,l} - x_\beta^{k,l-1}) \}. \end{aligned} \tag{3.57}$$

In order to obtain the internal forces from the above equation, the components of the Piola stress tensor have to be determined first. In the DR algorithm, the initial position vector with respect to the deformed configuration $\boldsymbol{r}^{k,l,0}$ is known since the position vector with respect to the reference configuration is known and the displacement vector $\boldsymbol{u}^0$ at the zero time step is given. The position vector $\boldsymbol{r}^{k,l,n}$ at time step n may be obtained from the previous time step. For all the variables are known in (3.52b), this gives the approximation of the zone-centered deformation gradient $\boldsymbol{F}$. Since the Cauchy-Green strain tensor is only a function of $\boldsymbol{F}$ in (2.2a), (2.2c) gives the approximation of the Cauchy-Green strain tensor $\boldsymbol{C}$, which is a zone-centered variable. The square of the

principal stretches are the two eigenvalues of the Cauchy-Green strain tensor. Equation (2.9) gives the two principal stretches λ and μ respectively. Obviously, the principal stretches λ and μ are two zone-centered variables. The principal directions with respect to the reference configuration $\boldsymbol{L}$ and $\boldsymbol{M}$ are the two eigenvalue vectors. Equation (2.10) gives the components of $\boldsymbol{L}$ and $\boldsymbol{M}$ as a function of the Cauchy-Green tensor $\boldsymbol{C}$, and the principal stretches λ and μ. From the definition of the unit vectors $\boldsymbol{l}$ and $\boldsymbol{m}$, (2.14) gives the components of the $\boldsymbol{l}$ and $\boldsymbol{m}$ respectively, as a function of the principal stretches λ and μ, the principal direction with respect to the reference configuration $\boldsymbol{L}$ and $\boldsymbol{M}$, and the deformation gradient $\boldsymbol{F}$. So, the principal direction with respect to the reference configuration $\boldsymbol{L}$ and $\boldsymbol{M}$, and the principal directions with respect to the deformed configuration $\boldsymbol{l}$ and $\boldsymbol{m}$ are the zone-centered variables. The spectral form of the Piola stress $\boldsymbol{T}$ is a function of the principal stresses w_λ and w_μ which may obtained by using the variational principle, and the principal directions with respect to the reference or the deformed configuration $\boldsymbol{L}$, $\boldsymbol{M}$ and $\boldsymbol{l}$, $\boldsymbol{m}$. Thus the components of the Piola stress may be given by (2.26).

The external forces considered in this work may be due to the uniform pressure loading or to pressure loading of the hydrostatic type. Body forces are neglected. In the presence of pressure loading of any kind, the external forces may be obtained by discretizing the term $\iint_D \boldsymbol{pJndA}$ in (2.29). The Jacobian $\boldsymbol{J}$ is a function of the principal stretches λ and μ, which are zone-centered variables, so $\boldsymbol{J}$ is also a zone-centered variable. The outward unit normal vector $\boldsymbol{n}$ is given by $\boldsymbol{n} = \boldsymbol{l} \times \boldsymbol{m}$, since $\boldsymbol{l}$ and $\boldsymbol{m}$ are zone-

centered variables, $\boldsymbol{n}$ determined by $\boldsymbol{l}$ and $\boldsymbol{m}$ is also a zone-centered variable, and the components of $\boldsymbol{n}$ may be expressed as:

$$n_i = e_{ijk} l_j m_k, \tag{3.58a}$$

where e_{ijk} is the three dimensional alternator symbol. In the presence of uniform pressure loading, the discretized zone-centered external force may be written as:

$$F_i^{k+1/2,J+1/2,n} = pn_i^{k+1/2,J+1/2,n} \lambda^{k+1/2,J+1/2,n} \mu^{k+1/2,J+1/2,n} A^{k+1/2,J+1/2,n}, \tag{3.59}$$

where the pressure $p = \text{constant}$. In the presence of a pressure loading of the hydrostatic type, the zone-centered p is obtained as the average:

$$p^{k+1/2,J+1/2,n} = \frac{1}{4}(p^{k+1,J,n} + p^{k+1,J+1,n} + p^{k,J,n} + p^{k,J+1,n}), \tag{3.60}$$

where the magnitude of the node-centered pressure p is given by $p^{k,J,n} = \varrho_l g \left| h_{ii}^{k,J,n} - r_i^{k,J,n} \right|$. Then, the discretized zone-centered external force $F^{k+1/2,J+1/2,n}$ can be obtained by substituting equation (3.60) into equation (3.59). Since the external force should be a node-centered variable, the node-centered external forces due to the pressure are taken to the average value of the zone-centered external force values whose zones are adjacent to the node. Thus, the node-centered external force is given by:

$$F_i^{k,J,n} = \frac{1}{4}(F_i^{k+1/2,J+1/2,n} + F_i^{k+1/2,J-1/2,n} + F_i^{k-1/2,J+1/2,n} + F_i^{k-1/2,J-1/2,n}). \tag{3.61}$$

The node-centered external force may be obtained with another approach as

$$F_i^{k,J,n} = p^{k,J,n} A^{k,J}, \tag{3.62}$$

where $p^{k,J,n} = \text{constant}$ for uniform pressure loading and $p^{k,J,n} = \varrho_l g \left| h_{ii}^{k,J,n} - r_i^{k,J,n} \right|$ for pressure loading of the hydrostatic type. The nodal area $A^{k,J}$ is given by equation (3.50).

These two approaches of computing the node-centered external force give the same solution.

3.3.4 Boundary Conditions

There are three kinds of boundary conditions: displacement boundary condition, traction boundary condition and mixed boundary condition (both displacement and traction boundary conditions exist). In order to enforce the boundary conditions, the mesh is arranged such that the boundary contains nodal points.

For displacement boundary condition, the displacements at the nodes on the boundary are imposed. In order to obtain the zone-centered deformation gradient from (3.52b) or (3.54), the position vectors with respect to the reference and deformed configuration on the boundary of the zone need to be known at every iteration. This can be automatically satisfied in the DR method. Thus the zone-centered deformation may be obtained. The internal forces at the nodes which are located on the boundary need not to be calculated, since the displacement of these nodes are already given. The internal forces at the interior nodes may be obtained from (3.57), since the variables of the equations are all determined from the previous time step in DR.

Only the case of displacement boundary conditions is studied in this work.

Chapter 4

DR Algorithm for Analysis of Membranes Subjected to Hydrostatic Pressure Loading

4.1 Introduction

A DR algorithm has been developed in this work for the static analysis of isotropic elastic membranes undergoing finite deformations, while subjected to pressure loading of the hydrostatic type. The possibility of wrinkling is taken into account by employing a relaxed strain energy density. The case of planar reference configurations and arbitrary displacement boundary conditions is considered.

This algorithm is based on the DR method which is suitable to the analysis of wrinkled membrane problems. The spatial discretization of the equation of motion at node (k, l) was obtained by using the Green's theorem differencing method:

$$m^{k,l}\ddot{u}^{n} + cm^{k,l}\dot{u}^{k,l,n} + P^{k,l,n} = F^{k,l,n}. \tag{4.1}$$

The static response of the membrane structure is obtained when the internal force $P^{k,l,n}$ is in equilibrium with the external force $F^{k,l,n}$.

4.2 The DR Algorithm

Parameters have to be chosen to start this algorithm. In this algorithm, the elements of the diagonal mass matrix are approximated by using the real mass density of elastic materials. The time step h is kept constant during the computation after it is selected by trail and error. The damping coefficient c is obtained from a numerical experiment: the program is run initially with $c = 0$, and the total kinetic energy of the whole membrane structure is calculated. Since the kinetic energy varies at twice of the fundamental frequency of the system, the fundamental frequency can be estimated, then from equation (3.37) the value of a damping coefficient which insures rapid convergence can be obtained.

The original DR method, instead of an adaptive DR method is used in this work, because of the following reasons: The difference between the original DR method and the adaptive DR method is that the fictitious mass matrix $\boldsymbol{M}$ and the damping coefficient c are evaluated at each iteration for the adaptive DR method. These two parameters are modified during the computation in order to maintain optimum convergence. The fictitious mass matrix $\boldsymbol{M}$ can be evaluated from equation (3.39), and the damping coefficient c can be evaluated from equation (3.40). Thus the stiffness matrix of the elements and the local stiffness matrix have to be calculated at each time step. These computations are very time consumming. Since the original DR version is simpler and reasonably efficient, it has been chosen in the present work. But this version may be easily modified to the adaptive DR version by adding a subroutine to calculate the

stiffness and the local stiffness, then compute $\boldsymbol{M}$ and c from (3.39) and (3.40) respectively, at each iteration.

Since the deformations occurring in membrane structures are mostly of the large rotation and/or large strain type, the internal force has to be obtained by using the variational principles, and the strain energy of the membrane material has to be given. The approximated internal force can be obtained from the membrane theory and the Green's theorem differencing method.

At step (I), described on the following page, the initial conditions $\boldsymbol{u}^0$ and $\dot{\boldsymbol{u}}^0$ are required to be given, and the iteration parameters which are the time step h, the damping coefficient c, and the elements of the diagonal mass matrix m_{ii} need to be chosen. The expression of the strain energy density of the material used is also needed. Only displacement boundary conditions are considered and have to be indicated. Steps (II), (III) and (IV) are the computational steps corresponding to the internal forces. At step (II) the zone centered variables deformation gradient and Cauchy-Green strain tensor are computed. At step (III) the zone centered variable Piola stress tensor is computed by using the relaxed strain energy density, and wrinkling is checked. At step (IV) the approximated internal forces are computed by using the Green's theorem differencing technique. At step (V) the external forces are computed, thus the density and the amount of liquid are needed in the case of a hydrostatic pressure loading, or the magnitude of the pressure in the case of a uniform pressure loading. At step (VI) the residual is computed. If the residual is approximately equal to zero (i.e. $\varepsilon < 10^{-6}$), it is considered that the equilibrium is satisfied, so the program stops. Otherwise, the velocity and displacement

are computed using the central difference time integrator at step (VIII) and (IX), and the next iteration is stated from step (II) to step(X).

Formally, this DR algorithm may be written as:

(I) initial conditions:

choose h, c and $\boldsymbol{M}$,

$\boldsymbol{u}^0$ given; $\dot{\boldsymbol{u}}^0 = \boldsymbol{0}$, $n = 0$,

$w(\lambda, \mu)$ given.

(II) compute zone-centered quantities:

deformation gradient $\boldsymbol{F}^n$,

Cauchy-Green strain $\boldsymbol{C}^n$,

principal stretches λ^n, μ^n, order $\lambda^n > \mu^n$,

principal vectors of strain $\boldsymbol{L}^n$, $\boldsymbol{M}^n$; $\boldsymbol{l}^n$, $\boldsymbol{m}^n$,

(III) check for wrinkling; compute zone centered Piola stress $\boldsymbol{T}^n$:

if $\lambda^n > (\mu^n)^{-1/2}, \mu^n > (\lambda^n)^{-1/2}$, tense zone;

$$w_R(\lambda^n, \mu^n) = w(\lambda^n, \mu^n),$$

$$T^n_{i\alpha} = w^n_\lambda l^n_i L^n_\alpha + w^n_\mu m^n_i M^n_\alpha;$$

if $\lambda^n > 1, \mu^n \le (\lambda^n)^{-1/2}$, wrinkled zone (tension field);

$$w_R(\lambda^n, \mu^n) = \hat{w}(\lambda^n),$$

$$T^n_{i\alpha} = \hat{w}(\lambda^n) l^n_i L^n_\alpha;$$

if $\mu^n > 1, \lambda^n \le (\mu^n)^{-1/2}$, wrinkled zone;

$$w_R(\lambda^n, \mu^n) = \hat{w}(\mu^n),$$

$$T_{i\alpha}^n = \hat{w}(\mu^n) m_i^n M_\alpha^n;$$

if $\lambda^n \leq 1, \mu^n \leq 1$, slack zone;

$$w_R(\lambda^n, \mu^n) = 0,$$

$$T_{i\alpha}^n = 0;$$

(IV) compute internal forces $\boldsymbol{P}^n$,

(V) compute external forces $\boldsymbol{F}^n$,

magnitude of pressure p given (uniform pressure loading)

mass density ϱ and total volume of liquid given (hydrostatic pressure loading)

(VI) compute residual $\boldsymbol{R}^n = \boldsymbol{F}^n - \boldsymbol{P}^n$,

(VII) If $\boldsymbol{R}^n \approx \boldsymbol{0}$ stop; otherwise continue

(VIII) compute velocity at time step n+1/2:

$$n=0, \quad \dot{u}_i^{1/2} = h(M_{ii}^0)^{-1} r_i^0 / 2$$

$$n \neq 0 \quad \dot{u}_i^{n+1/2} = \frac{(2-ch)}{(2+ch)} \dot{u}_i^{n-1/2} + 2h(m_{ii}^n)^{-1} r_i^n / (2+ch)$$

(IX) compute displacement at time step n+1:

$$\boldsymbol{u}^{n+1} = \boldsymbol{u}^n + h\dot{\boldsymbol{u}}^{n+1/2}$$

(X) $n=n+1$, return to (II).

The superscripts representing labels of nodes or labels of zone centers have been omitted to simplify the notation. The zone centered variables which are involved at steps (II) and (III) have been specified, the variables involved at the other steps are node-

centered variables. The superscripts used in this algorithm represent the time step. As the specified in other chapters, i indicates the range over $\{1,2,3\}$, α indicates the range over $\{1,2\}$.

The displacements, the principal stretches and the principal stresses and their directions may be obtained from the output files, as well as the presence and delimitation of the wrinkled regions.

Chapter 5

Applications for Rubber-like Materials

5.1 Introduction

The DR method developed in this work is applied to membranes made of rubber-like materials, with various boundary conditions and subjected to pressure loading of the hydrostatic type. The material is assumed as isotropic, homogenous, and incompressible. Four strain energy functions for rubber-like incompressible materials are considered: Varga, Mooney-Rivlin, neo-Hookean and Ogden strain energy functions, but results are presented only for the Ogden and the Mooney-Rivlin strain energies. Various displacement boundary conditions and total or partial pressure loading of the hydrostatic type as well as loading by uniform pressure and combined loading are used in the applications. The mesh is refined based on convergence considerations, but also to obtain a continuous deformed surface and a reasonably accurate delimitation of the wrinkled regions. The reference configuration of the membranes used here are square, circular and cylindrical. The deformed shapes, the principal stretches, the principal stresses and their directions are obtained. Graphs including numerical values of the results are presented and discussed. The presence of wrinkled regions as well as their delimitation is indicated.

5.2 Rubber-like Membrane Materials

The membrane materials used in the applications are rubber-like materials. It is assumed that these materials are isotropic, homogenous, and incompressible. Four strain energy functions are considered: Varga, Mooney-Rivlin, neo-Hookean and Ogden strain energy function.

For the Vagar material, the strain energy per unit of initial volume has the form (Varga, 1966):

$$U(\lambda_1,\lambda_2,\lambda_3) = \frac{2}{3}E(\lambda_1+\lambda_2+\lambda_3-3), \tag{5.1}$$

where λ_i are the principal stretches and E is Young's modules. For infinitesimal strain $E = 12kg/cm^2 = 1.076\times10^3 kN/m^2$ (Varga, 1966). For incompressible material, it is required that $\lambda_1\lambda_2\lambda_3 = 1$. If $\lambda_1 = \lambda$ and $\lambda_2 = \mu$, then $\lambda_3 = 1/\lambda\mu$. The corresponding strain energy function per unit initial area of membrane may be expressed as

$$w(\lambda,\mu) = \frac{2}{3}E(\lambda+\mu+\lambda^{-1}\mu^{-1}-3). \tag{5.2}$$

The two principal Piola stresses which are the forces per unit length in the reference configuration may be obtained for tense region as:

$$w_\lambda(\lambda,\mu) = \frac{2}{3}E(1-\lambda^{-2}\mu^{-1}),$$
$$w_\mu(\lambda,\mu) = \frac{2}{3}E(1-\mu^{-2}\lambda^{-1}). \tag{5.3}$$

When wrinkling occurs, the relaxed strain density is used in the wrinkled region. For $\lambda > 1$ and $\mu \le \nu(\lambda) \equiv \lambda^{-1/2}$, the relaxed strain density in uniaxial tension may be expressed as

$$\hat{w}(\lambda) = \frac{2}{3} E(\lambda + 2\lambda^{-1/2} - 3), \tag{5.4}$$

and the principal Piola stresses at this area which represents a tension field are obtained by the partial derivatives of (5.4)

$$\hat{w}_{\lambda}(\lambda) = \frac{2}{3} E(1 - \lambda^{-3/2}),$$
$$\hat{w}_{\mu} = 0. \tag{5.5}$$

For $\mu > 1$ and $\lambda \le \nu(\mu) \equiv \mu^{-1/2}$, the relaxed strain density in uniaxial tension may be expressed as

$$\hat{w}(\mu) = \frac{2}{3} E(\mu + 2\mu^{-1/2} - 3), \tag{5.6}$$

and the principal Piola stresses are:

$$\hat{w}_{\mu}(\mu) = \frac{2}{3} E(1 - \mu^{-3/2}),$$
$$\hat{w}_{\lambda} = 0. \tag{5.7}$$

For $\lambda \le 1$ and $\mu \le 1$, a slack area is obtained, and the two principal stresses are both zero:

$$\hat{w}_{\mu}(\mu) = 0,$$
$$\hat{w}_{\lambda} = 0. \tag{5.8}$$

For the Mooney-Rivlin material, the strain energy per unit of initial volume has the form (Ogden, 1984):

$$U(\lambda_1,\lambda_2,\lambda_3)=c_{10}(\lambda_1^{\,2}+\lambda_2^{\,2}+\lambda_3^{\,2}-3)+c_{01}(\lambda_2^{\,2}\lambda_3^{\,2}+\lambda_3^{\,2}\lambda_1^{\,2}+\lambda_1^{\,2}\lambda_2^{\,2}-3)\,, \tag{5.9}$$

where c_{10} and c_{01} are coefficients independent of the deformation. For a incompressible membrane, let $\lambda_1=\lambda$, $\lambda_2=\mu$ and $\lambda_3=1/\lambda\mu$, then the strain energy becomes

$$w(\lambda,\mu)=\frac{G_1}{2}(\lambda^2+\mu^2+\lambda^{-2}\mu^{-2}-3)-\frac{G_2}{2}(\lambda^{-2}+\mu^{-2}+\lambda^2\mu^2-3), \tag{5.10}$$

where $G_1-G_2=\tilde{G}$, $\tilde{G}$ is the shear modules for infinitesimal strain. For incompressible material, $\tilde{G}=E/3=4\text{kg}/\text{cm}^2=3.58\times10^2 kN/m^2$ (Varga, 1966). G_1 and G_2 may be determined when applying the relaxed strain density.

As for the Varga material, the principal Piola stress can be obtained from the above equation:

$$\begin{aligned} w_\lambda(\lambda,\mu)&=G_1(\lambda-\lambda^{-3}\mu^{-2})+G_2(\lambda^{-3}-\lambda\mu^2)\,,\\ w_\mu(\lambda,\mu)&=G_1(\mu-\mu^{-3}\lambda^2)+G_2(\mu^{-3}-\mu\lambda^2)\,. \end{aligned} \tag{5.11}$$

From the definition of the natural width, when $\mu=\nu(\lambda)\equiv\lambda^{-1/2}$, $w_\mu=0$. Thus from equation (5.11):

$$\begin{aligned} w_\mu(\lambda,\nu(\lambda))&=G_1(\lambda^{-1/2}-\lambda^{7/2})+G_2(\lambda^{3/2}-\lambda^{3/2})\\ &=G_1(\lambda^{-1/2}-\lambda^{7/2}). \end{aligned} \tag{5.12}$$

Since $\lambda^{-1/2}-\lambda^{7/2}\neq0$, G_1 should be zero. Therefore $G_2=-\tilde{G}$. Thus, the relaxed strain density and the stresses may be expressed as:

For $\lambda>\nu(\mu)$ and $\mu>\nu(\lambda)$

$$w(\lambda,\mu)=\frac{G}{2}(\lambda^{-2}+\mu^{-2}+\lambda^2\mu^2-3)\,,$$

$$w_\lambda(\lambda,\mu)=-G(\lambda^{-3}-\lambda\mu^2)\,,$$

$$w_\mu(\lambda,\mu) = -G(\mu^{-3} - \mu\lambda^2);$$

For $\lambda > 1$ and $\mu \le \nu(\lambda)$ (wrinkled zone)

$$\hat{w}(\lambda,\nu(\lambda)) = \frac{G}{2}(\lambda^{-2} + 2\lambda - 3),$$

$$\hat{w}_\lambda(\lambda) = G(-\lambda^{-3} + 1),$$

$$\hat{w}_\mu(\mu) = 0;$$

For $\mu > 1$ and $\lambda \le \nu(\mu)$ (wrinkled zone)

$$\hat{w}(\mu,\nu(\mu)) = \frac{G}{2}(\mu^{-2} + 2\mu - 3),$$

$$\hat{w}_\mu(\mu) = G(-\mu^{-3} + 1),$$

$$\hat{w}_\lambda(\lambda,\mu) = 0;$$

For $\lambda \le 1$ and $\mu \le 1$ (slack zone)

$$w(\lambda,\mu) = 0; \qquad w_\lambda(\lambda,\mu) = 0; \qquad w_\mu(\lambda,\mu) = 0.$$

For the neo-Hooken material, the strain energy per unit of initial volume has the form (Ogden, 1984):

$$U(\lambda_1,\lambda_2,\lambda_3) = \frac{G}{2}(\lambda_1^2 + \lambda_2^2 + \lambda_3^2 - 3). \tag{5.13}$$

For an incompressible membrane, the strain energy may be expressed as

$$w(\lambda,\mu) = \frac{G}{2}(\lambda^2 + \mu^2 + \lambda^{-2}\mu^{-2} - 3). \tag{5.14}$$

The relaxed strain density and the stresses are then:

For $\lambda > \nu(\mu)$ and $\mu > \nu(\lambda)$

$$w(\lambda,\mu) = \frac{G}{2}(\lambda^2 + \mu^2 + \lambda^{-2}\mu^{-2} - 3),$$

$$w_\lambda(\lambda,\mu) = G(\lambda - \lambda^{-3}\mu^{-2}),$$

$$w_\mu(\lambda,\mu) = G(\mu - \mu^{-3}\lambda^{-2});$$

For $\lambda > 1$ and $\mu \le \nu(\lambda)$ (wrinkled zone)

$$\hat{w}(\lambda,\nu(\lambda)) = \frac{G}{2}(\lambda^2 - 2\lambda^{-1} - 3),$$

$$\hat{w}_\lambda(\lambda) = G(\lambda - \lambda^{-2}),$$

$$\hat{w}_\mu(\mu) = 0.$$

For $\mu > 1$ and $\lambda \le \nu(\mu)$ (wrinkled zone)

$$\hat{w}(\mu,\nu(\mu)) = \frac{G}{2}(\mu^{-2} + 2\mu - 3),$$

$$\hat{w}_\mu(\mu) = G(-\mu^{-3} + 1),$$

$$\hat{w}_\lambda(\lambda,\mu) = 0;$$

For $\lambda \le 1$ and $\mu \le 1$ (slack zone)

$$w(\lambda,\mu) = 0; \qquad w_\lambda(\lambda,\mu) = 0; \qquad w_\mu(\lambda,\mu) = 0.$$

For the Ogden material, the strain energy per unit of initial volume has the form (Ogden, 1984):

$$U(\lambda_1,\lambda_2,\lambda_3) = G\sum_{r=1}^{3} g_r(\lambda_1^{\alpha_r} + \lambda_2^{\alpha_r} + \lambda_3^{\alpha_r} - 3)/\alpha_r \tag{5.15}$$

where $\alpha_1 = 1.3$, $\alpha_2 = 5.0$, $\alpha_3 = -2.0$;

$g_1 = 1.491$, $g_2 = 0.003$, $g_3 = 0.0237$

The membrane strain energy may be expressed as

$$w(\lambda,\mu) = G\sum_{r=1}^{3} g_r(\lambda^{\alpha_r} + \mu^{\alpha_r} + (\lambda\mu)^{-\alpha_r} - 3)/\alpha_r . \tag{5.16}$$

The relaxed strain density and the stresses are then:

For $\lambda > \nu(\mu)$ and $\mu > \nu(\lambda)$

$$w(\lambda,\mu) = G\sum_{r=1}^{3} g_r(\lambda^{\alpha_r} + \mu^{\alpha_r} + (\lambda\mu)^{-\alpha_r} - 3)/\alpha_r ,$$

$$w_\lambda(\lambda,\mu) = G\sum_{r=1}^{3} g_r(\alpha_r\lambda^{\alpha_r-1} - \alpha_r\lambda^{-\alpha_r-1}\mu^{-\alpha_r})/\alpha_r ,$$

$$w_\mu(\lambda,\mu) = G\sum_{r=1}^{3} g_r(\alpha_r\mu^{\alpha_r-1} - \alpha_r\lambda^{-\alpha_r}\mu^{-\alpha_r-1})/\alpha_r ;$$

For $\lambda > 1$ and $\mu \le \nu(\lambda)$ (wrinkled zone)

$$\hat{w}(\lambda,\mu) = G\sum_{r=1}^{3} g_r(\lambda^{\alpha_r} + 2\lambda^{-\alpha_r/2} - 3)/\alpha_r ,$$

$$\hat{w}(\lambda,\mu) = G\sum_{r=1}^{3} g_r(\alpha_r\lambda^{\alpha_r-1} - \alpha_r\lambda^{-\alpha_r/2-1})/\alpha_r ,$$

$$\hat{w}_\mu(\mu) = 0 ;$$

For $\mu > 1$ and $\lambda \le \nu(\mu)$ (wrinkled zone)

$$\hat{w}(\lambda,\mu) = G\sum_{r=1}^{3} g_r(\mu^{\alpha_r} + 2\mu^{-\alpha_r/2} - 3)/\alpha_r ,$$

$$\hat{w}(\lambda,\mu) = G\sum_{r=1}^{3} g_r(\alpha_r\mu^{\alpha_r-1} - \alpha_r\mu^{-\alpha_r/2-1})/\alpha_r ,$$

$$\hat{w}_\lambda(\lambda,\mu) = 0 ;$$

For $\lambda \le 1$ and $\mu \le 1$ (slack zone)

$$w(\lambda,\mu)=0; \qquad w_{\lambda}(\lambda,\mu)=0; \qquad w_{\mu}(\lambda,\mu)=0.$$

For a cylindrical membrane, four strain energy functions were considered. The reference configuration of the membrane is a planar square membrane, then it is curled into a cylinder with the top and the bottom boundaries fixed. Next the membrane is subjected to an uniform non dimensional pressure. The lager principal stretch λ at a certain node varies with the pressures and the variation is shown in Fig. 5.1. From the Fig.5.1e it can be observed that the solutions for the four strain energies give very similar results under low pressure values, however the solutions have bigger differences when the membrane is subjected to higher pressures. For the case considered here, only the Varga material gives convergent solutions when the membrane is subjected to low pressures, the maximum non-dimensional pressure is near 0.4; the Mooney-Rivlin material gives convergent solutions when the non-dimensional pressures are lower than 2.0, the curve in Fig. 5.1b changes smoothly; the maximum non-dimensional pressure for which the neo-Hooken material gives convergent solutions is 0.45; Ogden material can also give convergent solutions when the non-dimensional pressures are lower than 2.0, but comparing with the solutions which are obtained by using the Moony-Rivlin material, the curve changes sharply when the membrane is subjected to non-dimensional pressures which are between 0.425 to 2.0. All these strain energy functions give faster convergence when the membrane is subjected to lower pressures, the Moony-Rivlin material gives the fastest convergence among these four materials and still gives convergent solutions when the pressure is increased and the other three materials won't give convergent solutions.

Figures 5.2 to 5.5 show that Mooney-Rivlin gives the largest strain energy and relaxed strain density when the stretches are over certain values, Ogden gives the second largest value, neo-Hooken gives the third largest, Varga gives the smallest.

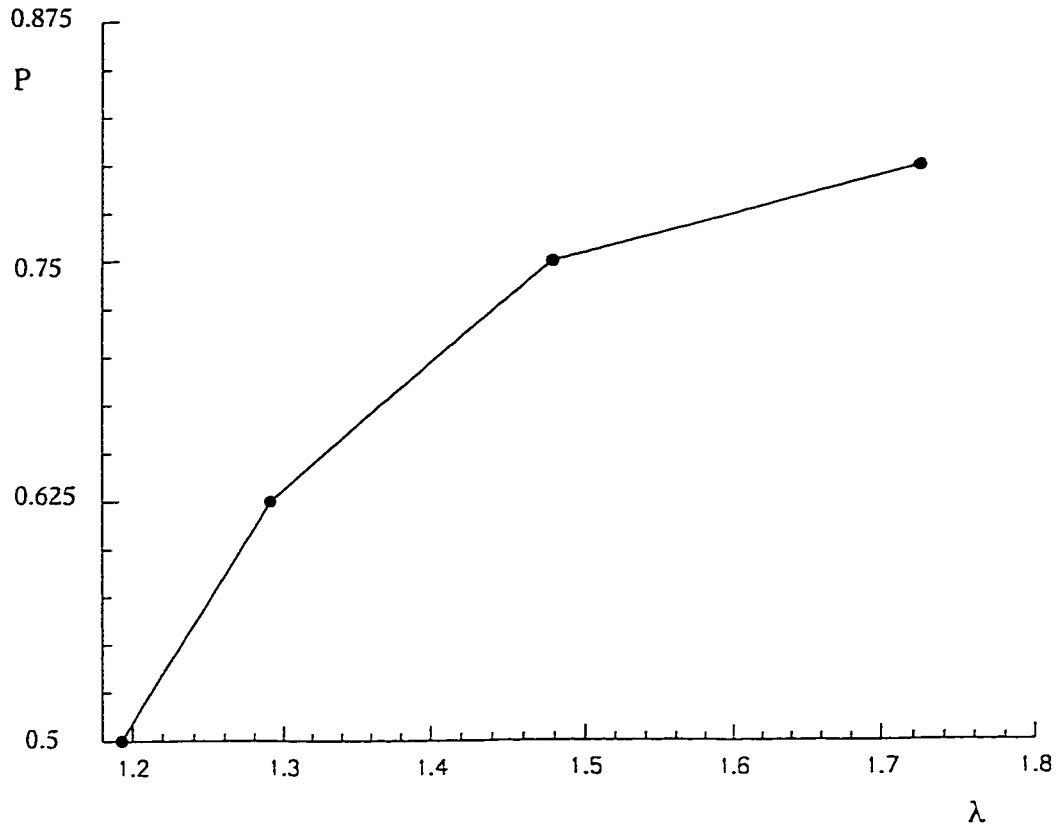

Fig. 5.1a Dimensionless pressure vs principal stretch λ, Varga material

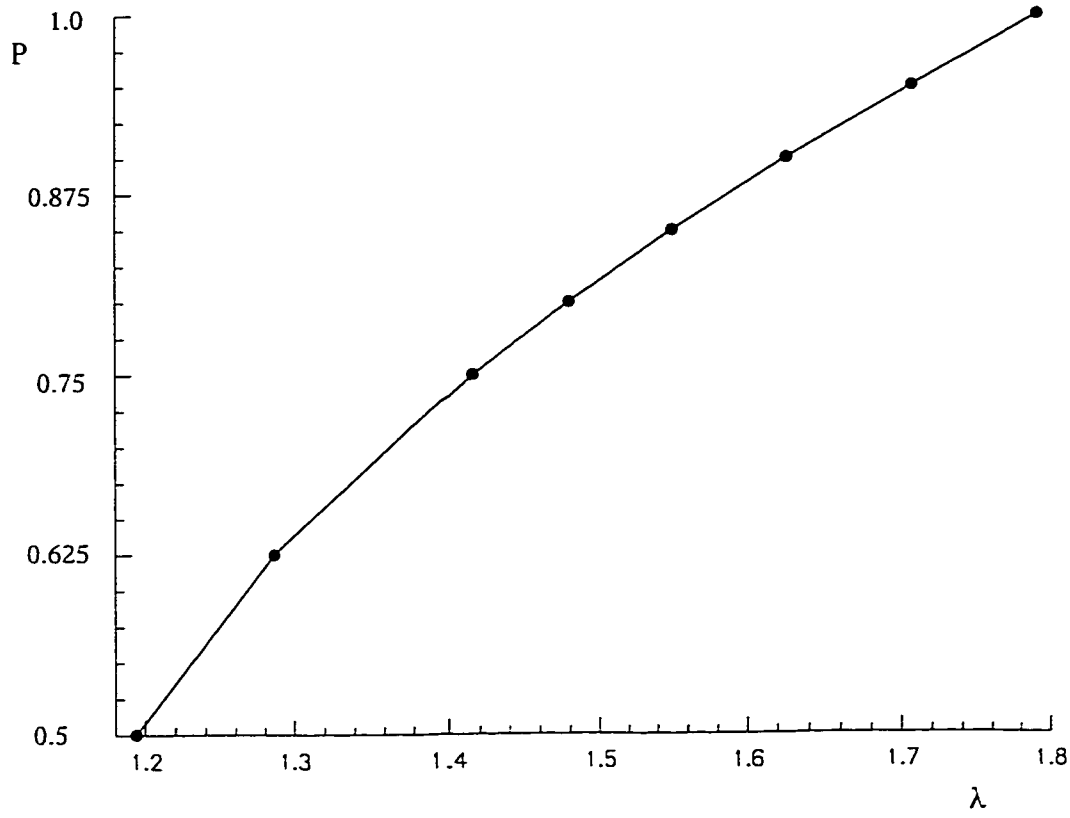

Fig. 5.1b Dimensionless pressure vs principal stretch λ, Mooney-Rivlin material

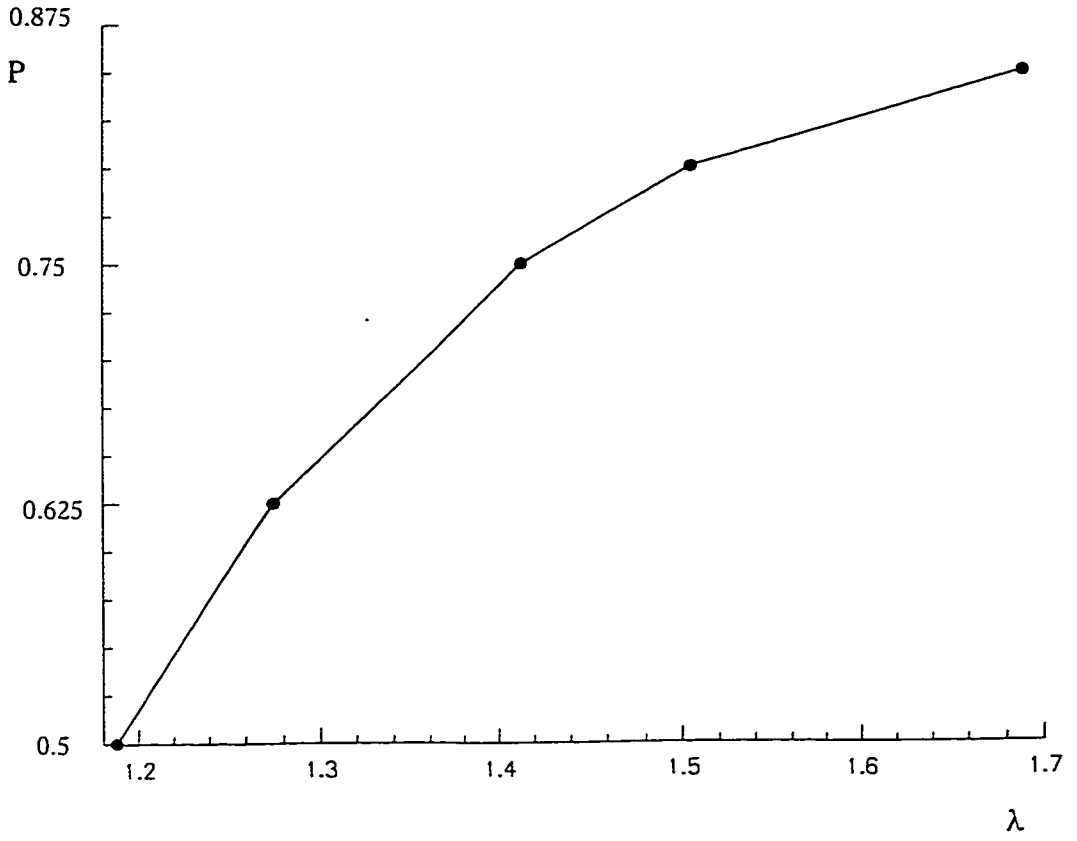

Fig. 5.1c Dimensionless pressure vs principal stretch λ, neo-Hooken material

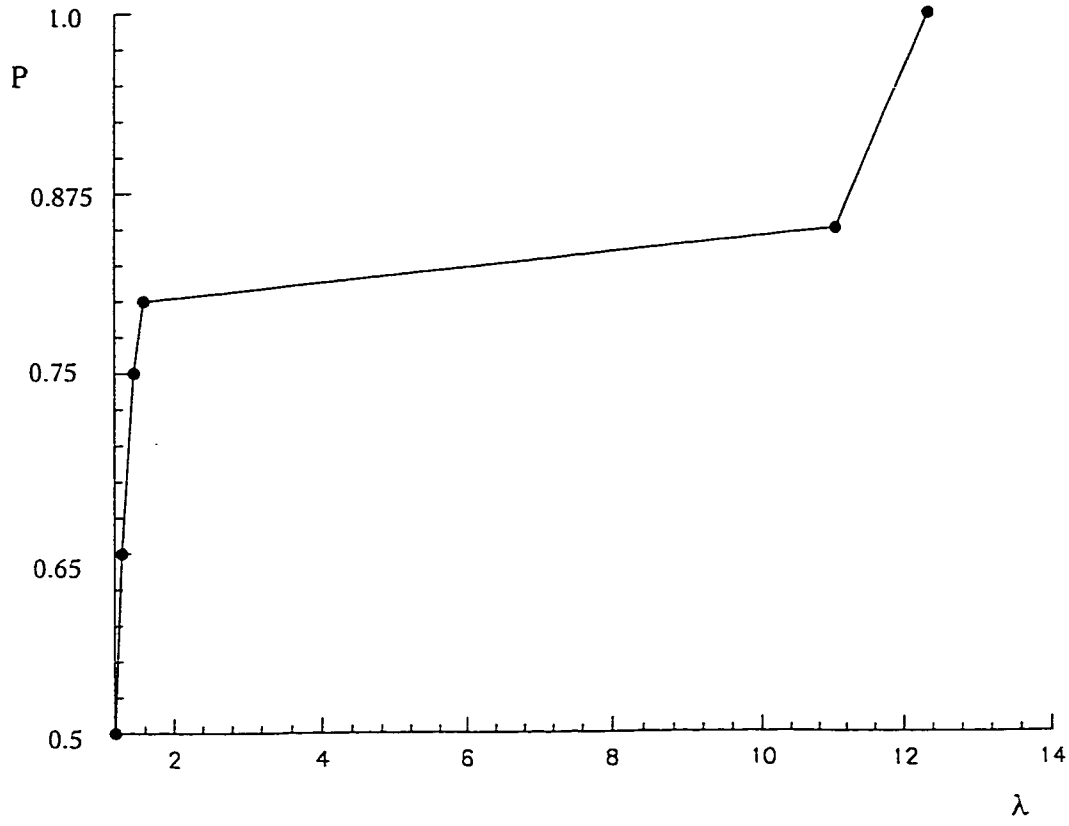

Fig. 5.1d Dimensionless pressure vs principal stretch λ, Ogden material

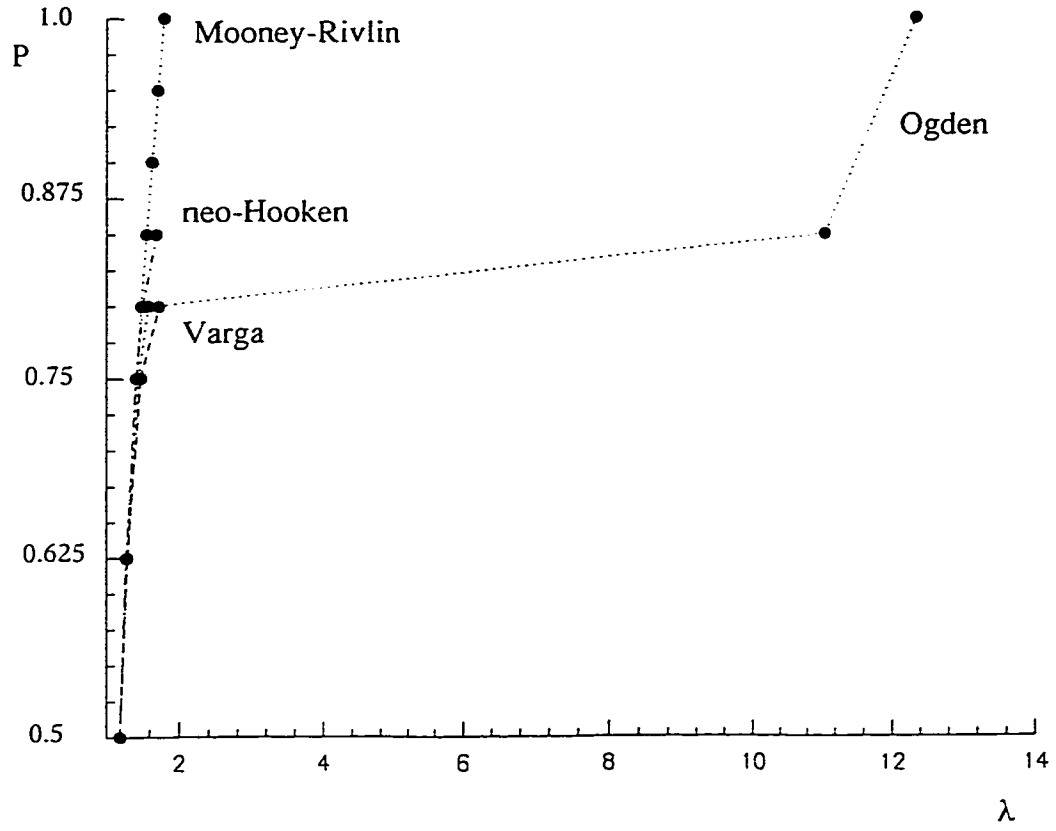

Fig. 5.1e Dimensionless pressure vs principal stretch λ,

Varga, Mooney-Rivlin, neo-Hooken, Ogden material

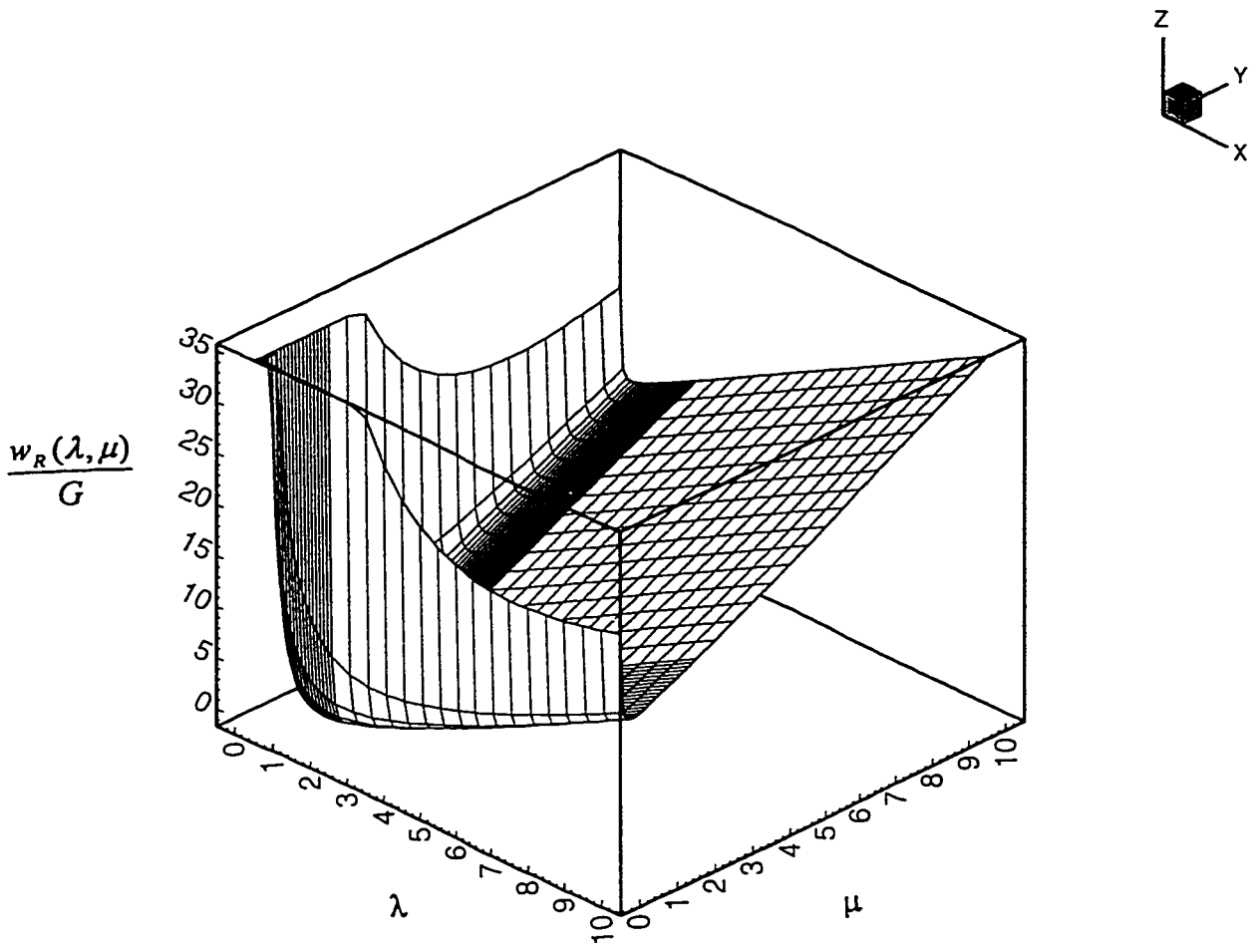

Fig. 5.2a Original Varga strain energy function,

for $0.02 \leq \lambda, \mu \leq 10.0$

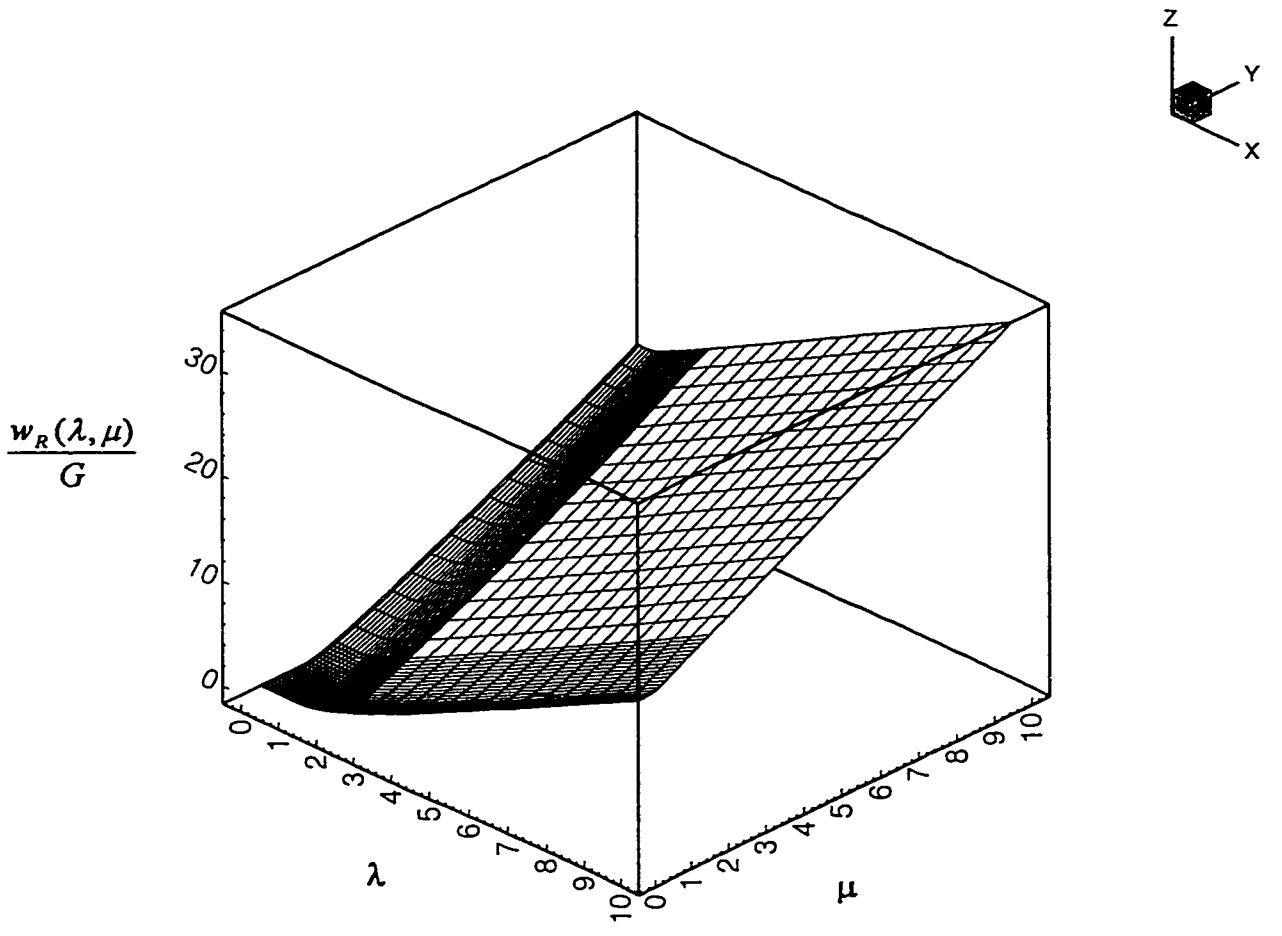

Fig. 5.2b Relaxed Varga strain energy function,

for $0.02 \leq \lambda, \mu \leq 10.0$

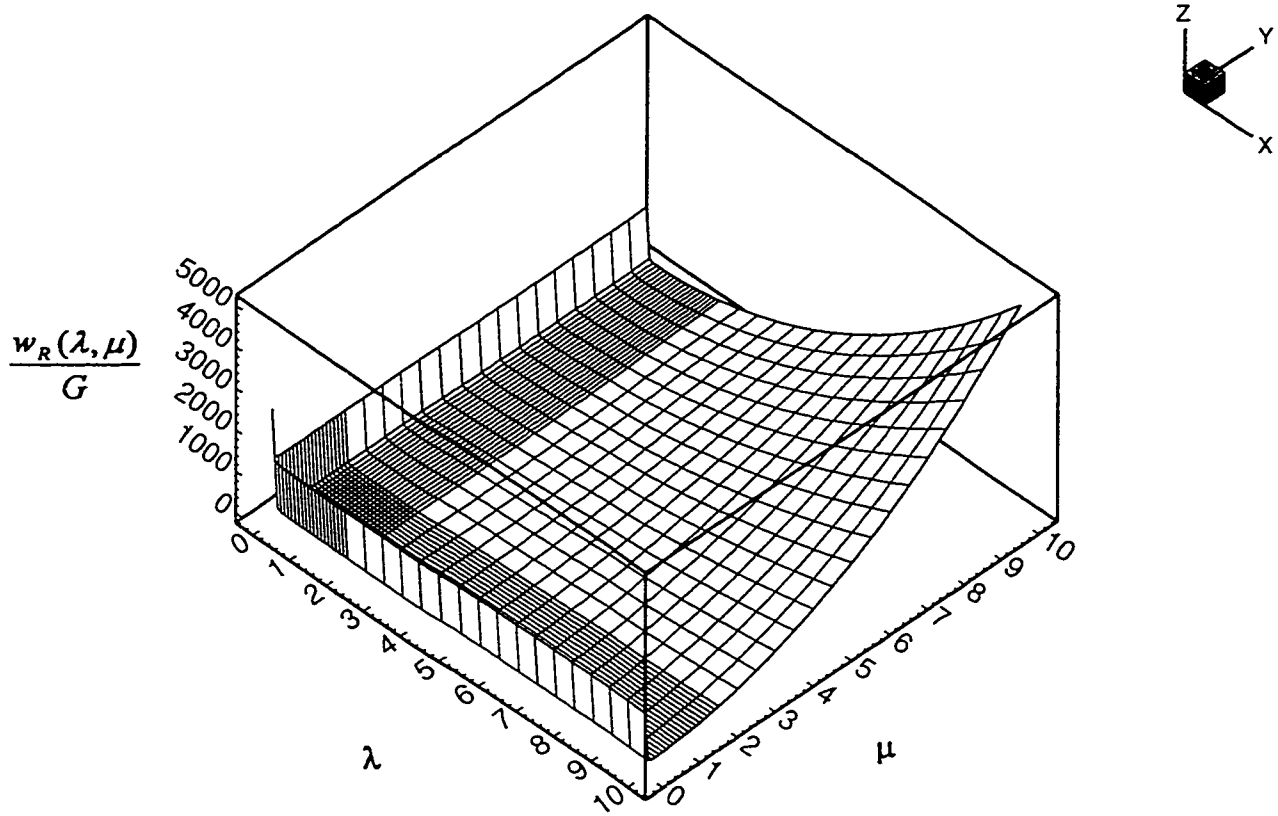

Fig. 5.3a Original Mooney-Rivlin strain energy function,

for $0.02 \leq \lambda, \mu \leq 10.0$

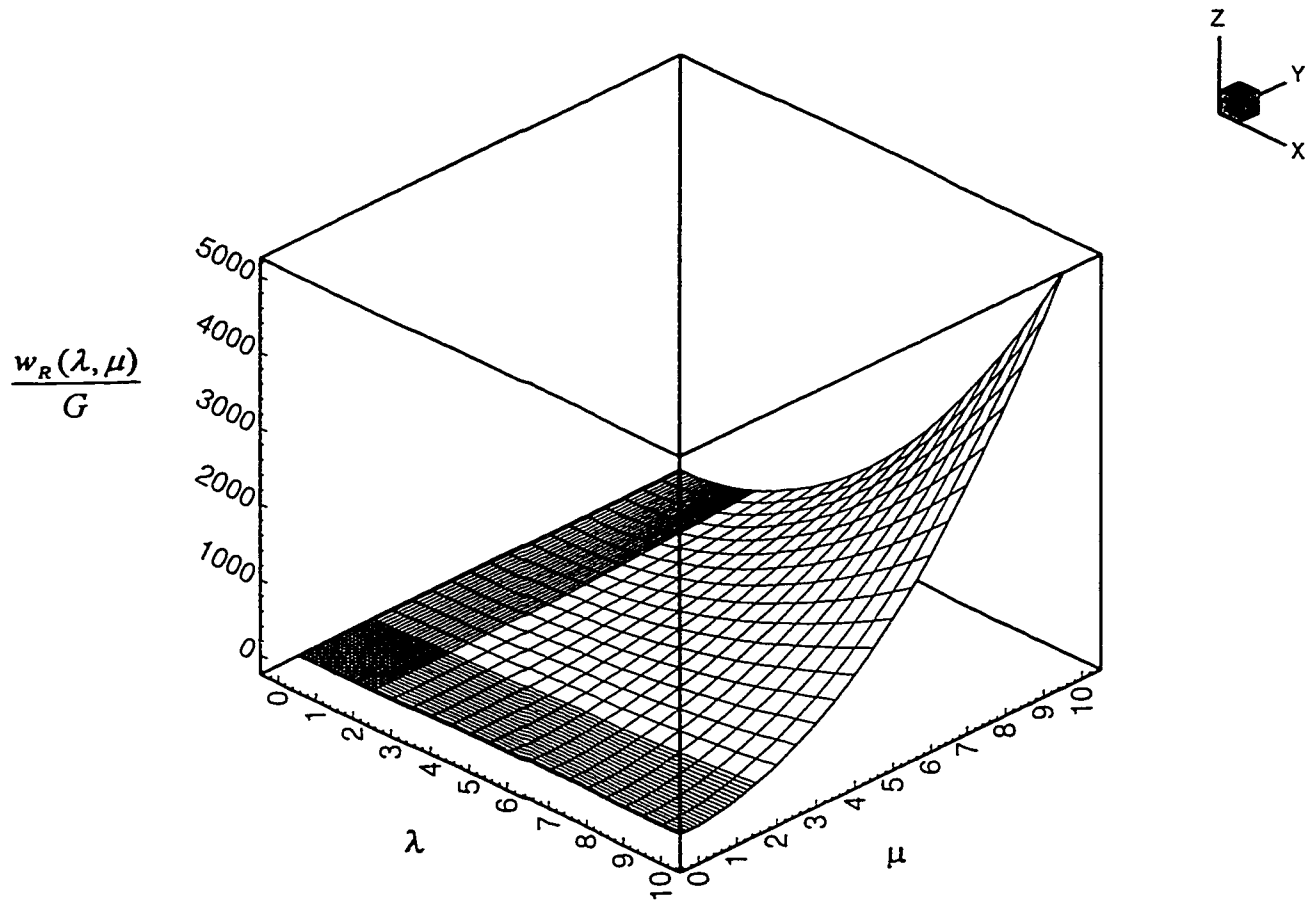

Fig. 5.3b Relaxed Mooney-Rivlin strain energy function,

for $0.02 \leq \lambda, \mu \leq 10.0$

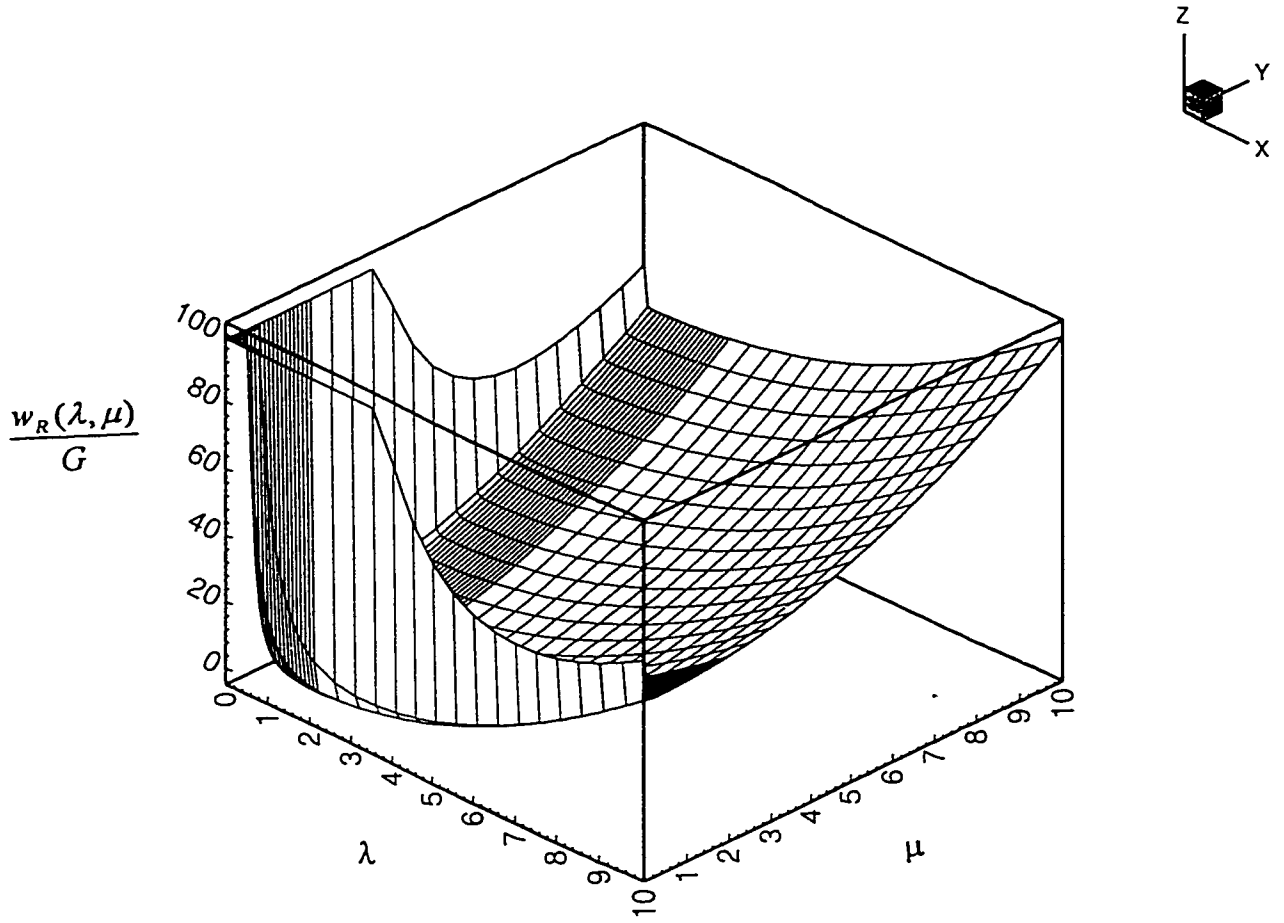

Fig. 5.4a Original neo-Hooken strain energy function,

for $0.02 \leq \lambda, \mu \leq 10.0$

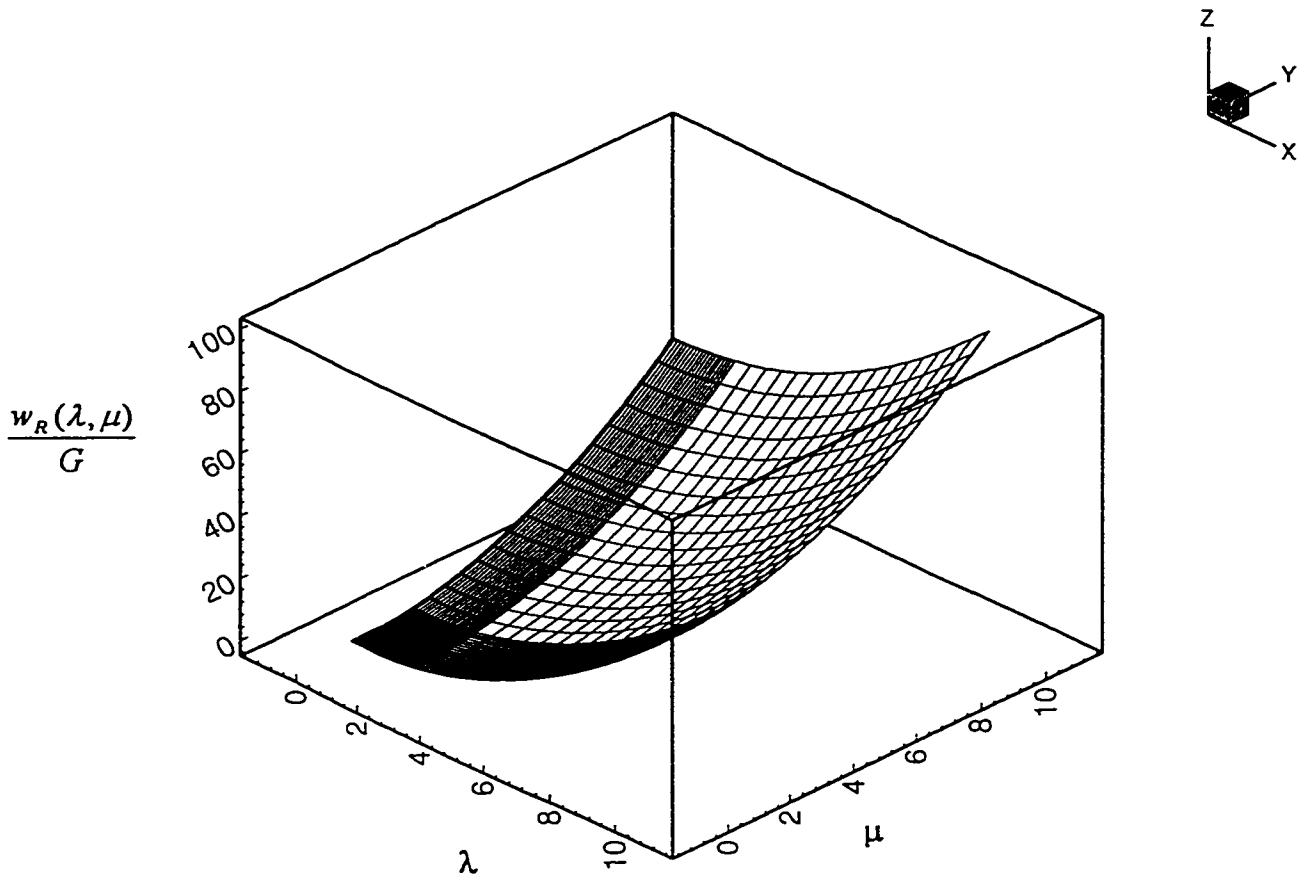

Fig. 5.4b Relaxed neo-Hooken strain energy function,

for $0.02 \leq \lambda, \mu \leq 10.0$

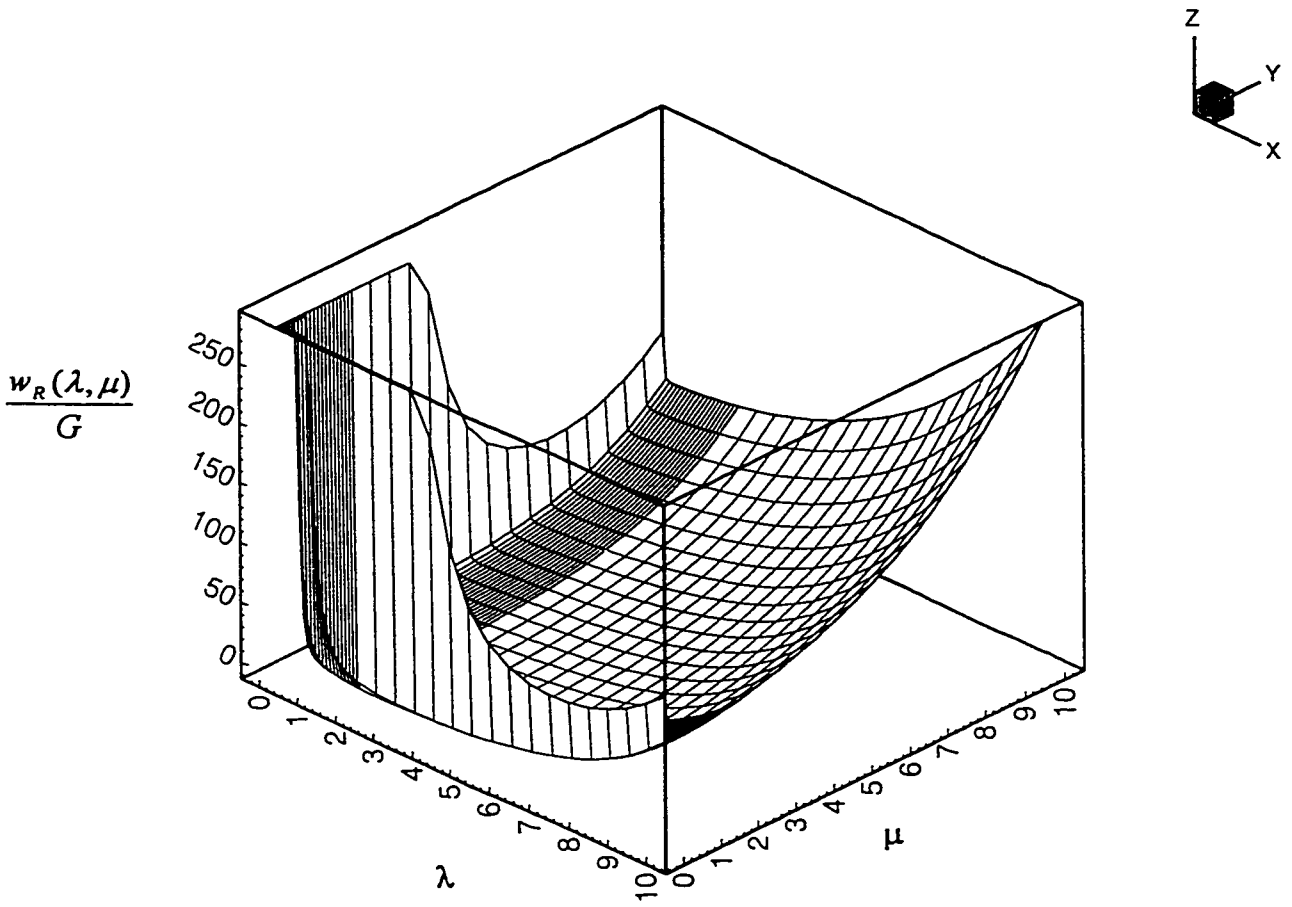

Fig. 5.5a Original Ogden strain energy function,

for $0.02 \leq \lambda, \mu \leq 10.0$

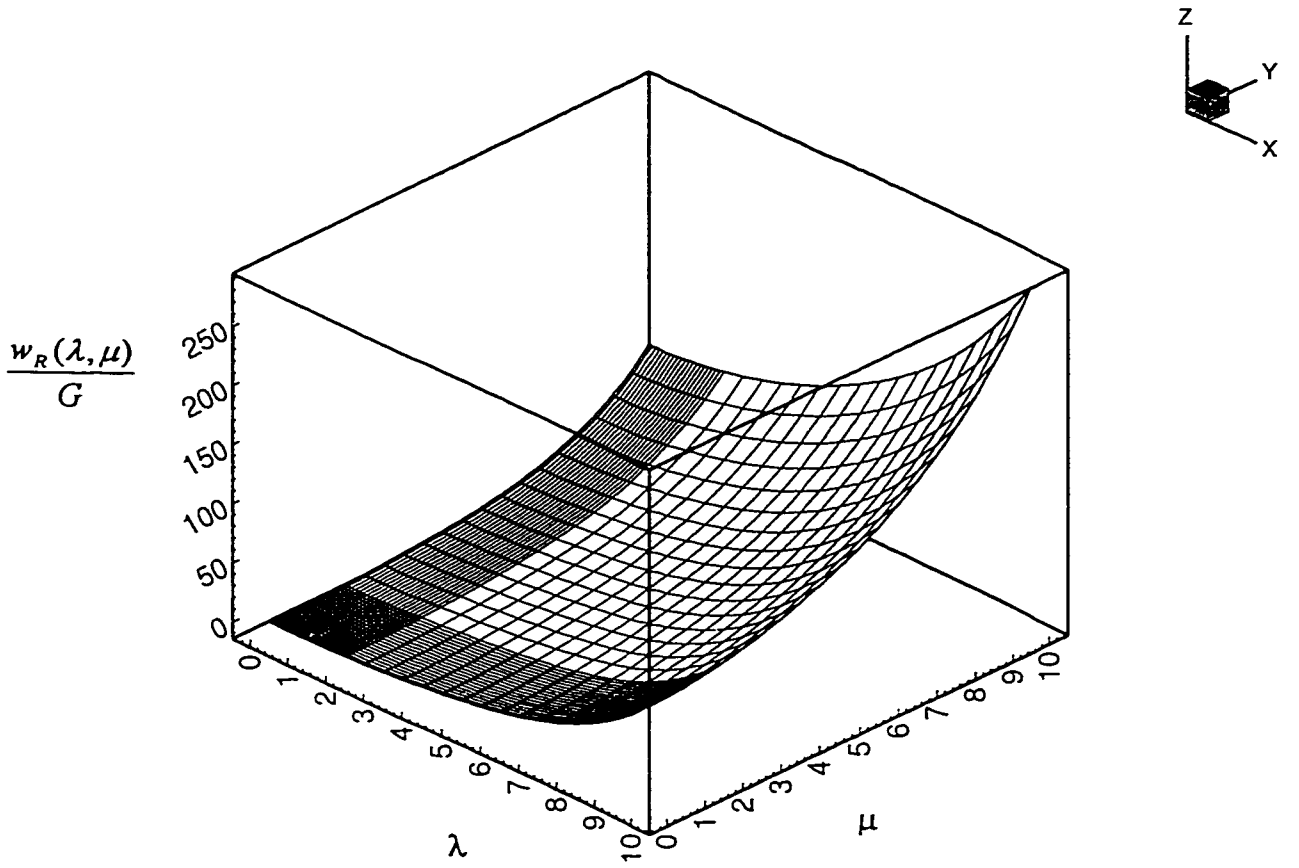

Fig. 5.5b Relaxed Ogden strain energy function,

for $0.02 \leq \lambda, \mu \leq 10.0$

5.3 Solutions to Problems Involving Ogden and Mooney-Rivlin Circular Membranes Subjected to Hydrostatic Pressure

A circular membrane with unit radius is considered. The reference configuration is shown in Fig. 5.6a. Ogden material is used first. The boundary is decreased from its initial value of 1.0 to 0.5, leading to a 50% contraction of the circumference, which is subsequently maintained fixed. Then, the entire membrane is subjected to pressure loading of the hydrostatic type. The hydrostatic pressure considered in this work is assumed as axisymmetic. Figure 5.6 shows the deformed configuration, which is nearly axisymmetric. Total wrinkling occurs in a region of constant width immediately adjacent to the boundary, followed by a partly wrinkled region. The tension trajectories are represented by dashed lines at the zone centered points, the lower part of the membrane is tense. Figure 5.6c shows the distribution of the principal stretch λ. The maximum computed value of λ is 1.1.6, and occurs at the zone-centered points situated in the vicinity of the parallel of maximum diameter. The principal direction of strain $\boldsymbol{l}$ is tangent to the meridian passing through each zone center. Fig. 5.6d shows the distribution of the principal stretch μ. The maximum computed value of μ is 1.15, and occurs at zone-centered points situated on a parallel immediately adjacent to the apex of the deformed surface. The principal direction of strain $\boldsymbol{m}$ is tangent to the parallel passing through zone centers. The distributions of the principal Cauchy stresses $w_\lambda u^{-1}$ and $w_\mu \lambda^{-1}$ along a meridian passing through zone-centered points are shown in Fig. 5.6e and Fig. 5.6f. The direction of $w_\lambda u^{-1}$ is along $\boldsymbol{l}$, tangent to the meridian. The maximum

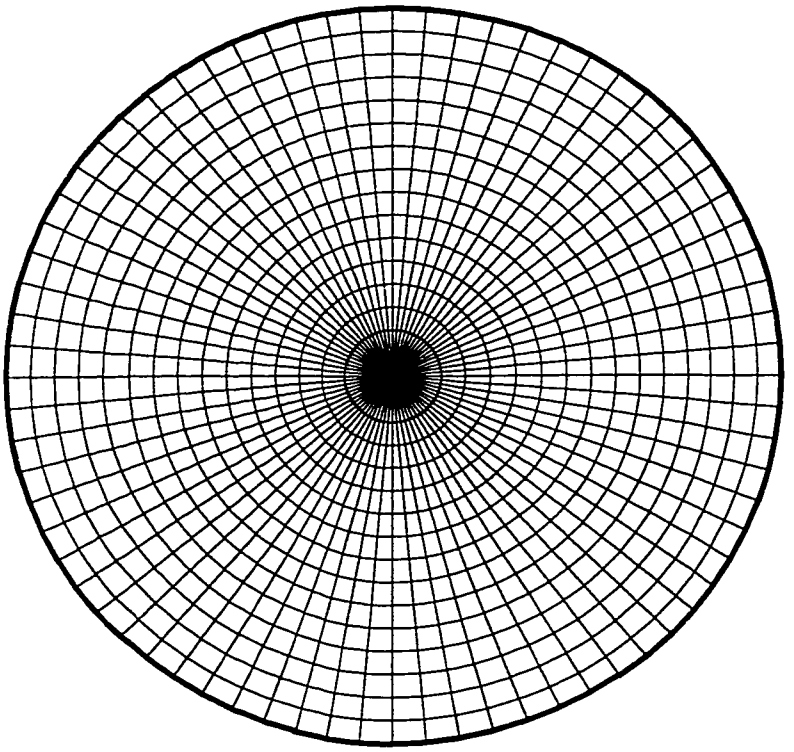

Fig. 5.6a Circular membrane;

meshed reference configuration

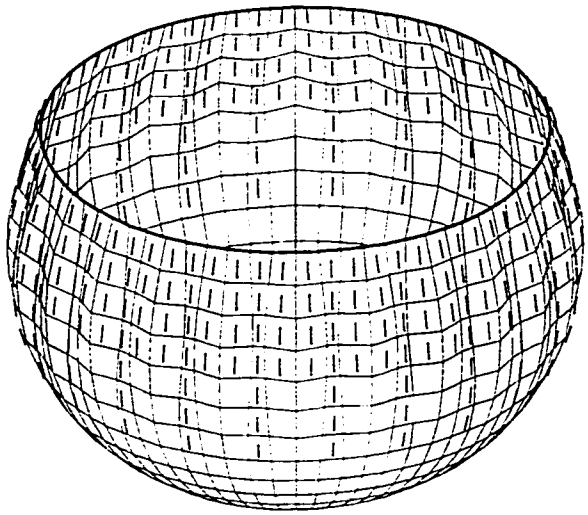

Fig. 5.6b Circular Ogden membrane

totally subjected to hydrostatic pressure,

combined with a 50% contraction of the boundary

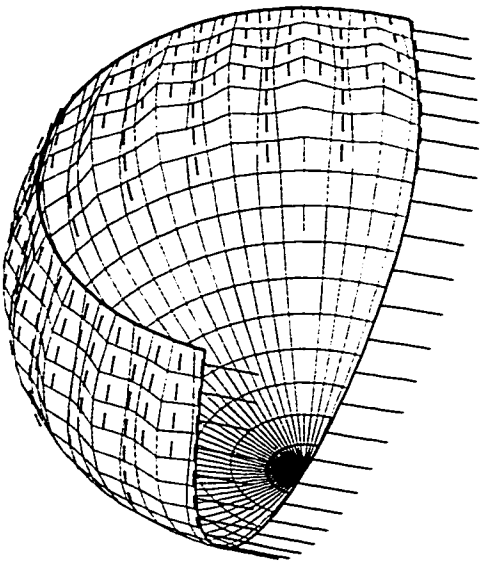

Fig. 5.6c Distribution of principal stretch λ

along a meridian passing through zone-centered points

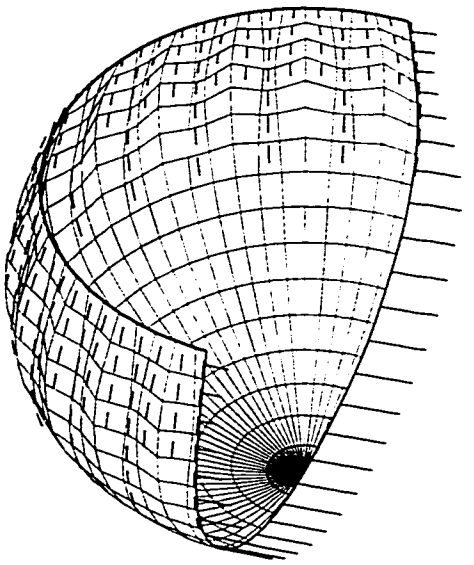

Fig. 5.6d Distribution of principal stretch μ

along a meridian passing through zone-centered points

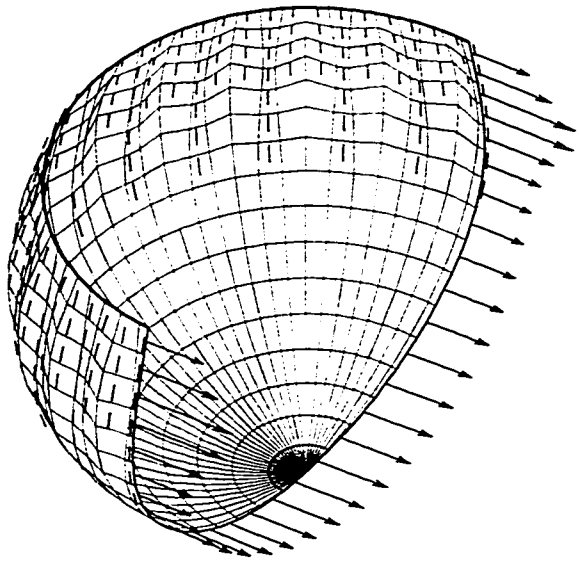

Fig. 5.6e Distribution of principal Cauchy stress $w_\lambda \mu^{-1}$

along a meridian passing through zone-centered points

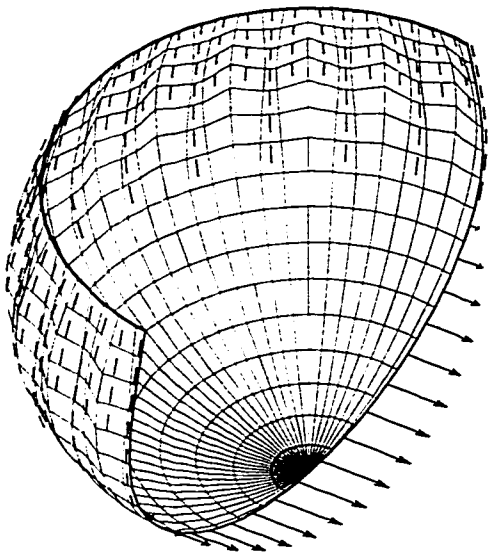

Fig. 5.6f Distribution of principal Cauchy stress $w_{\mu}\lambda^{-1}$

along a meridian passing through zone-centered points

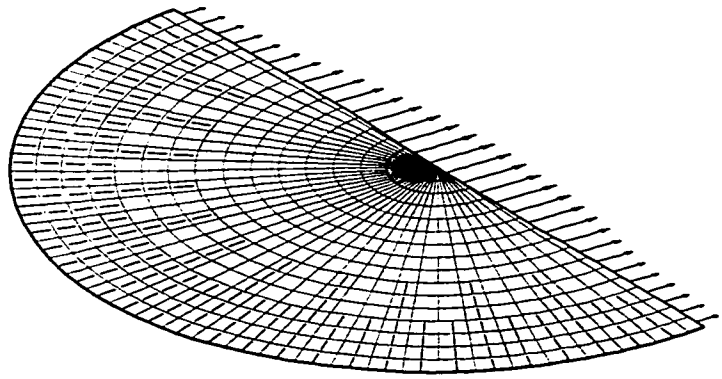

Fig. 5.6g Distribution of principal Piola stress w_λ

along a meridian passing through zone-centered points;

reference configuration

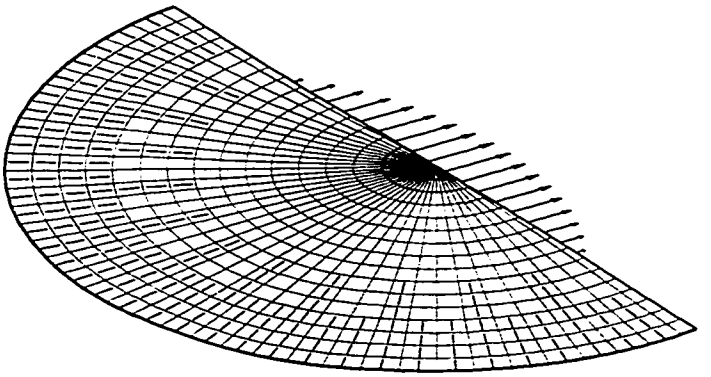

Fig. 5.6h Distribution of principal Piola stress w_{μ}

along a meridian passing through zone-centered points;

reference configuration

non-dimensional value of $w_\lambda u^{-1}$ is 0.840, and occurs at the zone-centered points situated along the parallel near the boundary. The direction of $w_\mu \lambda^{-1}$ is along $\boldsymbol{m}$, tangent to the parallel. The maximum non-dimensional value of $w_\mu \lambda^{-1}$ is 0.598, and occurs at the zone-centered points situated along the parallel immediately adjacent to the apex of the deformed surface. Fig. 5.6g and Fig. 5.6h show the distribution of the principal Piola stresses w_λ and w_μ along a meridian passing through zone-centered points. The direction of w_λ is along $\boldsymbol{L}$, tangent to the meridian (in the reference configuration), and the maximum non-dimensional value of w_λ is 0.695, occurring at the zone-centered points on the parallel immediately adjacent to the center of the undeformed configuration. The direction of w_μ is along $\boldsymbol{M}$, tangent to the parallel (in the reference configuration). The maximum non-dimensional value of w_μ is 0.693, occurring at the same zone-centered points as w_λ.

Next, the membrane is only partially subjected to a pressure loading of the hydrostatic type, while the boundary conditions remain unchanged. The non-dimensional volume of the liquid is 0.01. Fig. 5.7a shows the deformed configuration, which is almost axisymmetric, and Fig. 5.7b shows the liquid level. The unloaded region is completely wrinkled, whereas the loaded region is almost completely tense. The tension trajectories are represented by dashed lines at zone-centered points. Fig. 5.7c shows the distribution of the principal stretch λ along a meridian passing through zone centered points. The maximum computed stretch λ is 1.05, occurring at the zone-centered points situated along a parallel in the vicinity of the liquid level. The principal direction of strain $\boldsymbol{l}$

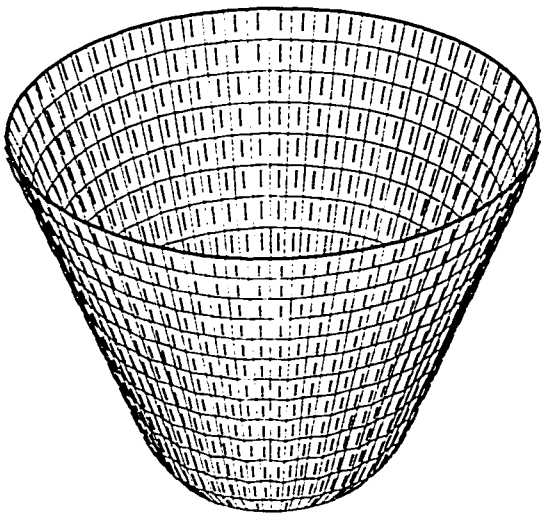

Fig. 5.7a Circular Ogden membrane

partly subjected to hydrostatic pressure,

combined with a 50% contraction of boundary

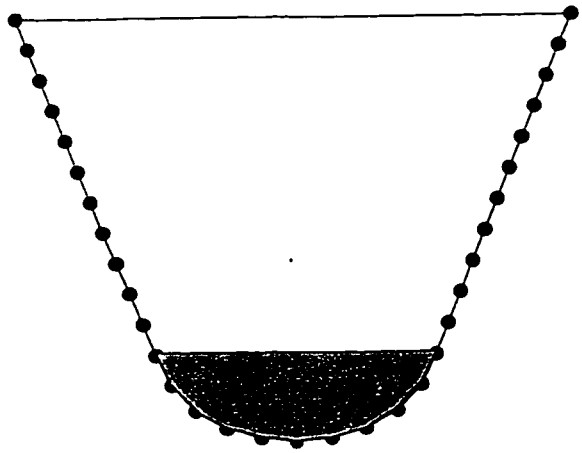

Fig. 5.7b Cross-section through a meridian of the deformed configuration;

liquid level shown

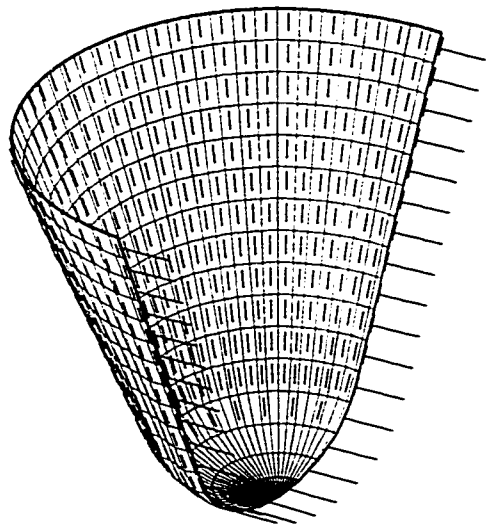

Fig. 5.7c Distribution of principal stretch λ

along a meridian passing through zone-centered points

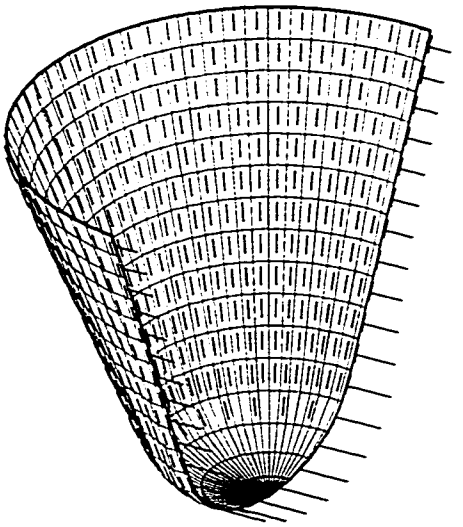

Fig. 5.7d Distribution of principal stretch μ

along a meridian passing through zone-centered points

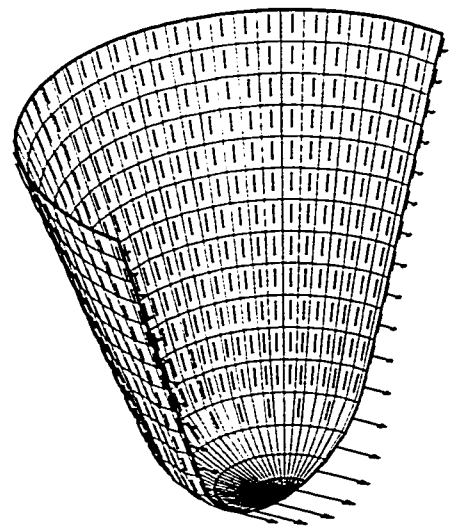

Fig. 5.7e Distribution of principal Cauchy stress $w_{\lambda}\mu^{-1}$

along a meridian passing through zone-centered points

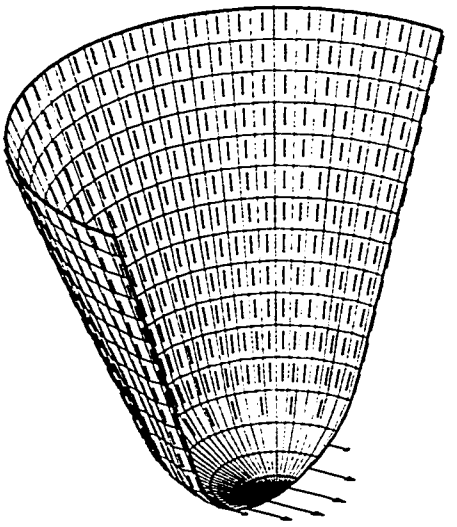

Fig. 5.7f Distribution of principal Cauchy stress $w_{\mu}\lambda^{-1}$

along a meridian passing through zone-centered points

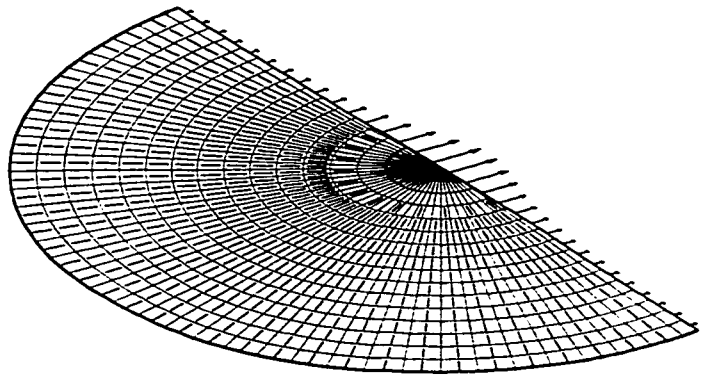

Fig. 5.7g Distribution of principal Piola stress w_{λ}

along a meridian passing through zone-centered points;

reference configuration

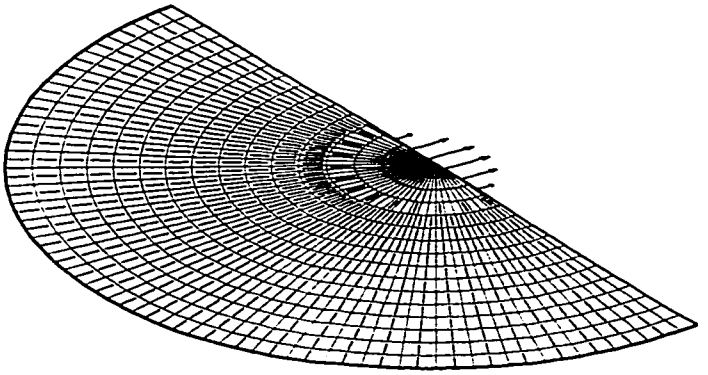

Fig. 5.7h Distribution of principal Piola stress w_{μ}

along a meridian passing through zone-centered points;

reference configuration

is tangent to the meridian passing through each zone center. Fig. 5,7d shows the distribution of the principal stretch μ along a meridian passing through zone-centered points. The maximum computed stretch μ is 1.04, and occurs at the zone-centered points situated along a parallel immediately adjacent to the apex of the deformed surface. The principal direction of strain $\boldsymbol{m}$ is tangent to the parallel passing through each zone center. The maximum non-dimensional values of the principal stresses $w_\lambda u^{-1}$ and $w_\mu \lambda^{-1}$ are 0.244 and respectively 0.233. Fig. 5.7e and Fig. 5.7f show their distributions along a meridian passing through zone-centered points. Both of the maximum non-dimensional values occur at the zone-centered points situated along the parallel immediately adjacent to the center of the reference configuration. The maximum non-dimensional intensity of the principal stresses w_λ and w_μ are 0.255 and respectively 0.246, and they both occur at zone centered points situated along the parallel immediately adjacent to the apex of the deformed surface. Fig. 5.7g and Fig. 5.7h show the distributions of w_λ and w_μ along a meridian passing through zone-centered points. The direction of w_λ is along $\boldsymbol{L}$, tangent to the meridian, and the direction of w_μ is along $\boldsymbol{M}$, tangent to the parallel (in the reference configuration).

Next, the Mooney-Rivlin material is used. For the same reference configuration, the radius of the boundary is reduced to zero. This model may be used to simulate the behavior of the biological tissues of a bladder. The deformed configuration is shown in Fig. 5.8a. Total wrinkling occurs in a region of constant width immediately adjacent to the boundary, whereas partly wrinkling occurs in the rest of the membrane surface. The deformation is not axisymmetric. The tension trajectories are represented by dashed

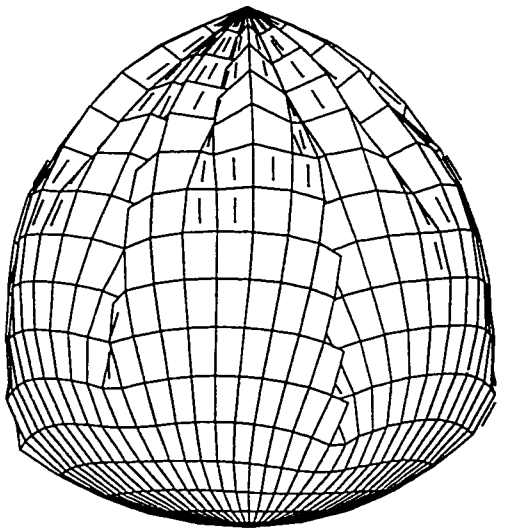

Fig. 5.8a Circular Mooney-Rivlin membrane

totaly subjected to hydrostatic pressure,

combined with a 100% contraction of boundary

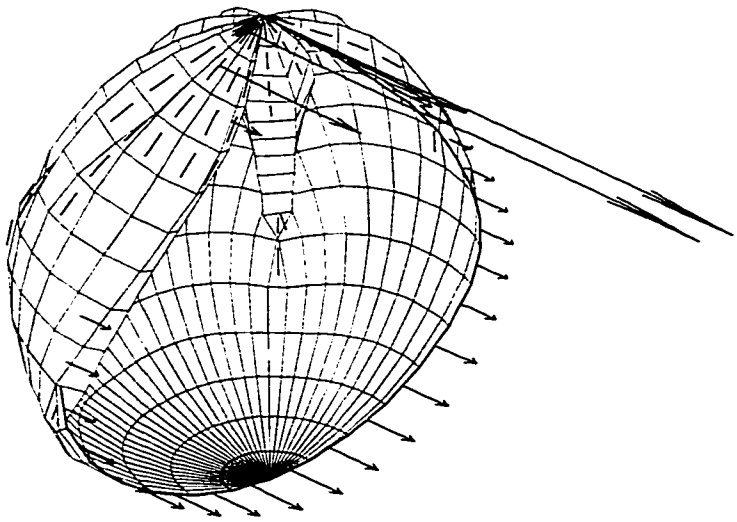

Fig. 5.8b Distribution of principal Cauchy stress $w_\lambda \mu^{-1}$

along a meridian passing through zone-centered points

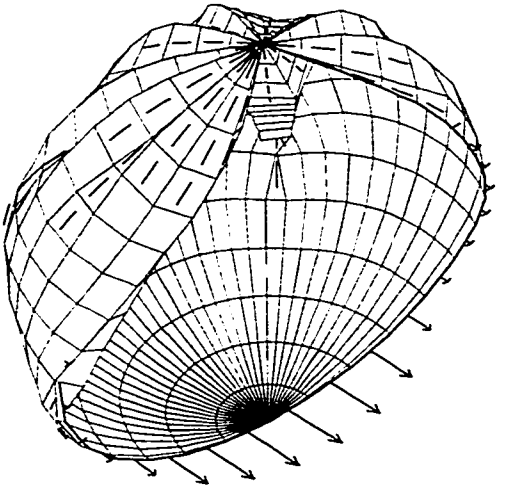

Fig. 5.8c Distribution of principal Cauchy stress $w_{\mu}\lambda^{-1}$

along a meridian passing through zone-centered points

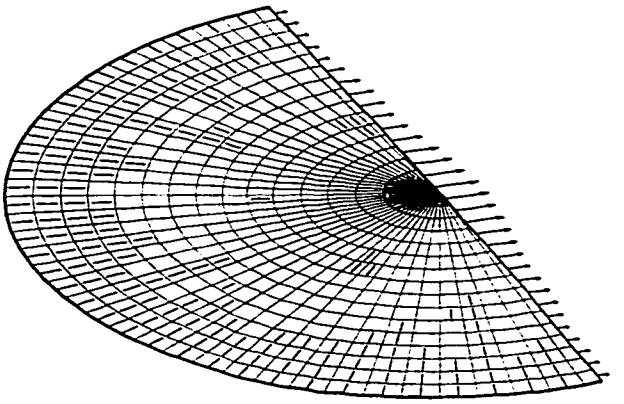

Fig. 5.8d Distribution of principal Piola stress w_λ

along a meridian passing through zone-centered points;

reference configuration

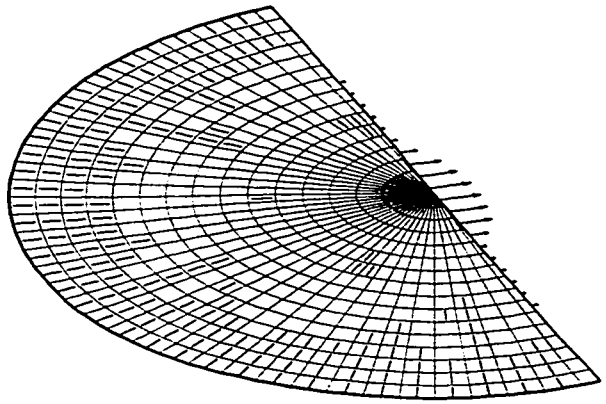

Fig. 5.8e Distribution of principal Piola stress w_{μ}

along a meridian passing through zone-centered points;

reference configuration

lines at zone-centered points. The principal directions are not shown in the tense regions. The maximum non-dimensional principal Cauchy stress $w_\lambda \mu^{-1}$ occurs at the zone-centered points situated along the parallel immediately adjacent to the boundary, and is much larger than the principal stresses at the other zone-centered points. The maximum non-dimensional value of $w_\mu \lambda^{-1}$ is 3.291. The direction of $w_\mu \lambda^{-1}$ is along $\boldsymbol{l}$, tangent to the meridian passing through the zone-centered points. The maximum non-dimensional value of the principal stress $w_\mu \lambda^{-1}$ is much smaller than the maximum non-dimensional values of $w_\lambda \mu^{-1}$. The maximum non-dimensional value of $w_\lambda \mu^{-1}$ is 0.377, and occurs at the zone-centered points situated along the parallel immediately adjacent to the apex. The direction of $w_\lambda \mu^{-1}$ is along $\boldsymbol{M}$, tangent to the parallel. The distributions of $w_\lambda \mu^{-1}$ and $w_\mu \lambda^{-1}$ along a meridian passing through zone-centered points are shown in Fig. 5.8b and Fig. 5.8c. The maximum Piola stresses w_λ and w_μ occur at the same zone-centered points situated along the parallel that is immediately adjacent to the apex. The distributions of w_λ and w_μ along a meridian passing through zone-centered points are shown in Fig. 5.8d and Fig. 5.8e. The maximum non-dimensional stress w_λ is 0.425 and the maximum non-dimensional stress w_μ is 0.411. The direction of w_λ is along $\boldsymbol{L}$, tangent to the meridian, and the direction of w_μ is along $\boldsymbol{M}$, tangent to the parallel (in the reference configuration).

The numerical results show a periodic non-axisymmetric structure of the deformation, corresponding to pleats in the membrane. The deformation contains regions of self

penetration of the membrane, which would not occur in practice. To model this behavior properly, the effects of self contact would need to be taken into consideration.

5.4 Solutions to the Ponding Problem

Planar inflatable membranes may be used as large-scale roof coverings. If an initial depression occurs at the apex, the Ponding Phenomenon may be observed to appear after rain or snow. This will cause geometric changes. In the present work, only axisymmetric liquid loading is considered. For safety considerations, the response of the structure to the overloading caused by hydrostatic pressure is of major importance.

An Ogden circular membrane with unit radius is considered. The reference configuration is plane, as shown in Fig 5.9a. A graded mesh is used in this application. The boundary conditions require that the radius of the membrane is reduced to 0.5 and then kept fixed. An uniform non-dimensional pressure $p = 2$ is applied upwards, and the configuration becomes spheroidal, as shown in Fig 5.9b. The deformed configuration is almost axisymmetric, wrinkling only occurring in the region near the boundary. The tension trajectories are represented by dashed lines at zone-centered points. The rest of the membrane is tense, and the principle directions of stress are not shown in the tense region. Next, if a depression occurs at the apex of the membrane structure and axisymmetric liquid loading is added into the depression, the Ponding Phenomenon can be observed. The response depends on the density of the liquid, the internal pressure and the geometric parameters of the membrane structure (Szyszkowski and Glockner, 1984). For the given internal pressure, the initial geometry and the displacement boundary conditions, the liquid density used here is such as to fill up to the depression's capacity with little additional deflection taking place. The deformed configuration is as

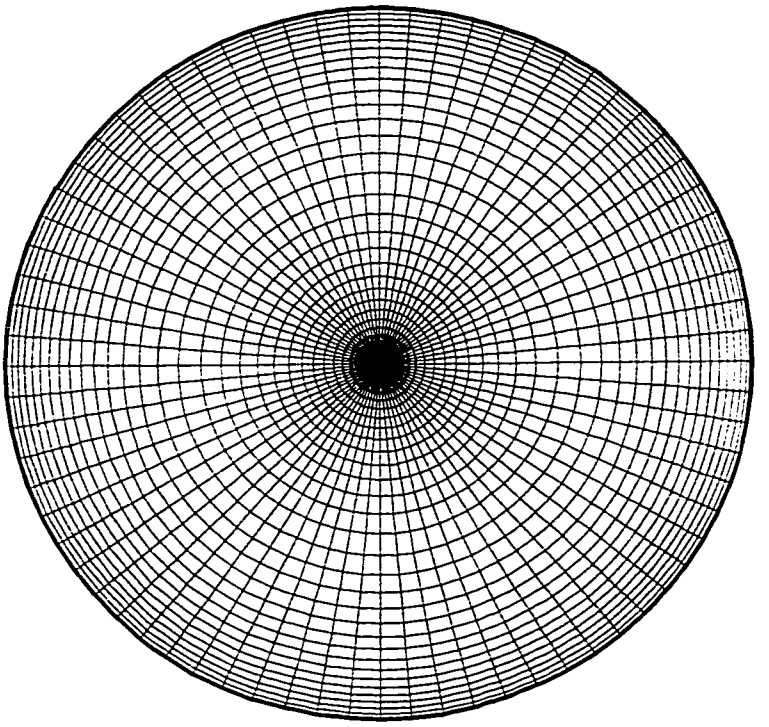

Fig. 5.9a Circular membrane;

meshed reference configuration

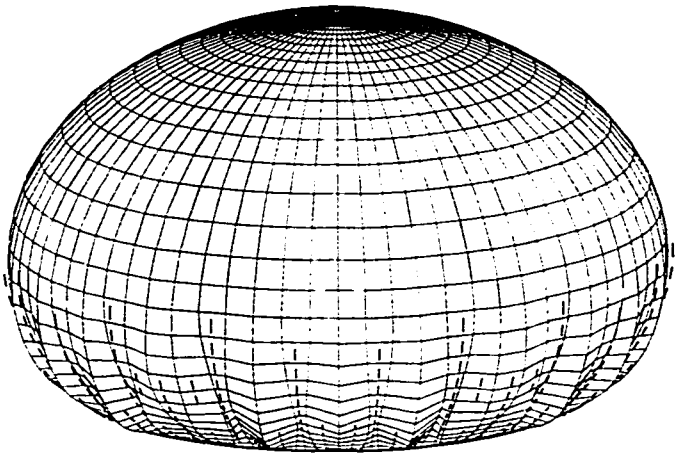

Fig. 5.9b Circular Ogden membrane

totally subjected to a uniform pressure,

combined with a 50% contraction of the boundary

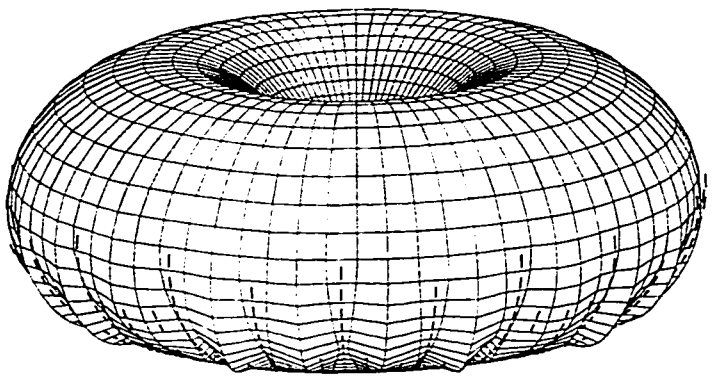

Fig. 5.9c Circular Ogden membrane simultaneously subjected to internal uniform pressure and external pressure loading of a hydrostatic type, combined with a 50% contraction of the boundary

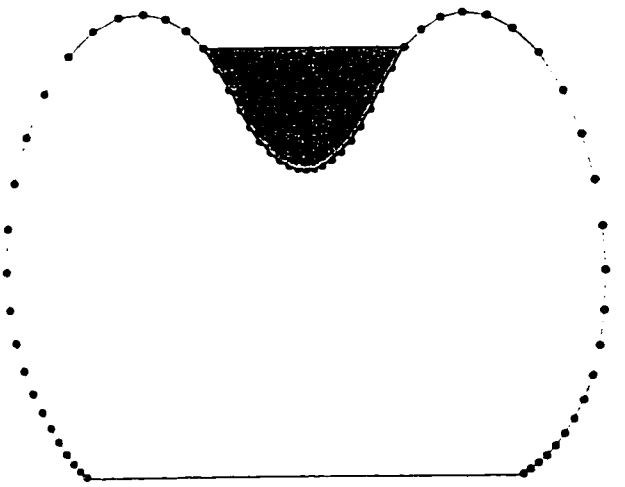

Fig. 5.9d Crosse-section through a meridian of the deformed configuration, liquid level shown

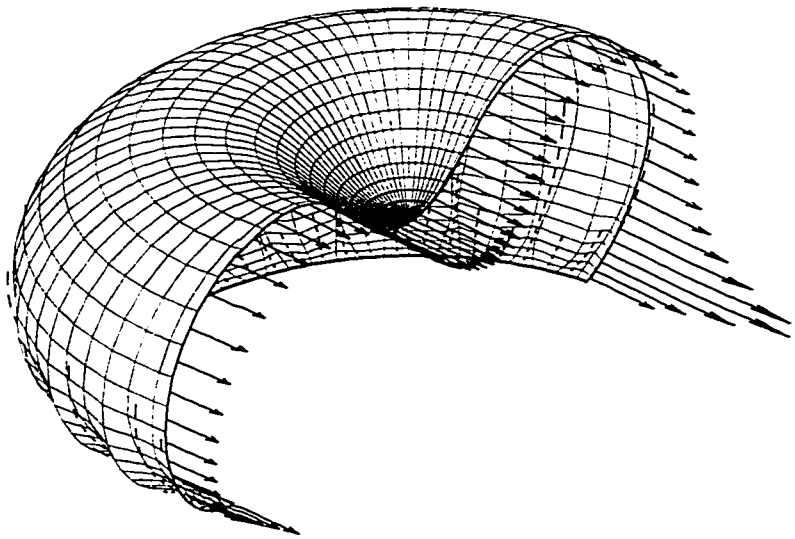

Fig 5.9e Distribution of principal Cauchy stress $w_\lambda \mu^{-1}$

along a meridian passing through zone-centered points

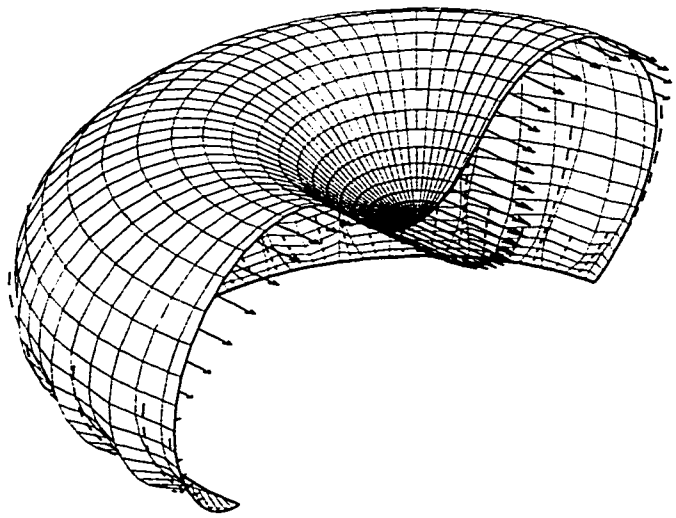

Fig. 5.9f Distribution of principal Cauchy stress $w_\mu \lambda^{-1}$

along a meridian passing through zone-centered points

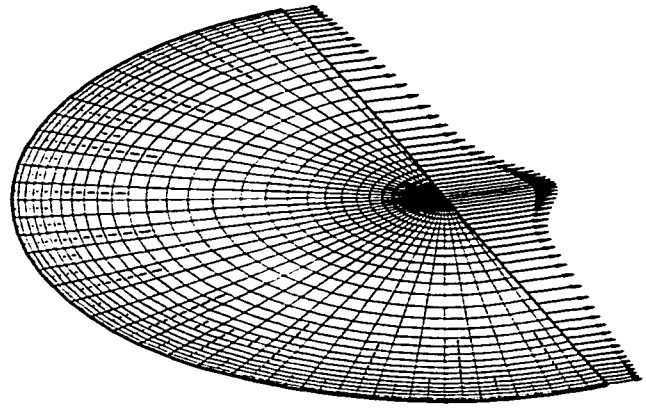

Fig. 5.9g Distribution of principal Piola stress w_λ

along a meridian passing through zone-centered points;

reference configuration

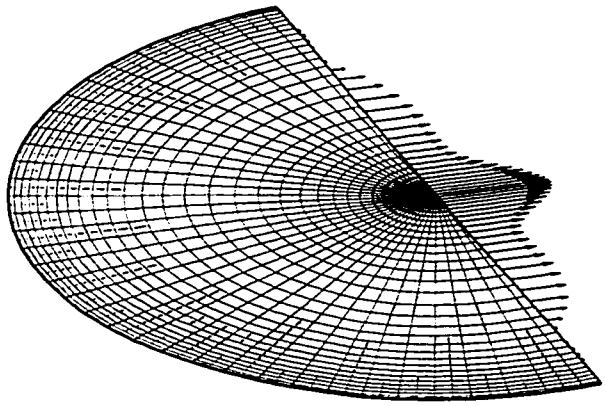

Fig. 5.9h Distribution of principal Piola stress w_{μ}

along a meridian passing through zone-centered points;

reference configuration

shown in Fig 5.9c. The wrinkling occurs at almost the same zone-centered points as in the case of the internal pressure loading only. The deformed configuration is almost axisymmetric. The tension trajectories are represented by dashed lines at zone-centered points. The principal directions of stresses are not shown in the tense region. Fig. 5.9d shows the liquid level. Fig. 5.9e shows the distribution of the principal Cauchy stress $w_\lambda \mu^{-1}$ along a meridian passing through zone-centered points. The direction of $w_\lambda \mu^{-1}$ is along l, tangential to the meridian. The maximum non-dimensional value of $w_\lambda \mu^{-1}$ is 1.22, and occurs at the zone-centered points situated along the parallel near the boundary. Fig. 5.9f shows the distribution of $w_\mu \lambda^{-1}$ along a meridian passing through zone-centered points, and the maximum non-dimensional value is 0.8543, which occurs at the zone-centered points situated along the parallel adjacent to the apex of the deformed surface. The direction of $w_\mu \lambda^{-1}$ is along $\boldsymbol{m}$, tangent to the parallel. Figure 5.9g shows the distribution of the principal Piola stress w_λ, with the maximum non-dimensional value of 1.13. Figure 5.9h shows the distribution of w_μ, and the maximum non-dimensional value is 1.12. The maximum values of w_λ and w_μ both happen at the zone-centered points situated along the parallel adjacent to the apex. The direction of w_λ is along $\boldsymbol{L}$, tangent to the meridian, and the direction of w_μ is along $\boldsymbol{M}$, tangent to the parallel (in the reference configuration).

If too much liquid is accumulated in the depression at the apex of the membrane, the structure will fail. The quantity of the liquid corresponding to this critical situation can be easily predicted with this model.

5.5 Solutions to Problems Involving Mooney-Rivlin Cylindrical Membranes Totally Subjected to Pressure Loading

A cylindrical membrane with unit radius and a height of 2π is shown in Fig.5.10a. Since the numerical model developed in this work is suitable to membrane structures with plane reference configurations, the cylindrical membrane is developed into a square membrane, by cutting it along a generatrix. The resulting square has a side length of 2π. The meshed square membrane is shown in Fig. 5.10b. A graded mesh is used. To impose the boundary conditions, the cylindrical configuration is considered again. Then, while the radius of the top boundary is kept fixed, the radius of the bottom boundary is reduced to zero. First a non-dimensional uniform pressure of 1.0 is applied in order to compare the response with the one for the same boundary conditions but for a membrane subjected to hydrostatic pressure loading. The deformed configuration of the membrane subjected to the uniform pressure is shown in Fig. 5.10c. This is almost axisymmetric. Total wrinkling occurs in a region immediately adjacent to the bottom boundary, followed by a partly wrinkled region. The tension trajectories are presented by dashed lines at zone-centered points. The remaining part of the membrane is tense. The principal directions of the stress are not shown in the tense region. Fig. 5.10d shows the distribution of the principal Cauchy stress $w_\lambda \mu^{-1}$ along a generatix passing through zone-centered points, the maximum non-dimensional value being 2.8265, and occurring at the zone-centered points situated along the parallel adjacent to the bottom boundary. The direction of $w_\lambda \mu^{-1}$ is along l, tangent to the generatrix. Fig. 5.10e shows the distribution of $w_\lambda \mu^{-1}$

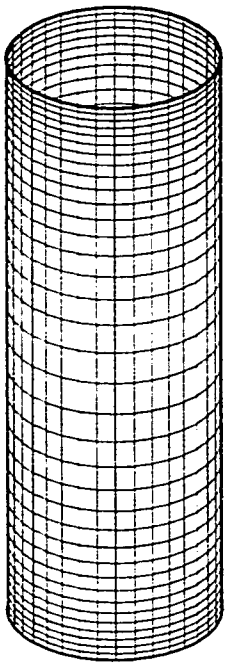

Fig. 5.10a Cylindrical Mooney-Rivlin membrane;

meshed reference configuration

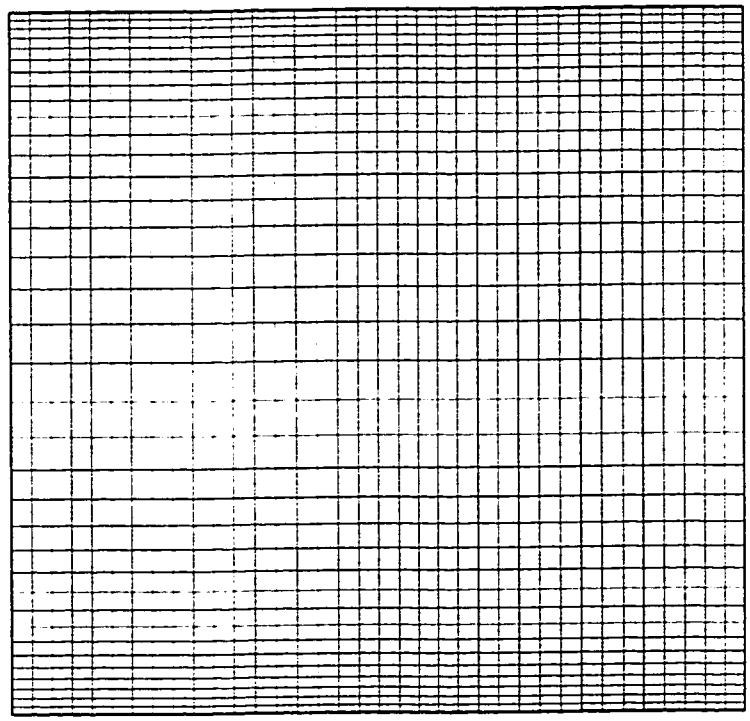

Fig. 5.10b Square Mooney-Rivlin membrane;

meshed reference configuration

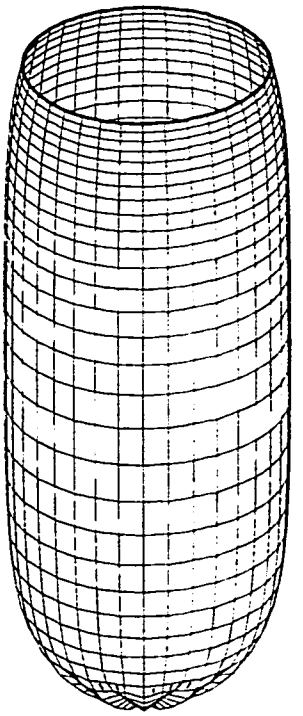

Fig. 5.10c Cylindrical Mooney-Rivlin membrane,

subjected to uniform pressure,

with fixed upper boundary and a 100% contraction of the lower boundary

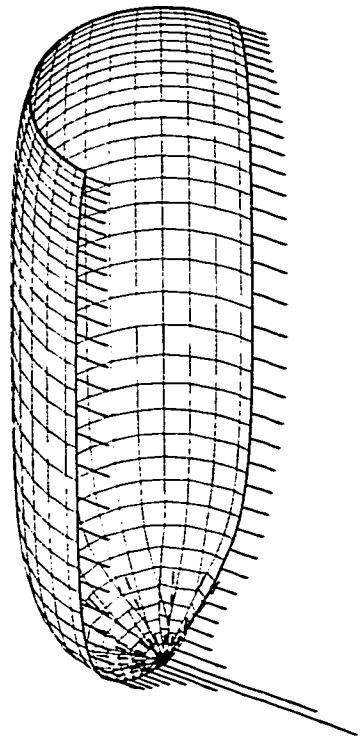

Fig. 5.10d Distribution of principal Cauchy stress $w_\lambda \mu^{-1}$

along a generatrix passing through zone-centered points

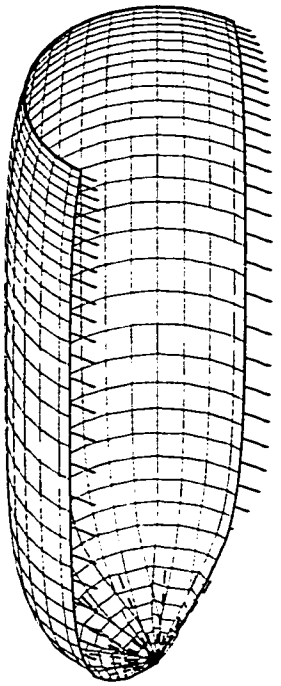

Fig. 5.10e Distribution of principal Cauchy stress $w_\mu \lambda^{-1}$

along a generatrix passing through zone-centered points

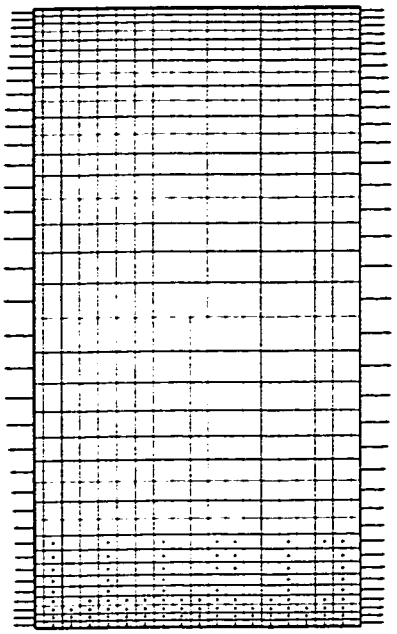

Fig. 5.10f Distribution of principal Piola stress w_λ

along a generatrix passing through zone-centered points;

reference configuration

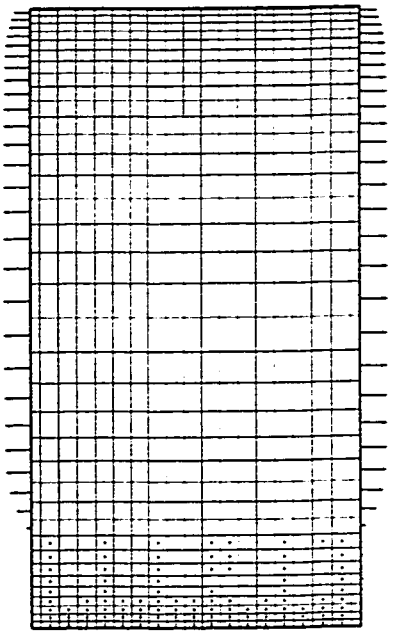

Fig. 5.10g Distribution of principal Piola stress w_μ

along a generatrix passing through zone-centered points;

reference configuration

along a generatrix passing through zone-centered points. The maximum non-dimensional value is 1.7423, and occurs at zone-centered points situated in the vicinity of the parallel of maximum diameter of the membrane. The direction of $w_\lambda \mu^{-1}$ is along $\boldsymbol{m}$, which is tangent to the parallel. For the Piola stresses, the distribution of w_λ along a generatrix passing through zone-centered points is shown in Fig. 5.10f. The maximum non-dimensional value of w_λ is 1.7423, and occurs at the zone-centered points situated in the vicinity of the parallel of the maximum diameter of the membrane. The direction of w_λ is along $\boldsymbol{L}$, tangent to the generatrix. The maximum non-dimensional value of w_μ occurs at the same zone-centered points as w_λ, its value being 1.4092. Fig. 5.10g shows the distribution of w_μ along a generatrix passing through zone-centered points. The direction of w_μ is along $\boldsymbol{M}$, tangent to the parallel (in the reference configuration).

Then the membrane is totally subjected to hydrostatic instead of uniform pressure. Figure 5.11a shows the deformed configuration, which is almost axisymmetric. Wrinkling also occurs only at the bottom of the membrane, as shown in Fig. 5.11b, representing the bottom view. The distribution of the principal Cauchy stress $w_\lambda \mu^{-1}$ along a generatrix passing through zone-centered points presented in Fig. 5.11c. The maximum non-dimensional value is 2.667, and occurs at the zone-centered points situated along the parallel adjacent to the bottom. The direction of $w_\lambda \mu^{-1}$ is along $\boldsymbol{l}$, tangent to the generatrix. Figure 5.11d shows the distribution of $w_\mu \lambda^{-1}$ along a generatrix passing through zone-centered points. The maximum non-dimensional value is 1.4625, and occurs at zone-centered points situated in the vicinity of the parallel of maximum

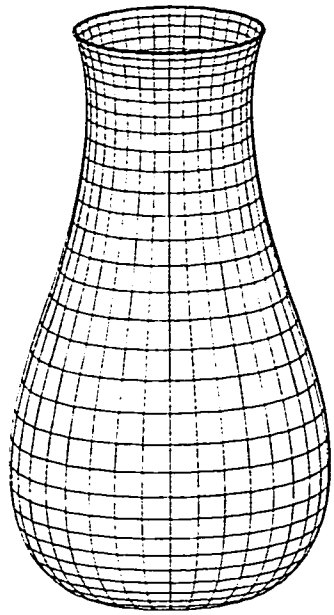

Fig. 5.11a Cylindrical Mooney-Rivlin membrane

with fixed upper boundary and a 100% contraction of the lower boundary,

totally subjected to hydrostatic pressure

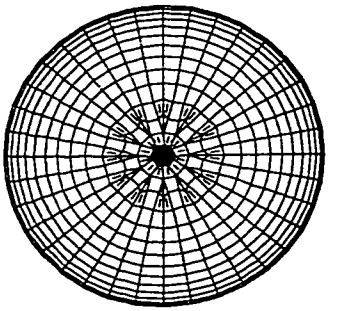

Fig. 5.11b Bottom view

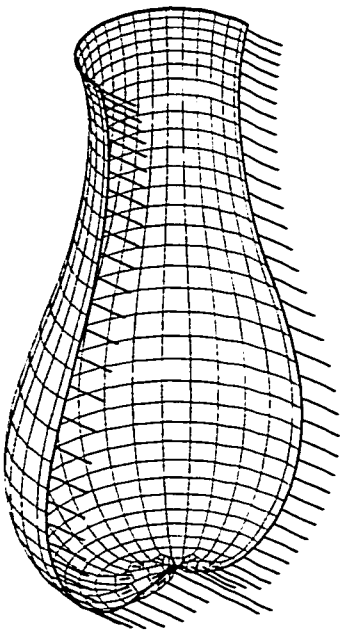

Fig. 5.11c Distribution of principal Cauchy stress $w_{\lambda}\mu^{-1}$

along a generatrix passing through zone-centered points

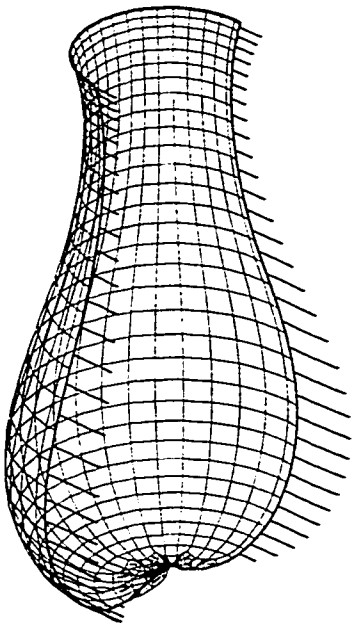

Fig. 5.11d Distribution of principal Cauchy stress $w_{\mu}\lambda^{-1}$

along a generatrix passing through zone-centered points

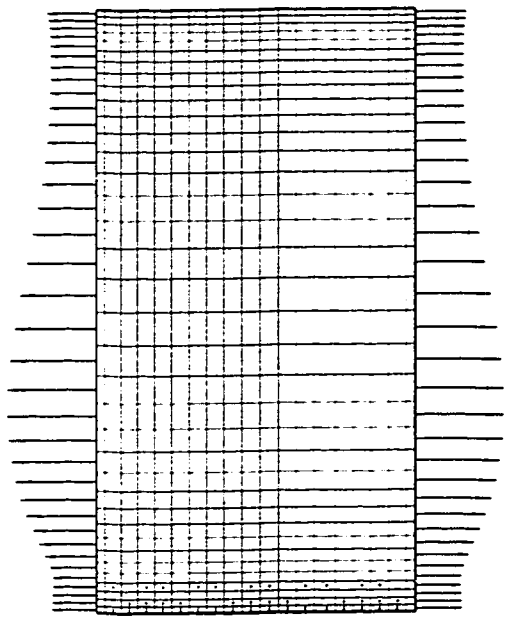

Fig. 5.11e Distribution of principal Piola stress w_λ

along a generatrix passing through zone-centered points;

reference configuration

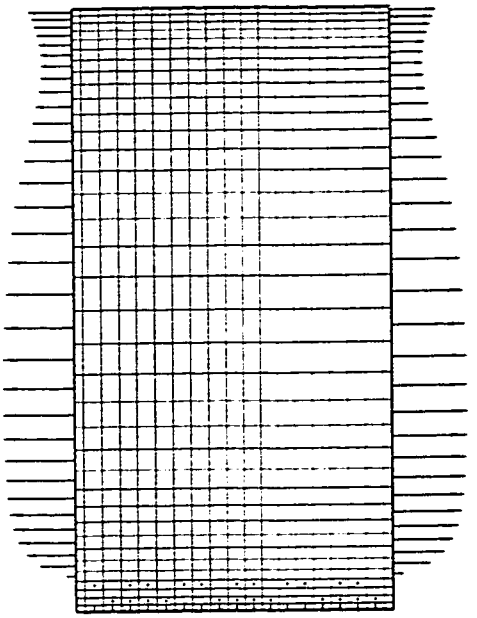

Fig. 5.11f Distribution of principal Piola stress w_μ

along a generatrix passing through zone-centered points;

reference configuration

diameter. The direction of $w_\mu \lambda^{-1}$ is along $\boldsymbol{m}$, tangent to the parallel. The distribution of the principal Piola stress w_λ is shown in Fig. 5.11e. Its maximum non-dimensional value is 1.0813, and occurs at the zone-centered points situated in the vicinity of the parallel to the maximum diameter. The direction of w_λ is along $\boldsymbol{L}$, tangent to the generatrix. Figure 5.11f shows the distribution of w_μ along a generatrix passing through zone-centered points. The maximum non-dimensional value is 1.0574, and occurs at the same zone-centered points as w_λ. The direction of w_λ is along $\boldsymbol{M}$, tangent to the parallel (in the reference configuration).

From the above figures it can be observed that the deformed configurations of the cylindrical membrane with similar boundary conditions but subjected first to uniform pressure and subsequently to hydrostatic pressure are very different. The distributions of the principal Cauchy stresses and of the Piola stresses are also different.

Chapter 6

Experimental Validation

6.1 Introduction

Numerical solutions of static problems involving isotropic elastic membranes undergoing finite deformations can be obtained by using the numerical technique based on the DR method. All the membranes considered here started with plane reference configurations and ended with 3D surfaces as deformed configurations. An experiment has been designed with the objective to verify the numerical model developed in this work. It would be desirable to design an experiment and obtain experimental results for one of the problems given in Chapter 5, but there are technical difficulties to achieve this. Pressure loading of the hydrostatic type on an elastic membrane with displacement boundary conditions is challenging to model experimentally. Therefore the validation of a simple problem with numerical as well as exact solutions already given by Haseganu (1994) is chosen. Also due to the limitations of the measuring equipment, only the trend of the experimental results is presented in this work.

6.2 Numerical Model

For the numerical model, the reference configuration is a square membrane with sides of unit length. Fig. 6.1a shows the meshed reference configuration. The mesh density is 21×21. The Ogden strain energy function is employed. The following displacement boundary conditions are imposed: the boundary of the square is deformed into a rhombus while maintaining the lower boundary fixed until the left boundary forms an angle of 35° and then 45° with the vertical. The deformed configuration is shown in Fig. 6.1b, respectively Fig. 6.1c. The trajectories of tensile stress are represented by dashed lines at zone-centered points, indicating wrinkling over the entire membrane. Computed numerical results for the displacement of every node, the principal stretches and the principal directions at every zone-centered point were obtained.

6.3 Experimental Model

Strain gages are generally used to measure the strain at a material particle of an elastic material, then the stress may be obtained from the constitutive equation. But the common strain gages cannot be used here, since by mounting the gages a substantial variation in the local stiffness of the membrane material would occur, and this would considerably alter the response of the membrane. Also these gages are used for infinitesimal strain. Thus in this work, the principal stretches λ and μ and the principal direction l were obtained from an experiment by measuring the coordinates at chosen testing point.

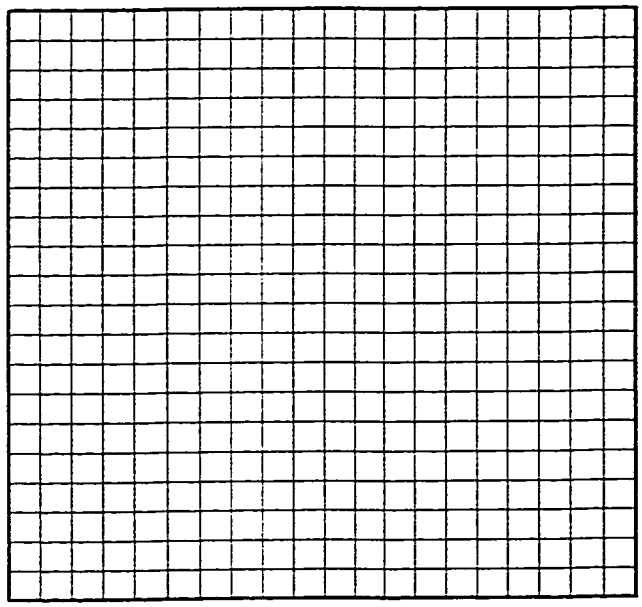

Fig. 6.1a Square membrane;

meshed reference configuration

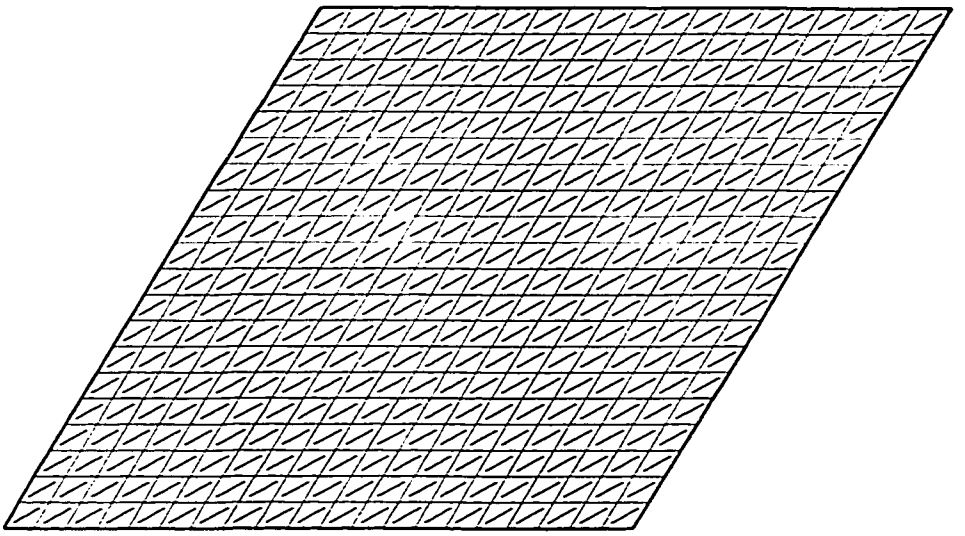

Fig. 6.1b Square membrane subjected to shearing (35°)

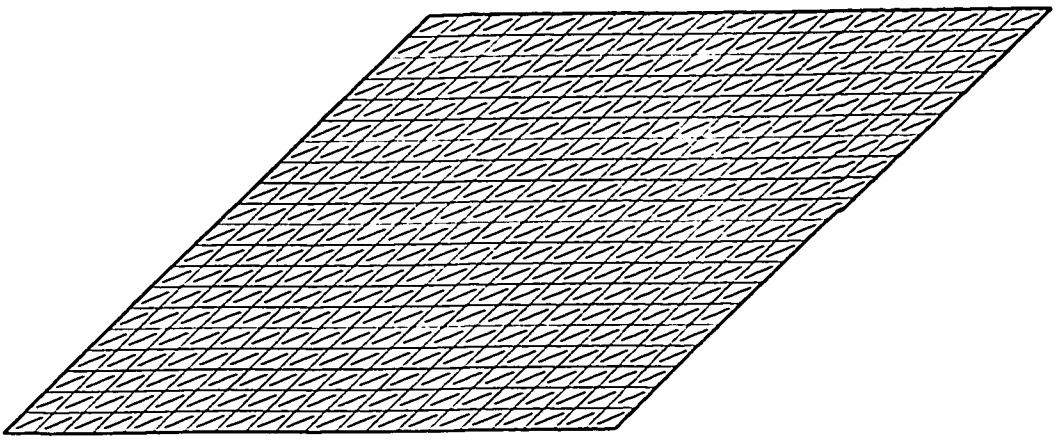

Fig. 6.1c Square membrane subjected to shearing (45°)

For the experimental model, a square wooden frame is used to clamp the membrane. The membrane material used in this experimental is polyethylene material. Before the square membrane was mounted on the frame, four dots were plotted on the membrane. The dimensions of this frame and the locations of the dots are shown in Fig. 6.1d. Dots 1 to 4 are the dots situated at four zone-centered points. The 48 dots around each zone-centered dot were plotted to find the maximum and the minimum stretches and their directions. The same mesh density as for the numerical model was chosen, but only the dots were plotted on the sheet, the mesh was omitted. Fig. 6.1e shows the reference configuration of the square membrane having all four margins attached to the frame by 20 C-clamps. Fig. 6.1f and Fig. 6.1g show the deformed configurations for a shear angle of 35° and 45° respectively. The strain energy employed in the numerical model is suitable for some biological materials (biomembranes) as well as polyethylene material (Humphrey, 1990). To get the experimental results for the principal stretches and the principal directions, three photographs were taken, the first one is the picture of the reference configuration, the other two are the pictures of the deformed configurations with the two shear angles. Coordinates of every dot plotted on the membrane sheet were measured by digitizing the photographs.

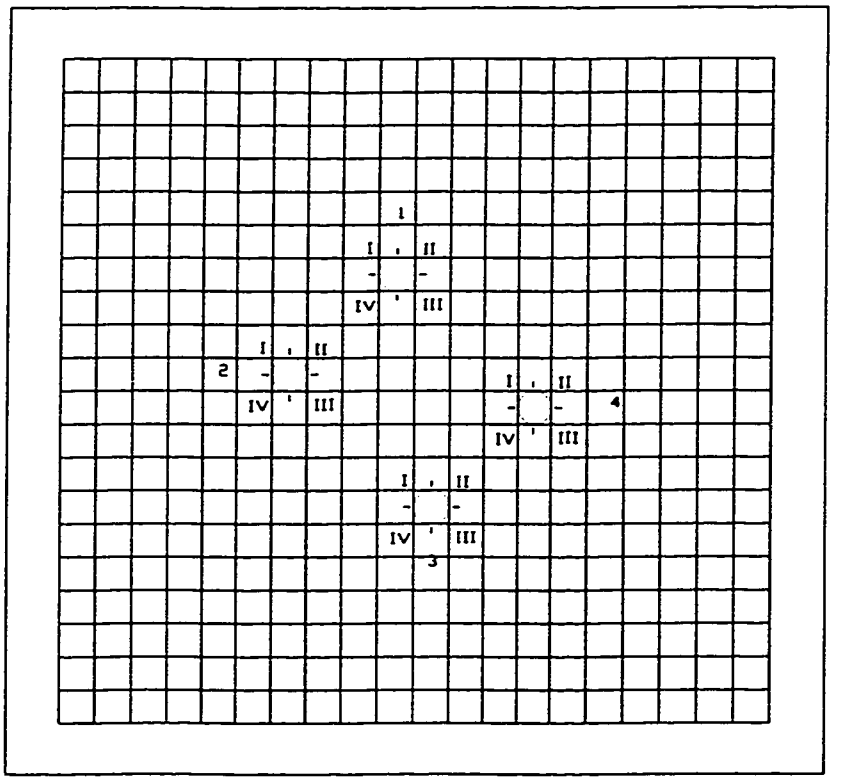

Fig. 6.1d Experimental model of square membrane;

location of testing dots shown

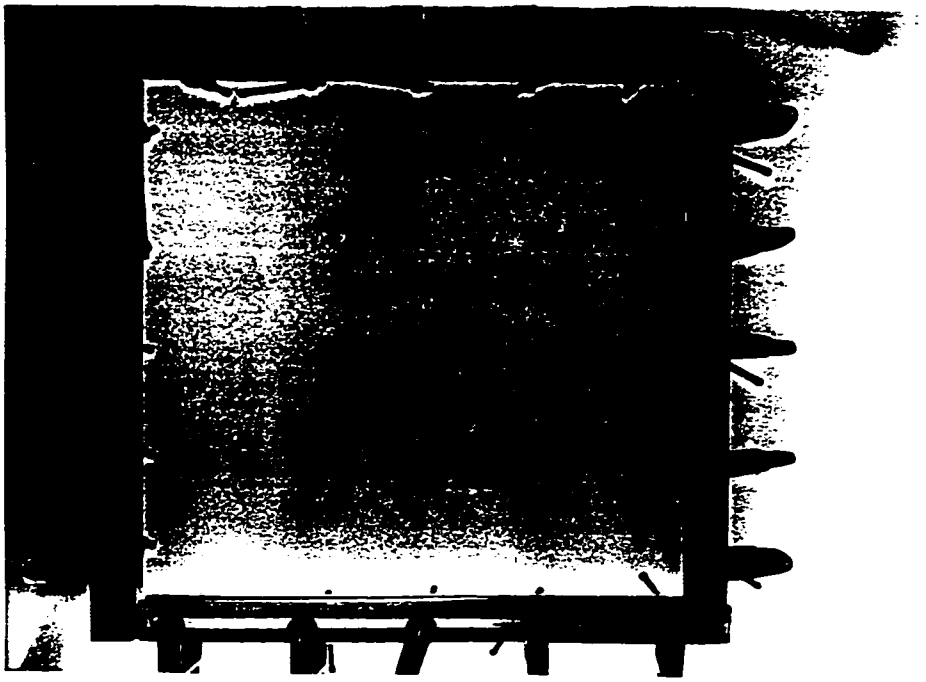

Fig. 6.1e Experimental model of square membrane;

initial configuration

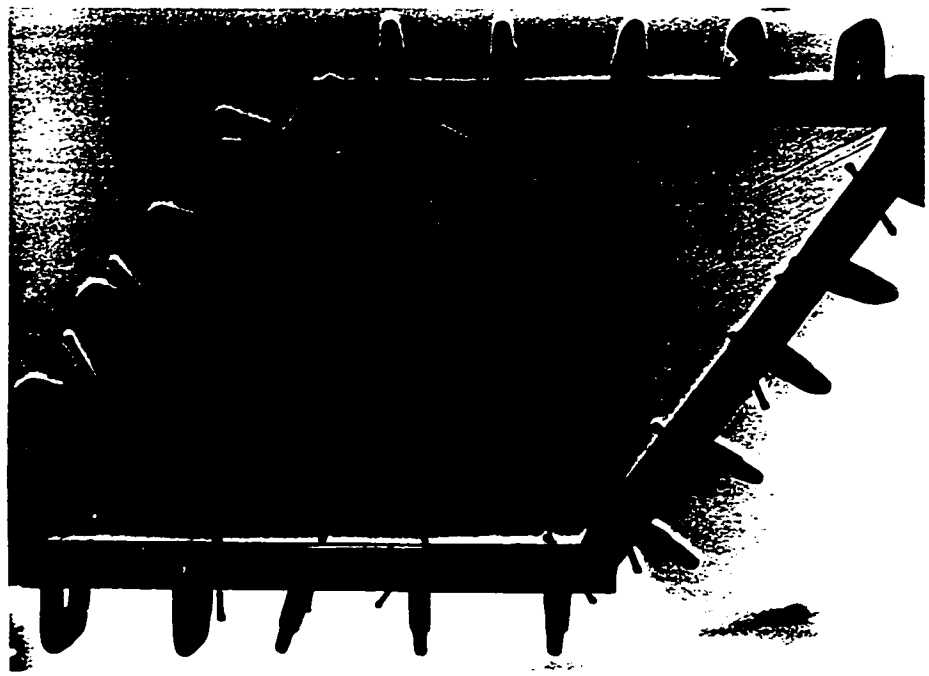

Fig. 6.1f Experimental model of square membrane

subjected to shearing (35°)

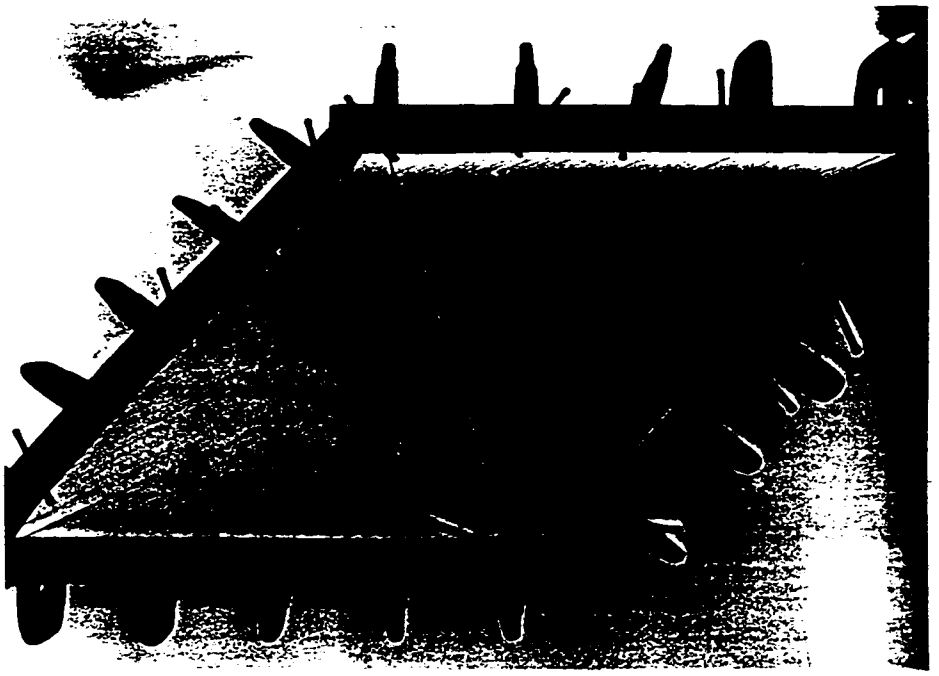

Fig. 6.1g Experimental model of square membrane

subjected to shearing (45°)

6.4 Results

For the case of a shear angle equal with 35°, the comparison of the experimental results and the numerical solutions obtained with the numerical model developed in this work are shown in Fig. 6.1h. At point 1, the difference between the computed λ and the measured λ is 0.23, for μ the difference is 0.05, and for the direction of l the difference is 2.5°. At point 2, the difference between the numerical solution and the experimental one is 0.007 for λ, 0.04 for μ, and 5° for the direction of l. At point 3, the difference between the experimental results and the numerical solutions is 0.17 for λ, 0.01 for μ, and 2.5° for the direction of l. At point 4, the difference between the experimental results and the numerical solution is 0.02 for λ, 0.07 for μ, and 5.5° for the direction of l.

For the case of a shear angle equal with 45°, the comparison of the numerical solutions and the experimental results are shown in Fig. 6.1i. At point 1, the difference between the experimental results and the numerical solution is 0.25 for λ, 0.03 for μ, and 2.5° for the direction of l. At point 2, the difference between the experimental results and the numerical solution is 0.15 for λ, 0.03 for μ, and 2.5° for the direction of l. At point 3, the difference between the experimental results and the numerical solution is 0.11 for λ, 0.08 for μ, and 1.5° for the direction of l. At point 4, the difference between the experimental results and the numerical solution is 0.07 for λ, 0.08 for μ, and 2° for the direction of l.

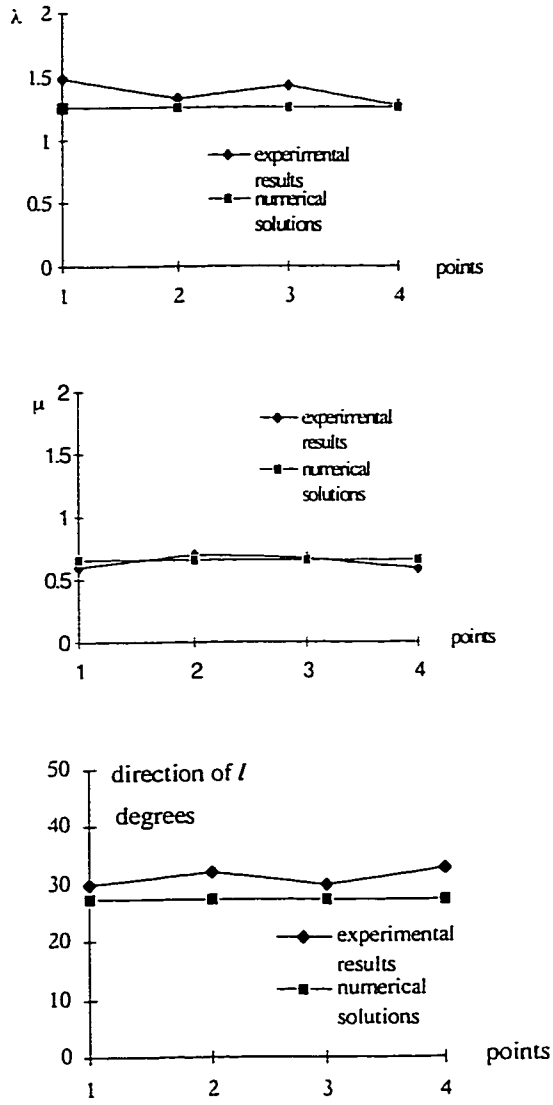

Fig. 6.1h Comparison of numerical results and experimental solutions;

shearing angle of 35°

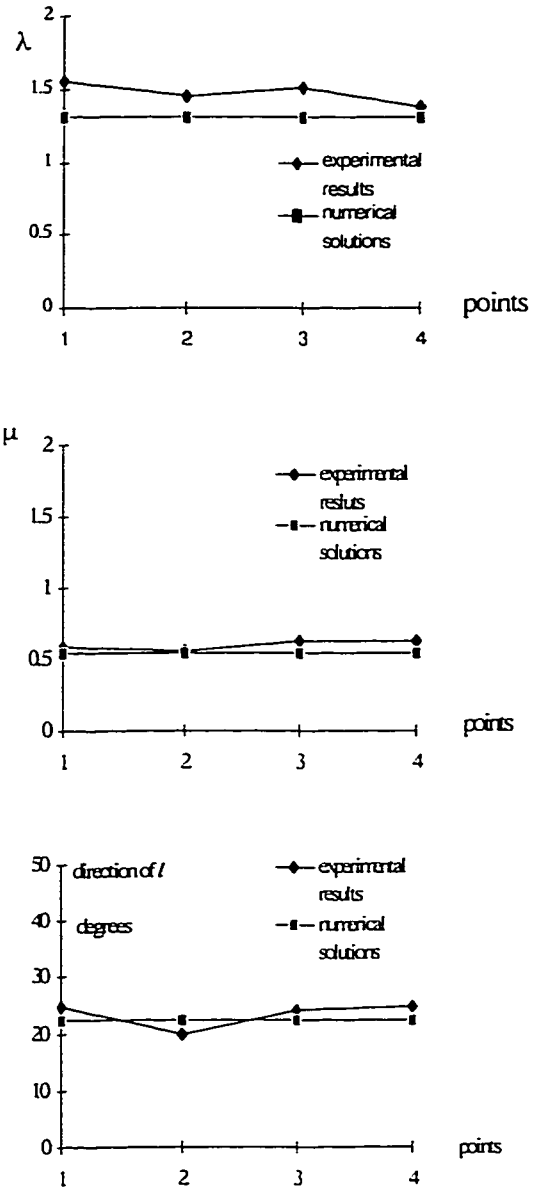

Fig. 6.1i Comparison of numerical results and experimental solutions;

shearing angle of 45°

The inconsistencies in the measured results come from the mounting of the membrane and from the measurement technique. Twenty C-clamps were used to clamp the edges of the membrane to the frame. Although two intermediate wooden lamellae were employed to uniformly distribute the pressure on each clamped side of the membrane, load variations in pressure would still occur. Thus not every material particle of the membrane on the boundary got the exact displacement boundary conditions. The errors also come from the measurement technique, which is primitive. Due to lack of appropriate equipment, the way the coordinates were measured from the photographs cannot give very accurate results. In order to get more accurate experimental results, better instruments, such as laser measurement instruments should be used.

Although causes for errors exist in the experiment, the experimental results still indicate the same trend as the numerical solution. Wrinkling occurs in the whole membrane, as the numerical model shows and the stretches increase with increasing shear angle. It is concluded that, for available equipment the experimental results agree sufficiently well with the numerical solution.

Chapter 7

Summary, Conclusions and Future Work

7.1 Summary and Conclusions

A numerical model has been developed for stress analysis in isotropic elastic membranes undergoing finite deformations, while partly or totally subjected to pressure loading of the hydrostatic type. The possibility of wrinkling is taken into account. The presence of tension fields generated by wrinkling is a problem of concern in the design and analysis of membrane structures. Wrinkling occurs due to the loss of prestress and appearance of compressive stresses, under the action of certain loads and/or certain boundary conditions. It represents a local bucking phenomenon. The configuration of the wrinkled region depends on the small bending stiffness of the material. Membrane theory cannot be applied directly to the wrinkled region, since the bending stiffness is neglected in this theory, and compressive stresses are obtained. Solutions with compressive stresses are unstable, and therefore not observable as equilibrium states. Shell theory may be used in the wrinkled region to get solutions, but it is more complicated in comparison to membrane theory. Tension field theory may also be used to analyze the wrinkled region, and this is much simpler from the point of view of analysis. However tension field theory

can be automatically incorporated into ordinary membrane theory by replacing the strain energy function by a relaxed stain energy. In this work, a ***Relaxed Strain Energy Density*** is used in the modeling process, in order to consider the wrinkling effect while retaining the analytical simplicity of membrane theory.

This numerical model is based on the ***Dynamic Relaxation*** (DR) method. This is an explicit iterative method developed to solve static structural mechanics problems. The static problem is transformed into an equivalent dynamic problem by adding inertia and damping terms. The static solution may be then obtained as the steady state part of the transient response of the structure. The numerical model is obtained from the spatial and temporal discretization of the PDEs describing the damped motion of the structure. The spatial discretization technique used here is a finite difference technique derived from Green's theorem (Wilkins, 1964, Silling, 1985). In addition to its simplicity, this method is suitable to any shape of the boundary. Uniform or irregular meshes may be used. The resulting system of ODEs is then integrated in time by employing a central difference time integrator. This numerical technique is particularly well suited for the class of the problems considered here, since it does not require the construction or inversion of the stiffness matrix, which in the presence of wrinkling is ill-conditioned. DR also has these advantages:

- it is an explicit, iterative technique with low storage;
- it is easy to program;
- fictitious mass and damping characteristics may be chosen for rapid convergence in time;

- it is simple, reliable and flexible with regard to constitutive equations;
- it delivers asymptotically dynamically stable solution.

This numerical model has been used to analyze the response of isotropic elastic membranes subjected to pressure loading of hydrostatic type for various planar reference configurations and different boundary conditions. The deformed shapes, the principal stretches, the principal stresses and their directions and the delimitation of the wrinkled regions were obtained form the output files.

An experimental model consisting of a square membrane subjected to shear and stretch was investigated in order to validate this numerical technique. The principal stretches, the principal stresses and their directions were determined. The numerical results obtained with the experimental model were in good agreement with the numerical solution.

This method can be used for stress analysis of in lightweight constructions, it can be applied to the problems involving ponding of inflatables, a condition frequently encountered in large scale roof coverings, such as protective enclosures for recreational facilities or exposition pavilions. The method is also applicable to biomembranes as well as to membranes used in prosthetics.

7.2 Future Work

The DR algorithm used in this work may be modified to an adaptive one, by adding subroutines to calculate the fictitious mass matrix and the damping coefficient at each

time step. This would lead to a faster convergence of the damped dynamic response toward the static solution.

This numerical model can be further adapted to analyze problems involving initially curved surfaces, the case of orthtropic materials as well as anisotropic materials. Temperature effects may be also included.

Improved experimental techniques, based on better equipment, such as measurements with laser instruments, may be chosen to improve the accuracy of the experimental results.

Bibliography

Alwar, R.S., Ramachandra R., N., 1975, An Alternative Procedure in Dynamic Relaxation, *Computers and Structures*, **5**, 271-274.

Barnes, M. R., 1974, Dynamic Relaxation Analysis of Tension Networks, *Proc. of Int. Conf. on Tension Structures*, London, 1-11.

Bunce, J.W., 1972, A Note on the Estimation of the Critical Damping in Dynamic Relaxation, *Int. J. for Numerical Methods in Engineering,* **4**, 301-304.

Cassel, A. C., 1970, Shells of Revolution under Arbitrary Loading and the Use of Fictitious Densities in Dynamic Relaxation, *Proc. of Inst. of Civil Engineers*, London, **45**, 65-78.

Cohen, H., Wang, C.C., 1984, On the Response and Symmetry of Elastic and Hyperelastic Membrane Points, *Arch. Rat. Mech. Anal.*, **85**, 343-79.

Courant, R., Friedrichs, K., Lewy, H., 1928, On the Partial Differential Equations of Mathematical Physics, Mathematische Annallen, **100**, 32-74, English translation in: *IBM Journal*, 215-234, (1967).

Cundall, P.A., 1976, Explicit Finite Difference Methods in Geomechanics, *Proc. of E.F. Conf. on Numerical Methods in Geomechanics*, Blacksburg, VA.

Day, A.S., 1965, An Introduction to Dynamic Relaxation, *The Engineer*, London, **219**, 218-221.

Frankel, S.P., 1950, Convergence Rates of Iterative Treatments of Partial Differential Equations, Mathematical Tables and other Aids to Computation, *National Research Council, Washington*, **4**, 65-75.

French, D.A., Jensen, S., 1991, Behaviour in the Large of Numerical Solutions to One-Dimensional Nonlinear Viscoelasticity by Continuous Time Galerkin Methods, *Computer Methods in Applied Mechanics and Engineering*, **86**, 105-124.

Graves, L.E., 1939, The Weierstrass Condition for Multiple Integral Variation Problems, *Duke Math. Journal*, **5**, 656-660.

Haseganu, E.M., Steigmann, D.J., 1994, Analysis of Partly Wrinkled Membranes by the Method of Dynamic Relaxation, *Computational Mechanics*, **14**, 596-614..

Haseganu, E.M., 1994, Analytical Investigation of Tension Fields in Lightweight Membrane Structures, Ph.D. Thesis Dept. of Mech. Eng., University of Alberta, Edmonton.

Haug, E., Powell, G.H., 1971, Finite Element Analysis of Non-linear Membrane structures, *Proc. of IASS Pacific Symp.*, Part II, On Tension Structures and Space Frames, Tokyo, 165-175.

Herrmann, W., Bertholf, L.D., 1983, Explicit Lagrangian Finite-Difference Methods, in: *Computational Methods for Transient Analysis*, Belytschko, T., Hughes, T.J.R., editors, Elsvier, Amsterdam, 361-416.

Hilgers, M.G., Pipkin, A.C., 1992, Elastic Sheets with Bending Stiffness, *Q. Jl. Mech. Appl. Math.*, **45**, 93-110.

Humphrey, J.D., Strumpf, R.K., and Yin, F.C.P., 1990, Determination of A Constitutive Relation for Passive Myocardium: I. A New Functional Form, *ASME Journal of Biomechanical Engineering*, **112**, 333-339.

Knops, R.J., Wilkes, E.W., 1973, Theory of Elastic Stability, in: *Handbuch der Physik*, Flügge, S., editor, Vol. VIa/3, Springer Verlag, Berlin.

Kodkhodayan, M., Zhang, L. C., 1995, Consistent DXDR Method for Elastic-plastic Problems, *Int. J. for Numerical Methods in Engineering,* **38**, 2413-2431.

Kommineri, J.R., Kant, T., 1995, Pseudo-transient Large Deflection Elastic Analysis of Composite and Sandwich Shells with A Refined Theory, *Computer Methods in Applied Mechanics & Engineering*, **123**, 1-13.

Leech, J. W ., 1965, Stability of Finite-Difference Equations for the Transient Response of a Flat Plate, *AIAA Jour.*, 3, 1772-1773.

Lewis, W.J., Gosling, P.D., 1993, Stable Minimal Surfaces in Form-Finding of Lightweight Tension Structures, *Int. J. of Space Structures*, 8, 149-166.

Liu, Y., Haseganu, E.M., 1997, Dynamic Relaxation Analysis of Elastic Membrane Subjected to Hydrostatic Pressure, *Proc. of the 1997 CSME forum*, Laval University, Québec, 35-36.

Liu, Y., Haseganu, E.M., 1998, Response of Pneumatic Structures Subjected to Hydrostatic Loading, Submitted for presentation and publication in the Porc. of the 1998 CSME Forum, Ryerson Polytechnic University, Toronto, ON.

Lynch, R.D., Kelsey, S., Saxe, H. C., 1968, The Application of Dynamic Relaxation to the Finite Element Method of Structural Analysis, Technical Report No. Themis-Und-68-1, University of Notre Dame, Indiana.

Miller, R.K., Hedgepeth, J.M., 1982, An Algorithm for Finite Element Analysis of Partly Wrinkling Membranes, *AIAA Jour.*, **20**, 1761-1763.

Motro, R., 1984, Forms and Forces in Tensegrity Systems, *Proc. of Third Int. Conf. on Space Structures*, Guilford, 283-288.

Motro, R., Najari, S., Jouanna, P., 1986, Tensegrity Systems, from Design to Realization, *Proc. of First Int. Conf. on Lightweight Structures in Architecture*, Sydney, 690-697.

Naghdi, P.M., 1972, Theory of Shells and Plates, in: *Handbuch der Physik*, Flügge, S., editor, Vol. VI/2, pp. 425-640, Spring Verlag, Berlin.

Oakely, D.R, Knight, N. F Jr, Warner, D.D., 1995a, Adaptive Dynamic Relaxation Algorithm for Non-linear Hyperelastic Structures. Part I. Parallel Implementation, *Computer Methods in Applied Mechanics & Engineering*, **126**, 67-89.

Oakely, D.R, Knight, N. F Jr, Warner, D.D., 1995b, Adaptive Dynamic Relaxation Algorithm for Non-linear Hyperelastic Structures. Part II. Parallel Implementation, *Computer Methods in Applied Mechanics & Engineering*, **126**, 91-109.

Oakely, D.R, Knight, N. F Jr, Warner, D.D., 1995c, Adaptive Dynamic Relaxation Algorithm for Non-linear Hyperelastic Structures. Part III. Parallel Implementation, *Computer Methods in Applied Mechanics & Engineering*, **126**, 111-129.

Ogden, R.W., 1984, *Nonlinear Elastic Deformations*, Ellis-Horwood, Chichester, U. K.

Otter, J.R.H., 1965, Computations for Prestressed Concrete Reactor Pressure Vessels using Dynamic Relaxation, *Nuclear Structural Engineering*, Amsterdam, 1, 61-75.

Otter, J.R.H., Cassell, A.C., Hobbs, R.E., 1966, Dynamic Relaxation, *Proc. of the Inst. of Civil Engineers*, London, 35, 633-656.

Papadrakakis, M., 1981, A Method for the Automatic Evaluation of the Dynamic Relaxation Parameters, *Computer Methods in Applied Mechanics and Engineering*, **25**, 35-48.

Pipkin, A.C., 1986, The Relaxed Energy Density for Isotropic Elastic Membranes, *IMA J. Appl. Math*, Vol. 36, pp. 85-99.

Rushton, K.R., 1968, Large Deflection of Variable-Thickness Plates, *Int. J. Mech. Sci.*, **10**, 723-735.

Salehi, M., Shahidi, A., 1994, Large Deflection Analysis of Elastic Sector Mindlin Plates, *Computer & Structures*, **52**, 987-998.

Sauve, R.G., Badie, N., 1993, Non-Linear Shell Formulation for Time-Dependent Deformation, *Proc. of 1993 Pressure Vessels and Piping Conference*, Denver, CO, 269-275.

Siddiquee, M S A, Tanaka, T., Tatsuoka, F., 1995, Tracing The Equilibrium Path by Dynamic Relaxation in Materially Nonlinear Problems, *Int. J. for Numer. & Analytical Method in Geomechanics*, **19**, 749-767.

Silling, S.A., 1985, CHIMP - A Computer Program for Finite Elastostatics, Report 54 California Institute of Technology, Division of Engineering and Applied Science.

Silling, S.A., 1987, Incompressibility in Dynamic Relaxation, *J. of Applied Mechanics*, **54**, 539-544.

Silling, S.A., 1988a, Finite Difference Modeling of Phase Changes and Localization in Elasticity, *Computer Methods in Applied Mechanics and Engineering*, **70**, 251-273.

Silling, S.A., 1988b, Numerical Studies of Loss of Elipticity near Singularities in an Elastic Material, *J. of Elasticity*, **19**, 213-239.

Silling, S.A., 1989, Phase Changes induced by Deformation in Isothermal Elastic Crystals, *J. of the Mechanics and Physics of Solids*, **3**, 293-316.

Steigmann, D.J., 1986, Proof of a Conjecture in Elastic Membrane Theory, *ASME J. Appl. Mech.*, **53**, 955-956.

Steigmann, D.J., 1990, Tension-Field Theory, *Proc. of Roy. Soc. of London*, A, 429, 141-173

Steigmann, D.J., 1991, A Note on Pressure Potentials, *J. Elast.*, 26, 87-93.

Strang, G., 1976, *Linear Algebra and its Applications*, Academic Press, New York.

Szyszkowski, W., Glockner, P.G., 1984, Finite Deformation and Stability Behavior of Spherical Inflatable under Axisymmetric Concentrated Loads, *Int. J. Non-Linear Mech.*, **19**, 489-496.

Tarakanov, S.I., 1984, Convergence of the Dynamic Relaxation Method in Problems of Loading of Elastic Shells of Revolution, *Moskow University Mechanics Bulletin*, **39**, 53-56.

Turvey, G.J., Osman, M.Y., 1993, Large Deflection Initial Failure Analysis of Angle-Ply Laminated Plates, *Composite Structures*, **25**, 529-539.

Underwood, P., 1983, Dynamic Relaxation, in: *Computational Methods for Transient Analysis*, Belytschko, T., Hughes, T. J. R. editors, Elsvier, Amsterdam, 245-265.

Varga, O.H., 1966, *Stress-Strain Behavior of Elastic Materials*, Wiley, New York.

Wagner, H., 1929, Ebene Blechwandträger mit sehr dünnen Stegblech, *Z. Flugtechnik u. Motorluftschiffahrt*, **20**, Nos 8-12.

Welsh, A.K., 1967, in Discussion on Paper "Dynamic Relaxation" by Otter, J.H.R. et al., *Proc. of Inst. of Civil Engineers, London*, **37**, 723-750.

Wilkins, M. L., 1964, Calculation of Elastic-Plastic Flow, in: *Methods in Computational Physics*, V.3, Alder, B., Fernbach, S., Rotenberg, M., editors, Academic Press, New-York, 211-163.

Wilkins, M.L., 1969, Calculation of Elastic-Plastic Flow, Lawrence Radiation Laboratory, Rept. UCRL-7322, Revised, Univ. of California. Livermore.

Zhang, L.C., Kadkhodayan, M., Mai, Y-W, 1994, Development of The maDR Method, *Computer and Structures*, 52, 1-8.

Zhang, L.G., Yu, T. X., 1989, Modified Adoptive Dynamic Relaxation Method and its Application to Elastic-Plastic Bending and Wrinkling of Circular Plates, *Computers and Structures*, 33, 609-614.

Zhang, L.G., Yu, T. X., Wang, R., 1989, New Approach of Predicting Points of Elastic-Plastic Buckling of Plates and Shells, *Acta Mechanica Sinica*, 5, 145-151.

Zienkiewicz, O.C., Löhner, R., 1985, Accelerated "Relaxation" or Direct Solution? Future Prospects for FEM, *Int. J. for Numer. Methods in Engineering*, **21**, 2-11.